LBNL-39127
UC-404

ERNEST ORLANDO LAWRENCE
BERKELEY NATIONAL LABORATORY

Solid-State Sodium Batteries Using Polymer Electrolytes and Sodium Intercalation Electrode Materials

Y. Ma
Materials Sciences Division

August 1996
Ph.D. Thesis

LBNL--39127

Solid-State Sodium Batteries Using Polymer Electrolytes and Sodium Intercalation Electrode Materials

Yanping Ma

(Ph.D. Thesis)

Department of Materials Science and Mineral Engineering

University of California, Berkeley

and

Materials Sciences Division

Lawrence Berkeley National Laboratory

University of California

Berkeley, CA 94720-1760

Fall, 1996

Work supported by the Director, Office of Energy Research, Office of Basic Energy Sciences, Materials Sciences Division of the U.S. Department of Energy under Contract No. DE-AC03-76SF00098.

Solid-State Sodium Batteries Using Polymer Electrolytes and Sodium Intercalation Electrode Materials

By

Yanping Ma

B.E. (Tsinghua University) 1986
M.Eng. (Tsinghua University) 1989

DISSERTATION

Submitted in partial satisfaction of the requirements for the degree of

DOCTOR OF PHILOSOPHY

in

ENGINEERING
MATERIALS SCIENCE AND MINERAL ENGINEERING

in the

GRADUATE DIVISION

of the

UNIVERSITY of CALIFORNIA, BERKELEY

Committee in Charge:

Professor Lutgard C. De Jonghe
Professor Alan W. Searcy
Professor John Newman

Fall, 1996

ABSTRACT

Solid-State Sodium Batteries Using Polymer Electrolytes and Sodium Intercalation Electrode Materials

By

Yanping Ma

Doctor of Philosophy in Materials Science and Mineral Engineering

University of California, Berkeley

Professor Lutgard C. De Jonghe, Chair

Solid-state sodium cells using polymer electrolytes (polyethylene oxide mixed with sodium trifluoromethanesulfonate: $PEO_nNaCF_3SO_3$) and sodium cobalt oxide positive electrodes are characterized in terms of discharge and charge characteristics, rate capability, cycle life, and energy and power densities. The experimental results are the best ever reported in the literature for sodium/polymer cells. The P2 phase Na_xCoO_2 can reversibly intercalate sodium in the range of $x = 0.3$ to 0.9, giving a theoretical specific energy of 440 Wh/kg and energy density of 1600 Wh/l. Over one hundred cycles to 60% depth of discharge have been obtained at 0.5 mA/cm^2 (C/1h). Experiments show that the electrolyte/Na interface is stable and is not the limiting factor to cell cycle life.

$Na_{0.7}CoO_2$ composite electrodes containing various amounts of carbon black additive are investigated. The electronic conductivity of these electrodes is found to be dominated by the volume fraction of carbon. The additive is also critical to cell cycle life.

The transport properties of polymer electrolytes are the critical factors for performance. These properties (the ionic conductivity, salt diffusion coefficient, and ion

transference number) are measured for the $PEO_nNaCF_3SO_3$ system over a wide range of concentrations at 85°C. The ionic conductivity and the salt diffusion coefficient are measured using the ac-impedance technique and the restricted-diffusion method, respectively. A novel method to measure the ion transference number is developed and used in the present study. This method is based on dc polarization experiments in combination with concentration cell measurements, and is theoretically rigorous for any binary electrolyte and also experimentally simple. The thermodynamic factor (a factor that is related to the mean activity coefficient) of the electrolytes is determined, as well, using this method. All the three transport properties of the $PEO_nNaCF_3SO_3$ system are very salt-concentration dependent. The ionic conductivity exhibits a maximum at about n = 20. The transference number, diffusion coefficient, and thermodynamic factor all vary with salt concentration in a similar fashion, decreasing as the concentration increases, except for a local maximum. These results verify that polymer electrolytes cannot be treated as ideal solutions.

The measured transport-property values are used to analyze and optimize the electrolytes by computer simulation and also cell testing. Salt precipitation is believed to be the rate limiting process for cells using highly concentrated solutions, as a result of lower values of these properties, while salt depletion is the limiting factor when a dilute solution is used. Moderately concentrated solutions (about n = 20) are found to have the optimum rate capability for the $PEO_nNaCF_3SO_3$ system.

TABLE OF CONTENTS

To

my parents, and my daughter Emily

Acknowledgments

I wish to express my acknowledgment to Professor Lutgard C. De Jonghe for his valuable guidance. I also gratefully thank Dr. Marca M. Doeff for her valuable assistance, proof reading this thesis, and friendship.

Special appreciation goes to Marc Doyle in the Department of Chemical Engineering at U.C. Berkeley for his major contribution in the development of transference number theory, computer simulations, and valuable discussion. Thanks also go to Professor John Newman for his contribution in the development of transference number theory.

I gratefully acknowledge Professor Alan W. Searcy and Professor John Newman for reviewing this thesis and their valuable comments.

I wish to express my appreciation to Dr. Carl M. Lampert for his financial support during the transition period to my Ph. D. program and his valued friendship. It is wish pleasure that I express my gratitude to all the friendly members of my research group. Special thanks go to Steve Visco, Mark Sixta, Marianna Niu, Mani Gopal, and Kazu Noda for the help they gave for this study.

I am most grateful to my dear husband, Joe, for his constant love and support, and to my lovely daughter, Emily, for the wonderful time and joy with her.

Chapter 1 Introduction

In recent years, consumer demand for electronic products such as portable computers, cellular phones, and video camcorders as well as environmental interests in promoting electric-powered vehicles have heralded the call for more advanced batteries. The criteria for superior batteries for these applications are high energy and/or high power density and long cycle lives. A great deal of attention has been given to lithium batteries [1] because lithium has an extremely high charge capacity and very negative electrode potential.

Alongside efforts to develop lithium batteries, there has also been exploration of similar systems that substitute lithium with other alkali metals or even divalent metals. Among the various proposed alternatives to lithium cells, the sodium battery is the most attractive. Sodium has a reasonably low equivalent weight and very negative electrode potential. More importantly, it is readily available and inexpensive. In addition, sodium ion conductors tend to have slightly higher ionic conductivity than their lithium analogues. Sodium, unlike lithium, does not form alloys with aluminum, making it feasible to use aluminum as current collectors in place of the heavier and more expensive nickel used in lithium cells. Though sodium has a lower charge capacity and less negative electrode potential than lithium, and consequently a lower cell energy density, the advantages of sodium make the development of sodium battery a compelling goal. [2]

The most attractive positive electrodes for lithium and sodium cells are intercalation materials, which contain a continuous network of empty sites of appropriate sizes. Mobile guest species can intercalate into and deintercalate out of these sites easily

without strongly perturbing the host structures. In intercalation processes, the kinetics are favorable because the reactions maintain a close structural relationship between the existing phase and the product so that the nucleation and growth of product phases are rapid. In addition, these intercalation materials contain empty sites that are connected so that guest species diffuse at high rates.

A wide range of host structures has been investigated. These materials include 1) three-dimensional network structures containing empty sites that form channels, 2) two-dimensional layered structures with van der Waals gaps between the layers, and also 3) one-dimensional chain structures or amorphous materials. Layered materials have been proven to be particularly versatile host materials, as they can adapt to guest species of very different sizes by changing interlayer spacing. The high degree of dimensional stability that is required of a host lattice stipulates strong and directional bonding. This is only obtained in compounds with an appreciable degree of covalence, such as metal oxides, or chalcogenides (sulfides, selenides, and tellurides), or in carbon-based materials such as graphite. Great attention has been paid to transition metal oxides as host materials.[3] Oxides possess potentially higher specific energy and energy density as well as lower toxicity than chalcogenides.

The first row transition metal oxides have been extensively studied for lithium and sodium cells, some second row and third row transition metal oxides and sulfides have also been studied, but the capacity density of these materials is expected to be lower due to the higher equivalent weight of these transition metal elements. The most widely studied materials are lithium-intercalating titanium disulfide, [4] vanadium oxides, [5-9] manganese oxides, [10-15] and cobalt and nickel oxides [16-20] for lithium cells, and the

sodium analogues of these for sodium cells. [21-36]

Lithium and sodium batteries are attractive not only for their potential high energy density but also because a battery assembly that is completely solid state is possible using solid-state lithium or sodium ion conducting electrolytes. Solid-state polymer electrolytes were proposed by Armand in 1979 for lithium battery use, [37] and have attracted great attention since then. The adhesiveness and elastomerity of a polymer allow good contact between electrolytes and electrodes, which is problematic when solid ceramic electrolytes are used. Most importantly, polymer electrolytes allow a greater flexibility in cell design and cell assembly due to their plastic characteristics.

The first part of this work explores further the feasibility of solid-state sodium batteries, employing polymer electrolytes and sodium intercalation electrode materials. [38] Preliminary studies on sodium batteries using vanadium oxides [23,24,27,35] and other materials [34,36] demonstrate that sodium cells can function with solid polymer electrolytes. However, improvement in energy density, rate capability, and cycle life is required before sodium/polymer electrolyte batteries can be considered for practical uses. Sodium cobalt oxide, which has recently been shown to exhibit promising intercalation/deintercalation characteristics and excellent performance in nonaqueous liquid electrolyte sodium cells, [22] was chosen as the positive electrode material for the present study.

For polymer electrolytes to be useful they must be nonreactive with positive electrodes which are usually very oxidizing, and nonreactive with negative electrodes, as well, which are usually very reducing. They should have an appropriate electrochemical window in order to be stable within the entire operating potential range during charge and

discharge. They also need to be stable at elevated temperatures since polymer electrolytes usually need to be heated to the melting state in order to be conductive. Other than these basic requirements, good transport properties are the primary factors in determining the performance of electrolytes. [39-41] The most widely studied polymer electrolytes are poly(ethylene oxide) complexed with one of the various lithium salts ($LiCF_3SO_3$, $LiClO_4$, $LiAsF_6$, $LiPF_6$, or $LiN(CF_3SO_2)_2$). [42]

Transport properties of an electrolyte determine how fast a cell can be discharged and charged while still attaining reasonable utilization. Knowledge of these properties is essential to understand transport processes in the electrolyte, to optimize the solution, and also to scale-up. These properties are determined by the interaction parameters [43] between the cation and solvent, between the anion and solvent, and between the cation and anion for a binary electrolyte. For a dilute solution, interactions between the cation and anion are usually ignored; therefore two parameters are sufficient to describe the transport processes in the solution. This interaction parameter, however, can not be ignored for polymer electrolytes, as demonstrated from studies of activity coefficients, [44] ion-pairing, [45,46] and the concentration dependence of ionic conductivity. [47,48] Therefore, three independent transport properties that result from the three interaction parameters are necessary to describe completely a polymer electrolyte. Much attention has been given to the conductivity of the lithium-conducting electrolytes based on polyethylene oxide. Attempts are also been made to measure the ion transference number in these solutions. Since polymers are solid materials, traditional methods of measuring the transference number such as the Hittorf method [49] have met with much difficulty. Several novel methods have been developed, the most well-known of which are the

potentiostatic polarization method (steady-state current method) [50-53] and the ac impedance method. [54] However, there has been many variations among the results obtained with these methods and other methods. [55,56] The discrepancies can probably be explained by invalid assumptions made in the analysis, including not accounting for the concentration dependence of transport properties or the assumption of an ideal solution. Detailed critiques of the potentiostatic polarization method and the ac-impedance methods from the standpoint of concentrated-solution theory have appeared in literature. [57,58] There has been no comprehensive study on the transport properties of any single polymer electrolyte due foremost to the difficulties in transference number measurements. Clearly, there is a need for new approaches to measure the ion transference number that are theoretically rigorous and are also experimentally easy to perform.

The second part of the present work focuses on these issues. A novel method to measure the transference number that satisfying the above criteria is developed from concentrated solution theory. [59] The new method is based on galvanostatic polarization experiments in combination with concentration-cell measurements. A complete set of transport properties of a polymer system ($PEO_nNaCF_3SO_3$), which is the analogue of the widely used $PEO_nLiCF_3SO_3$, is determined over a wide range of concentration. These properties are used to analyze and optimize the electrolyte system to achieve the best rate capability. This is done with computer simulation using the measured property values and also with cell testing.

References for Chapter 1

1. M. Gauthier, A. Belanger, B. Kapfer, G. Vassort, and M. Armand, "Solid Polymer Lithium Batteries," in Polymer Elelctrolyte Reviews - 2, Eds., J. R. MacCallum and C. A. Vincent, Elservier Applied Science, London, 1989.

2. K. West, "Solid-State Sodium Batteries," in *Lithium Batteries – New materials, Developments and Perspecties*, Ed. G. Pistoia, Elsevier, 1994.

3. T. Ohzuku and A. Ueda, "Why Transition Metal (Di)oxides are the Most Attractive Materials for Batteries," *Solid State Ionics*, **69**, 201-211 (1994).

4. M. Gauthier, D. Fauteux, G. Vassort, A. Belanger, M. Duval, P. Ricoux, J.-M. Chabagno, D. Muller, P. Rigaud, M. B. Armand, and D. Deroo, "Assessment of Polymer-Electrolyte Batteries for EV and Ambient Temperature Applications," *J. Electrochem. Soc.*, **132**, 1333-1340 (1985).

5. F. Bonino, M. Ottaviani, and B. Scrosati, "A Polymeric Electrolyte Rechargeable Lithium Battery," *J. Electrochem. Soc.*, **135**, 12-15 (1988).

6. C. Lampe-Onnerud, J. O. Thomas, M. Hardgrave, and S. Yde-Anderson, "The Performance of Single-Phase V_6O_{13} in the Lithium Polymer Electrolyte Battery," *J. Electrochem. Soc.*, **142**, 3648-3651 (1995).

7. K. West, B. Zachau-Christiansen, M. J. L. Ostergard, and T. Jacobsen, "Vanadium Oxides as Electrode Materials for Rechargeable Lithium Cells," *J. Power Sources*, **20**, 165-172 (1987).

8. A. Hooper and J. M. North, "The Fabrication and Performance of All Solid State Polymer-Based Rechargeable Lithium Cells," *Solid State Ionics*, **9&10**, 1161-1166 (1983).

9. M. Z. A. Munshi and B. B. Owens, "Performance of Polymer Electrolyte Cells at +25 to +100°C," *Solid State Ionics*, **26**, 41-46 (1988).

10. J. M. Tarascon, E. Wang, F. K. Shokoohi, W. R. McKinnon, and S. Colson, "The Spinel Phase of $LiMn_2O_4$ as a Cathode in Secondary Lithium Cells," *J. Electrochem. Soc.*, **138**, 2859 (1991).

11. M. M. Thackeray, A. de Kock, M. H. Rossouw, D. Liles, R. Bittihn, and D. Hoge,

"Spinel Electrodes from the Li-Mn-O System for Rechargeable Lithium Battery Applications," *J. Electrochem. Soc.*, **139**, 363 (1992).

12. J. M. Tarascon and D Guyomard, "Li Metal-Free Rechargeable Batteries Bassed on $Li_{1+x}Mn_2O_4$ Cathodes ($0 \leq x \leq 1$) and Carbon Anodes," *J. Electrochem. Soc.*, **138**, 2864 (1991).

13. D. Guyomard and J. M. Tarascon, "Li Metal-Free Rechargeable $LiMn_2O_4$/Carbon Cells: Their Understanding and Optimization," *J. Electrochem. Soc.*, **139**-948 (1992).

14. Q. Xu and G. Wan, "Rechargeable Li/$LiMn_2O_4$ Batteries with a Polymeric Solid Electrolyte," *J. Power Sources*, **41**, 315-320 (1993).

15. M. M. Thackeray, M. H. Rossouw, A. de Kock, A. P. de la Harpe, R. J. Gummow, K. pearce, and D. C. Liles, "The Versatility of MnO_2 for Lithium Battery Applications," *J. Power Sources*, **43-44**, 289 (1993).

16. T. Ohzuku and A Ueda, "Solid-State Redox Reactions of $LiCoO_2$ (R3-m) for 4 Volt Secondary Lithium Cells," *J. Electrochem. Soc.*, **141**, 2972 (1994).

17. E. Plichta, S. Slane, M. Uchiyama, M. Salomon, O. Chua, W. B. Ebner, and H. W. Lin, "An Improved Li/Li_xCoO_2 Rechargeable Cell," *J. Electrochem. Soc.*, **136**, 1865-1869 (1989).

18. C. Delmas and I. Saadoune, "Electrochemical and Physical Properties of the $Li_xNi_{1-y}CoO_2$ Phases," *Solid State Ionics*, **53-56**, 370 (1992).

19. J. R. Dahn, U. von Sacken, M. W. Juzkow, and H. Al-Janaby, "Rechargeable $LiNiO_2$/Carbon Cells," *J. Electrochem. Soc.*, **138**, 2207 (1991).

20. A. Ueda and T. Ohzuku, "Solid State Redox Reactions of $LiNi_{1/2}Co_{1/2}O_2$ (R-3m) for 4 Volt Secondary Lithium Cells," *J. Electrochem. Soc.*, **141**, 2010 (1994).

21. C. Delmas, J-J Braconnier, C. Fouassier, and P. Hagenmuller, "Electrochemical Intercalation of Sodium in Na_xCoO_2 Bronzes," *Solid State Ionics*, **3/4**, 165-169 (1981).

22. L. W. Shacklette, T. R. Jow, and L. Townsend, "Rechargeable Electrodes from Sodium Cobalt Bronzes," *J. Electrochem. Soc.*, **135**, 2669-2674 (1988).

23. S. Skaarup, K. West, B. Zachau-Cristiansen, and T. Jacobsen, "Solid State Sodium Batteries," *Proceedings of the International Seminar on Solid State Ionic Devices*, eds., B. V. R. Chowdari and S. Radhakrishna, Singapore, 75-86 (1988).

24. K. West, B. Zachau-Christiansen, T. Jacobsen, and S Skaarup, "Sodium Insertion in Vanadium Oxides," *Solid State Ionics*, **28-30**, 1128-1131 (1988).

25. J. P. Pereira-Ramos, R. Messina, S. Bach, and N. Baffier, "Influence of the Synthesis via a Sol-Gel Process on the Electrochemical Lithium and Sodium Insertion in β-$Na_{0.33}V_2O_5$," *Solid State Ionics*, **40/41**, 970-973 (1990).

26. S. Bach, N. Baffier, J. P. Pereira-Ramos, and R. Messina, "Electrochemical Sodium Intercalation in $Na_{0.33}V_2O_5$ Bronze Synthesized by a So-Gel Process," *Solid State Ionics*, **37**, 41-49 (1989).

27. M. Z. A. Munshi, A. Gilmour, W. H. Smyrl, and B. B. Owens, "Sodium/V_6O_{13} Polymer Electrolyte Cells," *J. Electrochem. Soc.*, **136**, 1847-1848 (1989).

28. A. Mendiboure, C. Delmas, and P. Hagenmuller, "Electrochemical Intercalation and Deintercalation of Na_xMnO_2 Bronzes," *J. Solid State Chemistry*, **57**, 323-331 (1985).

29. M. M. Doeff, M. Y. Peng, Y. Ma, and L. C. De Jonghe, "Orthorhombic Na_xMnO_2 as a Cathode Material for Secondary Sodium and Lithium Polymer Batteries," *J. Electrochem. Soc.*, **141**, L145-147 (1994).

30. M. M. Doeff, L. Ding, and L. C. De Jonghe, "Electrochemical Characterization of Orthorhombic Na_xMnO_2 for Alkali Metal Polymer Batteries," *Mat. Res. Soc. Symp. Proc.*, **393**, 107-112 (1995).

31. J. M. Tarascon, D. G. Guyomard, and B. Wilkens, "Chemical and Electrochemical Insertion of Na into the Spinel λ-MnO_2 Phase," *Solid State Ionics*, **57**, 113-120 (1992).

32. M. M. Doeff, Y. Ma, M. Peng, S. J. Visco, and L. C. De Jonghe, "Solid Sodium Polymer Electrolyte Batteries," Proceedings of the *28th Intersociety Energy Conversion Engineering Conference*, # 93039, Atlanta, GA, 1993.

33. J. M. Tarascon and G. W. Hull, "Sodium Intercalation into the Layer Oxides $Na_xMo_2O_4$," *Solid State Ionics*, **22**, 85-96 (1986).

34. K. West, B. Zachau-Christiansen, T. Jacobsen, and S Atlung, "A Rechargeable All-Solid-State Sodium Cell with Polymer Electrolyte," *J. Elctrochem. Soc.*, **132**, 3061-3062 (1985).

35. K. West, B. Zachau-Christiansen, T. Jocobsen, and S. Skaarup, "Layered

Potassium Vanadium Oxides as Host Materials for Lithium and Sodium Insertion," *Solid State Ionics*, **40/41**, 585-588 (1990).

36. R. Kosbang, S. Yde-Andersen, K. West, B. Zachau-Christiansen, and S. Skaarup, "Lithium and Sodium Insertion in Ternary Chromium Oxides," *Solid State Ionics*, **28-30**, 868-872 (1988).

37. M. Armand, "Polymer Solid Electrolytes - An Overview," *Solid State Ionics*, **9&10**, 745-754 (1983).

38. Y. Ma, M. M. Doeff, S. J. Visco, and L. C. De Jonghe, "Rechargeable Na/Na_xCoO_2 and $Na_{15}Pb_4/Na_xCoO_2$ Polymer Electrolyte Cells," *J. Electrochem. Soc.*, **140**, 2726-2733 (1993).

39. M. Doyle, T. F. Fuller, and J. Newman, "Modeling of Galvanostatic Charge and Discharge of the Lithium/Polymer/Insertion Cell," *J. Electrochem. Soc.*, **140**, 1526-1533 (1993).

40. T. F. Fuller, M. Doyle, and J. Newman, "Simulation and Optimization of the Dual Lithium Ion Insertion Cell," *J. Electrochem. Soc.*, **141**, 1-10 (1994).

41. M. Doyle and J. Newman, "The Importance of the Lithium Ion Transference Number in Lithium/Polymer Cells", *Electrochemica. Acta*, **39**, 2073-2081 (1994).

42. L. A. Dominey, "Current State of the Art on Lithium Battery Electrolytes," in Lithium Batteries - New Materials, Developments and Perspectives, Ed., G. Pistoia, Elservier, 1994.

43. J. Newman, *Electrochemical Systems*, Prentice Hall, Englewood Cliffs, NJ (1991).

44. A. Bourdiah, F. Dalard, D. Deroo, and M. Armand, "Potentiometric Measurements of Ionic Transport Parameters in Poly(Ethylene Oxide)-LiX Electrolytes," *J. Appl. Electrochem.*, **17**, 625-634 (1987).

45. M. A. Ratner, "Aspects of the Theoretical Treatment of Polymer Solid Electrolytes: Transport Theory and Models," in *Polymer Electrolyte Reviews-1*, Eds., J. R. MacCallum and C. A. Vincent, Elsevier Applied Science, London, pp. 173-236 (1987).

46. P. G. Bruce and C. A. Vincent, "Effects of Ion Association on Transport in

Polymer Electrolytes," *Faraday Disc. Chem. Soc.*, **88**, 43 (1989).

47. C. D. Robitaille and D. Fauteux, "Phase Diagrams and Conductivity Characterization of Some PEO-LiX Electrolytes," *J. Electrochem. Soc.*, **133**, 315 (1986).

48. K. West, B. Zachau-Christiansen, T. Jacobsen, E. Hiort-Larenzen, and S. Skaarup, "Poly(Ethylene Oxide)-Sodium Perchlorate Electrolytes in Solid-State Sodium Cells," *British Polymer Journal*, **20**, 243-246 (1988).

49. P. G. Bruce, M. T. Hardgrave, and C. A. Vincent, "The Determination of Transference Number in Solid Polymer Electrolytes Using the Hittorf Method," *Solid State Ionics*, **53-56**, 1087 (1992).

50. J. Evans, C. Vincent, and P. Bruce, "Electrochemical Measurement of Transference Numbers in Polymer Electrolytes," *Polymer*, **28**, 2324-2328 (1987).

51. M. Watanabe, S. Nagano, K. Sanui, and N. Ogata, "Estimation of Li^+ Transference Number in Polymer Electrolytes by the Combination of Complex Impedance and Potentiostatic Polarization Measurements," *Solid State Ionics*, **28-30**, 911-917 (1988).

52. P. G. Bruce, J. Evans, and C. A. Vincent, "Conductivity and Transference Number Measurements on Polymer Electrolytes," *Solid State Ionics*, **28-30**, 918-922 (1988).

53. P. M. Blonsky, D. F. Shriver, P. Austin, and H. R. Allock, "Complex Formation and Ionic Conductivity of Polyphosphazene Solid Electrolytes," *Solid State Ionics*, **18/19**, 258-264 (1986).

54. P. R. Sorensen and T. Jacobsen, "Conductivity, Charge Transfer and Transport Number - An A.C. Investigation of the Polymer Electrolyte LiSCN-Poly(Ethylene Oxide)," *Electrochim. Acta*, **27**, 161 (1982).

55. A. Bourdiah, F. Dalard, D. Deroo, and M. Armand, "Potentiometric Measurements of Ionic Transport Parameters in Poly(Ethylene Oxide)-LiX Electrolytes," *J. Appl. Electrochem.*, **17**, 625-634 (1987).

56. P. R. Sorensen and T. Jacobsen, "Limiting Currents in the Polymer Electrolyte: $PEO_xLiCF_3SO_3$," *Solid State Ionics*, **9&10**, 1147 (1983).

57. M. Doyle and J. Newman, "Analysis of Transference Number Measurements

Based on the Potentiostatic Polarization of Solid Polymer Electrolytes," *J. Electrochem. Soc.*, **142**, 3465 (1995).

58. R. Pollard and T. Comte, "Determination of Transport Properties for Solid Electrolytes from the Impedance of Thin Layer Cells," *J. Electrochem. Soc.*, **136**, 3734-3748 (1989).

59. Y. Ma, M. Doyle, T. F. Fuller, M. M. Doeff, L. C. De Jonghe, and J. Newman, "The Measurement of a Complete Set of Transport Properties for a Concentrated Solid Polymer Electrolyte Solution," *J. Electrochem. Soc.*, **142**, 1859 (1995).

PART I SOLID STATE RECHARGEABLE SODIUM POLYMER BATTERIES

Chapter 2 Na_xCoO_2/PEO/Na and Na_xCoO_2/PEO/$Na_{15}Pb_4$ Cells

2.1 Introduction

Various transition metal oxides and chalcogenides have been investigated as host materials for lithium intercalation. The most popular of these include lithium titanium disulfide, [1] vanadium oxides ($Li_{1+x}V_3O_8$, V_6O_{13}), [2-6] lithium manganese oxides (Li_xMnO_2, $Li_xMn_2O_4$), [7-12] lithium cobalt and lithium nickel oxides (Li_xCoO_2, Li_xNiO_2, and $Li_xCo_yNi_{1-y}O_2$). [13-17] A comprehensive review on these materials is given by Desilvestro and Haas. [18] Parallel to the investigation of lithium intercalation materials, efforts have also been made in investigating sodium intercalation compounds. Abraham reviewed the development of intercalation materials for rechargeable sodium batteries in 1982. [19] Up to that time most of the attention had been given to layered structures, especially transition metal disulfides. Since then transition metal oxides and three dimensional network structures for sodium intercalation have also been extensively studied. This work has been reviewed by West. [20] Compared to sulfides, transition metal oxides have potentially higher specific energy and also higher energy density because they have lower equivalent weight, smaller volume, and higher electrode potential. [21]

The framework of these intercalation structures is mainly determined by oxygen or sulfur atoms that are nearly close packed. Small lithium ions (r = 0.068 nm) can usually fit into the octahedral interstitial sites and are able to move easily in these spaces. Larger ions such as sodium (r = 0.098 nm) are more sensitive to the size and shape of these sites. Layered structures are considered to be better host materials for sodium

intercalation since the interlayer space can be adapted to accommodate foreign ions quite easily. Typical layered structures of transition metal oxides or chalcogenides consist of sheets of edge-sharing transition metal polyhedra, MO_6. These sheets are kept together by van der Waals forces. The intercalation ions are accommodated between these layers in either octahedral sites, tetrahedral sites, or prismatic sites depending on the oxygen packing sequence. [22]

Among the sodium intercalation materials, sodium cobalt oxides are found to be particularly attractive. [23,24] Sodium cobalt bronzes are layered oxides in which layers are found in the sequence of OMOAOMOA (O = oxygen, M = Co, and A = Na.). Within the composition range $0.5 < x < 1$, up to four phases have been identified in which the sodium coordination is either octahedral or trigonal prismatic, depending on composition (x in Na_xCoO_2) and the method of preparation. In all structures the lattice is built up by sheets of edge-sharing CoO_6 octahedra between which sodium ions are inserted with trigonal prismatic (P) or octahedral (O) environment. The packing also differs in the number of sheets within the unit cell: 2 or 3. The monoclinic distortions of P3 and O3 packing result in P'3 and O'3 structures, respectively. During the electrochemical process the reversible structural transitions O3 $\leftrightarrow$ O'3 $\leftrightarrow$ P'3 occur. The transformations between these phases are kinetically favorable because the transformations predominantly involve only a relative displacement of adjacent cobalt-oxygen planes. Any transformation between the P2 structure and P3, O3, or O'3 structures, however, is energetically unfavorable since such a transformation would involve bond breaking and rotation of cobalt-oxygen octahedra. [23]

The intercalation characteristics of the four types of sodium cobalt oxide have been studied by Shacklette *et al.* [24] These compounds exhibit attractive properties as electroactive materials in ambient temperature secondary cells employing a nonaqueous electrolyte. The O3, O'3, and P3 phases have a reversible capacity of $\Delta x = 0.47$ and an average discharge potential of 2.71 V. These give a theoretical specified energy of 300 Wh/kg based on the weight of fully discharged composition, $NaCoO_2$. Most notably, the P2 phase has a reversible capacity of $\Delta x = 0.6$. The theoretical specific energy of this material can reach as high as 440 Wh/kg, based on a discharged composition of $Na_{0.9}CoO_2$.

The electrode potential of sodium cobalt oxides is lower than 4 V during the entire intercalation range. This implies that these compounds can function with polymer electrolytes since the commonly used electrolytes such as poly(ethylene oxide) are stable within this potential range. The suitability of the P2 phase sodium cobalt oxide in cells utilizing solid polymer electrolyte is investigated in the present work. [25] The commonly used poly(ethylene oxide) (PEO) complexed with sodium trifluoromethanesulfonate ($NaCF_3SO_3$) is employed as the electrolyte. Cells are characterized in terms of charge and discharge characteristics, rate capability, charging efficiency, and cycle life. A sodium alloy ($Na_{15}Pb_4$) is also used as an anode material. [26,27] $Na_{15}Pb_4$, which has a high melting point (375°C), can be used in place of sodium in cells that are operated at close or above the sodium melting temperature.

2.2 Experimental

The sodium cobalt bronze $Na_{0.7}CoO_2$ was prepared in the P2 phase through high temperature reaction of chemicals Na_2O_2 and Co_3O_4. Mixtures of Na_2O_2 and Co_3O_4 powders in the desired ratio were ground and well mixed, and then formed into pellets. The pellets were heated to 750°C under oxygen for 30 hours, and the resulting product was ground into powder of about 1 μm in diameter, as determined by scanning electron microscopy. The product was identified by x-ray diffraction. The density of $Na_{0.7}CoO_2$ was determined by Coning Incorporated, Corning, New York.

Composite electrodes were made by casting mixtures of the electroactive material, Shawinigan carbon black, poly(ethylene oxide), sodium trifluoromethanesulfonate, and brij (a carbon dispersant) in acetonitrile onto Taflon coated glass plates. The mixture without acetonitrile has 30 w/o electroactive material, 20 w/o carbon black, and 48 w/o poly(ethylene oxide) with $NaCF_3SO_3$ in a ratio of 8 ethylene oxide units per sodium, and 2 w/o brij. After air drying, the electrodes were cut to the desired size (3 cm^2 in a circular shape) and weighed, and then dried in vacuum for a week before use. Polymer electrolytes of composition $PEO_8NaCF_3SO_3$ were made in a similar fashion. The electrode and electrolyte membranes were about 40 to 100 μm in thickness.

Sodium, from Alfa, was purified through the following procedure. The metal was melted, filtered through coarse stainless steel wool, and then heated to 400°C with a small amount of titanium sponge. The purified sodium was rolled between sheets of polyethylene to form thin foil electrodes. $Na_{15}Pb_4$ alloy was made by melting sodium

with lead and then was purified as above. The alloy was heated in a stainless steel ring to form flat electrodes for use in cells.

Cathode-limited cells were assembled as shown in Figure 2-1 in a helium-filled glove box with O_2 levels below 1 ppm, and heated to 90°C (for sodium) or 100°C (for sodium/lead alloy) prior to use to render the polymer electrolytes conductive. Galvanostatic charges and discharges were performed at 0.1 to 3.0 mA/cm^2 using a computer controlled PAR 173 or 371 potentiostat/galvanostat and software developed in this laboratory. The current was interrupted periodically (for some experiments) in order to estimate cell open circuit voltages (OCVs).

A four-probe technique developed for solid polymer electrolyte cells [28] was used to evaluate how each component might limit the performance. Sodium foils were used as internal reference electrodes (Figure 2-2), and cells were subjected to galvanostatic charges and discharges as well as sequential bipolar square-wave current pulses.

2.3 Results and Discussion

2.3.1 Charge and Discharge Characteristics of $Na/Na_{0.7}CoO_2$ and $Na_{15}Pb_4/Na_{0.7}CoO_2$ Cells

The open-circuit potential of $Na/P(EO)_8NaCF_3SO_3/Na_{0.7}CoO_2$ cells is approximately 2.8 V (slightly lower when $Na_{15}Pb_4$ anodes are used). The cells are assembled in the halfway discharged state and are charged initially. Figure 2-3 shows a single galvanostatic charge and discharge for the cases with Na and $Na_{15}Pb_4$ anodes, respectively. The extent of intercalation, x in Na_xCoO_2, was calculated based on the

amount of charge passed and corresponds to $\Delta x = 0.55$ to 0.6. An assumption was made that the only charge-transfer process occurring during charge or discharge is electrochemical intercalation or deintercalation. The discharge curves appear quite similar to those obtained for P2 sodium cobalt bronze cells with liquid electrolytes at room temperature; [24] that is, they are quite sloping and show several small steps. Plateaus are typically associated with a two phase region (*i.e.*, a phase transition) and sloping curves with changes of composition of a single phase. However, no evidence for phase change has been found for this material over this range of intercalation; [24] instead the presence of steps in the potential profiles has been attributed to ordering transitions. Although the solid polymer electrolyte cells are operated at higher temperatures (90 to 100°C) than those with liquid electrolytes, the similarities in discharge characteristics strongly suggest the existence of a single phase under these conditions as well. Furthermore, previous structural studies by Delmas *et al.* [23] on the sodium cobalt bronzes indicate that interchange between the P2 and other phases occurs with difficulty and only at temperatures above 700°C.

Figure 2-4 shows one cycle of a $Na_{15}Pb_4/PEO_8NaCF_3SO_3/Na_xCoO_2$ cell that was overcharged (corresponding to the removal of Na to composition $Na_{0.1}CoO_2$). The subsequent discharge showed that this process was irreversible. It was possible to cycle this cell, but the discharge capacity was decreased. In all likelihood, it is not possible to remove sodium ions in the P2 sodium cobalt bronze beyond the composition of $Na_{0.3}CoO_2$ without disrupting the structure. Therefore, in order to obtain good cycling results, some care has to be taken in choosing the upper potential limit. If the OCV of the cell was allowed to reach 4.0 V, overextraction of the sodium cobalt bronze occurred,

causing reduced performance. Where fairly high current densities (0.5 mA/cm^2 or more) were used to charge the cell, the operating potential, however, could reach 4.0 V without adverse effect, because the open-circuit potential was actually somewhat lower. At low current densities, such as for the charge shown in Figure 2-4, there is little overpotential, and the operating potential is close to the open-circuit value. Thus, a lower potential limit is required at low current densities. Most cells were charged at 0.5 mA/cm^2 or higher, however, without any evidence of deleterious overcharge.

Figure 2-5 shows discharge curves at different current densities up to 2.5 mA/cm^2 for Na/$PEO_8NaCF_3SO_3$/$Na_{0.7}CoO_2$ cells. The rate capability of this system is clearly quite high. The entire capacity of the cell can be discharged as well as charged in under an hour at 0.5 mA/cm^2, and 2.5 mA/cm^2 can be sustained for several minutes, corresponding to a 25% depth of discharge. Similar behavior is seen when sodium/lead alloy anodes are used.

2.3.2 Cycling Results

Cycling results show that the P2 sodium cobalt bronze is very reversible when used in sodium or sodium/lead alloy SPE cells. Figure 2-6 shows cell capacity as a function of cycle number for an example cell discharged and charged at 0.5 mA/cm^2 continuously two hundred times. A rapid decrease in capacity is seen initially, but then the utilization levels out at more than 60% thereafter (the initial capacity of this cell corresponded to $\Delta x = 0.55$). Capacity fading is typical of all of the cells that were cycled under these conditions. Some capacity decrease may be attributed to mass transfer

effects; when cells were allowed to rest between cycles for several hours or discharged at lower current densities, the capacity of the subsequent cycle increased (but not to the level seen initially). As will be described in chapter 5, a large concentration profile is built up in the electrolyte upon passing a large current due to the small sodium-ion transference number for highly concentrated electrolyte solutions such as $PEO_8NaCF_3SO_3$. The salt solubility limit can be exceeded in the region near the electrodes at high current densities because of this. For cells that use thinner electrolyte and are charged or discharged at lower current densities like the cells used in the present study, mass transfer polarization is much less severe, but the electrolyte structure may not recover completely to its initial state due to the large composition change, perhaps forming salt complexes that do not easily relax back to the initial state. Mass transfer polarization could become severe upon continuous cycling because of the electrolyte modification. The strong operating-history dependence of the electrolyte may be a reflection of this point. It is found that the mass-transport limiting process (manifested as a rapid change in cell potential) occurs much earlier on the subsequent cycles than the initial cycle when pass a current through a cell $Na/PEO_8NaCF_3SO_3/Na$. (Detailed description of this can be found in chapter 5.) The transition time (time to reach the rapid potential change) also varies depending on the relaxation periods between cycles; a smaller transition time is obtained when a shorter rest period is used. Upon continuous cycling (allowing one hour relaxation period in between), the transition-time decreased and reached a stable value.

Figure 2-7 shows the charge efficiency for the same cell, defined as the ratio of coulombs passed during discharge to that passed during charge. For most cycles this is

close to one, but occasional overcharges are necessary to compensate for dendritic shorting during the charge process. (This shorting is manifested as a potential instability during charge.) Usually, overcharging below 4.0 V corrects the capacity loss associated with this phenomenon. However, after cycle 110 for this example, there was a dramatic decrease in capacity from which it was not possible to recover in spite of overcharging.

Besides the obvious decrease in capacity, there is a change in the shape of the discharge curve as cycling progresses (Figure 2-8). In particular, a long plateau at about 2.2 to 2.3 V appears as early as the 50th cycle. To test the hypothesis that structural changes in the cathode cause this modification in the potential profile, x-ray diffraction experiments were performed on cathodes that had been cycled to failure and compared to those obtained on fresh cathodes, but no differences were seen. While x-ray diffraction may be able to detect gross structural modifications, it is not certain whether subtle changes (such as increases in the number of defect sites) would be discernible. X-ray line broadening often is associated with a decrease in crystallinity or decrease in crystallite size, but this broadening was not detected in these experiments. Another possible explanation is that the sodium cobalt oxide reacts very slowly (perhaps with the polymer electrolyte) to give a product that is undetectable in the x-ray experiment but that has some (diminished) electrochemical activity.

Inadvertent rises in temperature occurred during some experiments, causing the sodium anodes to melt (the melting point of Na is 97°C). Although this sometimes caused shorting, there seemed to be no other deleterious effects. Cells that had completely shorted (potentials read zero) could often be rendered functional again simply

by removing excess sodium, lowering the temperature, and recharging. Complete recovery often occurred after several cycles.

Dendrite formation generally occurs less frequently in cells with sodium/lead anodes, and overcharging is not required as often as with sodium. Another advantage to the sodium/lead anode is its higher melting point, allowing a greater temperature range of operation. Two hundred medium to shallow depth cycles ($\Delta x = 0.1$ to 0.4 in Na_xCoO_2) have been obtained for a cell with a $Na_{15}Pb_4$ anode. (Figures 2-9 and 2-10). This is the same cell that was overcharged to composition $Na_{0.1}CoO_2$ (Figure 2-4), and the overcharge had a deleterious effect upon cycling (compare to Figure 2-6). The effect of various potential limits on performance is also shown. Whereas overcharging above 4.0 V tends to cause a decrease in capacity, cells are relatively impervious to overdischarge, and can withstand low potential cutoffs.

Cells with two sodium cobalt bronze electrodes of matched capacity and a polymer electrolyte separator were also assembled and tested. Initially, the potential was 0, but rose to 2.0 V upon charge, or dropped to -2.0 V upon discharge. This corresponds to a total range of intercalation equivalent to $\Delta x = 0.4$. Because $Na_{0.7}CoO_2$ is approximately halfway discharged, one electrode acts as a sodium ion acceptor, and the other as a sodium ion donor upon passage of current.

Figure 2-11 shows the results of three hundred cycles at 0.5 mA/cm^2. For this example, capacity fading is seen which has a similar pattern as the cell shown in Figure 2-6. This indicates that sodium/PEO interface is not a major factor causing capacity fading. The capacity decrease in this cell may be due to the mass-transfer effect as discussed earlier, or due to chemical or structural changes in the sodium cobalt bronze or

modifications in the structure of the composite positive electrode. AC impedance studies [29] on cycled intercalation electrodes show an increase in resistance that has been attributed to disconnection processes rather than structural changes in the electroactive material. The volume expansion and contraction associated with the deintercalation and intercalation of ions may cause exfoliation and cracking of the electroactive particles and concomitant disruption of the paths for electronic and/or ionic conductivity in the composite electrode, leading to lowered capacity and increased resistance.

While dendritic shorting may cause premature failure, the sodium electrode or sodium/PEO interface does not seem to be a major cause of capacity fading. (Further evidence for this is presented in the next section.) While more study is needed to determine how much each of the factors discussed above contributes to cycle life, it should be possible to improve performance simply based upon the information already obtained. Changes in the electrolyte may improve conductivity, sodium ion transference number, and salt diffusion coefficient or minimize reaction with the sodium cobalt bronze. Modifications in the fabrication of the composite electrodes (varying the amount or type of electronically conducting additive, loading levels, etc.) or in the way the cell is assembled may dramatically improve cycle life particularly if disconnection or loss of interfacial contact is occurring.

2.3.3 Four Probe DC Experiments

To determine how the various components in the $Na/PEO_8NaCF_3SO_3/Na_xCoO_2$ system contribute to performance, cells with two sodium foil reference electrodes were

constructed and tested. These are referred to the sodium anode. A polymer electrolyte layer separates each electrode for a total of three in the cell (Figure 2-2). [28] A simple arithmetic procedure then allows calculation of the overpotentials due to each component (*i.e.*, the cathode, the polymer electrolyte, and the Na/PEO interface) during galvanostatic charge and discharge or pulsing. Because it is performed *in situ,* this experiment can provide much information about processes occurring during conditions of actual cell use.

Sequential bipolar square-wave current pulses were applied to the four-probe cell, and the response of the overall cell potential and the reference electrodes were recorded. This allows determination of the contribution of the various components to the resistance of the cell with a minimum of disturbance to the system. The pulse time was chosen to minimize complications due to mass transport and double-layer charging. This procedure was done by applying single pulses of varying times to the cell and observing the potential response. On application of a current pulse, the interfacial polarization rises rapidly (within a few milliseconds or less) due to double-layer charging and reaches a plateau. After a much longer period of time (many seconds), the interfacial polarization increases greatly due to mass-transfer effects. A pulse width of about 50 ms allowed the potential response to reach the plateau after double-layer charging but before mass-transfer polarization. Subtraction of the response of reference 1 (the electrode closest to the negative) from that of reference 2 gives the resistance due to the polymer electrolyte (ohmic response). The reference 1 response less the ohmic response gives the resistance due to Na and the Na/PEO interface, and the overall cell overpotential less the response of reference 2 and the ohmic response gives the resistance due to the cathode. Results of this experiment performed after the second cell discharge are shown in Figure 2-12. By

far the major contributor to overall cell resistance under these conditions is the cathode (157.5 $\Omega \cdot cm^2$). The polymer electrolyte (6.0 $\Omega \cdot cm^2$) and the sodium and sodium/PEO interface (12.6 $\Omega \cdot cm^2$) make only minor contributions to cell resistance.

The four-probe method was also be applied to cells undergoing galvanostatic charge and discharge at 0.3 mA/cm^2. The sodium/PEO interface resistance is low throughout the course of the experiment. There is, however, an initial increase in the resistance of the PEO electrolyte as charging or discharging progresses (Figure 2-13), which then levels to a constant value, indicating the transition to steady state due to the nonunity sodium-ion transference number. (The detailed discussion of this matter is given in chapter 4.)

Figure 2-14 shows the change in resistance of the various cell components as a function of the cycle number, determined by pulsing after charge or discharge. The electrolyte and sodium/PEO interface contribute only slightly to the overall resistance increase seen in the cell in the first few cycles. The cell impedance increase is dominated by the cathode. Previous AC impedance results [30] on Na/PEO_8NaClO_4 systems, in contrast, suggest that corrosion at the sodium/electrolyte interface is the major factor contributing to increasing cell resistance upon cycling. Corrosion processes, however, are expected to be highly dependent upon the purity of the sodium and dryness of components. Results of AC experiments can also be quite different from those obtained during DC polarization of cells. The high interfacial impedance that were seen in the previous study always decreased upon passage of a DC current, suggesting that the corrosion layer breaks down upon cell polarization. The four probe experiments, cycling results on Na and $Na_{15}Pb_4/PEO_8NaCF_3SO_3/Na_xCoO_2$ cells, and cycling results on

positive/positive cells in this study all indicate that the sodium/PEO interface is stable in these cells and is not the limiting factor to cycle life.

Figure 2-14 also shows that the cathode resistance is consistently higher after discharge than after charge. This indicates that the conductivity of Na_xCoO_2 increases with decreasing x. For the sodium stoichiometric phase $NaCoO_2$, the t_{2g} band is fully filled, resulting in a poor conductivity at this state. When sodium ions are removed from the intersheet space, an equivalent number of cobalt ions are tetravalent; correspondingly holes are formed in the band. Smaller x corresponds to a larger amount of holes in the band and greater electronic conductivity. One other contribution to the higher resistance after discharge may come from a higher electrode resistance due to Na_xCoO_2 contraction upon intercalation, which may lead to disconnection for some particles with others.

2.3.4 Power and Energy Density Calculations

High theoretical energy densities of 1600 and 1470 Wh/l are calculated for the P2 sodium cobalt bronze with sodium and sodium/lead alloy anodes respectively, based upon the discharge characteristics and measured density of 4.81 g/cm^3. The theoretical specific energy of 440 Wh/kg for Na and 350 Wh/kg for $Na_{15}Pb_4$ are also very attractive. In cells with liquid electrolytes, it is usually possible to attain practical energies of only about one-fourth that of the theoretical. One advantage to using solid state components, however, is that light weight ultra thin current collectors may be used in order to maximize practical energy densities, because there is no danger of electrolyte leakage. To illustrate this point, practical energy densities are estimated and given in Figure 2-15,

assuming 5 μm metallized plastic current collectors with sodium cobalt bronze electrodes, 10 μm thick polymer electrolyte separators, and a two-fold excess of sodium are used. These calculations show that up to 150 Wh/kg for this configuration is attainable, depending upon the loading level and capacity of the positive electrode. It may be possible to increase this further by increasing the loading level in the cathode, but this has not yet been tested here.

Practical power densities based upon the configuration described above and the data shown in Figure 2-5 are presented in Figure 2-16. At 0.5 mA/cm^2, the entire capacity of the positive electrode can be discharged in less than an hour (this time varies somewhat depending upon the cell capacity). This corresponds to a practical power density of 335 W/l for continuous operation. Up to 2.7 kW/l is attainable for short periods of time (several minutes) for a depth of discharge of 25% of the available capacity in the positive electrode.

Because less capacity can be discharged at higher current levels, cells designed for high rate and thus high power density applications should use thinner electrodes (*i.e.*, fewer coulombs per unit area in the cathode). If energy density is the primary consideration, cells with larger capacities should be built. The Ragone plot presented in Figure 2-17 indicates the relationship between energy and power densities. For some applications such as electric vehicles, both high energy densities and high power densities for at least short periods of time are important attributes. It appears that the $Na_xCoO_2/PEO_8NaCF_3SO_3/Na$ system has the potential for fulfilling these requirements.

2.3.5 Comparison with Other Sodium Systems

As with lithium batteries, various transition metal oxides, especially the first row transition metal oxides, have been studied for sodium intercalation. These materials, besides sodium cobalt oxides (Na_xCoO_2), include vanadium oxides ($Na_xV_2O_5$, [31-34] $Na_{1+x}V_3O_8$, [43,32] $Na_xV_6O_{13}$, [35]), manganese oxides (Na_xMnO_2), [36-40] molybdenum oxide ($Na_xMo_2O_4$), [41] and amorphous MoS_3, [42] and also ternary host structures ($Na_xKCr_3O_8$ and $Na_xKV_3O_8$). [43,44] The performance of these compounds is briefly reviewed to compare with the sodium cobalt oxide results.

α-phase V_2O_5, a layered structure, has been studied for sodium cells using PEO-$NaClO_4$ polymer electrolytes at 80°C. [31,32] This compound undergoes two sequential irreversible phase transformations. With the final phase (unknown structure), 1.7 sodium atoms can be intercalated and deintercalated quite reversibly, while the other 0.3 sodium atoms strongly bond to the lattice. The new phase intercalates sodium at higher potential, indicating that the new structure has higher affinity to the intercalation ions. The theoretical specific energy and energy density of the system calculated from the second discharge are 430 Wh/kg and 1040 Wh/l, respectively. This cell was cycled at 0.075 mA/cm^2 (C/8h rate), and 100 cycles had been achieved before the electrode capacity dropped below 40% of the electrode capacity (of the second discharge).

The three-dimensional structure β-$Na_xV_2O_5$ has been tested in sodium cells using PEO-$NaClO_4$ polymer electrolytes at 80°C. [31,32] This material was able to intercalate sodium electrochemically from $x = 0.25$ to $x = 1.6$, but the structure was believed to break down during the process, probably to an amorphous state. In spite of the phase transformation, 30 cycles at 0.075 mA/cm^2 (C/25h) were obtained with a capacity larger

than 1 sodium per V_2O_5 unit. The stoichiometric energy density calculated from the first discharge is 245 Wh/kg. In addition to high temperature synthesis, β-$Na_{0.33}V_2O_5$ has been synthesized by a sol-gel process and tested in a liquid cell at room temperature. [33,34] The structure of this material was maintained during cycling, manifested by the similar shape of the discharge curves. A total of one sodium per mole of bronze can be intercalated into the structure between 3.4 V and 2 V at 0.1 mA/cm^2, corresponding to an electrode capacity of 100 mAh/g. This cell was cycled at 0.03 mA/cm^2 in the potential range of 3.6 to 2.4 V; the capacity was 85 mAh/g for the initial discharge and decreased to 50 mAh/g after 30 cycles.

$Na_{1+x}V_3O_8$ is a layered structure made of edge sharing VO_6 octahedra sheets. One sodium ion per formula unit must be present to stabilize the structure. This structure was studied in a polymer electrolyte cell and was found to be able to intercalate two extra sodium atoms per formula, [31,32] giving a stoichiometric energy density of 340 Wh/kg. One cell using $Na_{1+x}V_3O_8$ and PEO-$NaClO_4$ polymer electrolyte was cycled at 0.05 mA/cm^2; the cell capacity decreased during the first 40 cycles but gradually increased in later cycles to almost its original capacity at about 80 cycles before it quickly dropped to a very low value. Another cell which was cycled at 0.1 mA/cm^2, however, showed much less utilization and a decreasing capacity with cycling. No phase transformation upon cycling was detected with this material.

A three-dimensional network structure V_6O_{13} was tested in polymer electrolyte (PEO-$NaCF_3SO_3$) sodium cells. [35] This material intercalates only a limited amount of sodium and has rather poor retention of capacity.

Sodium manganese oxide bronzes have been extensively studied. Several phases were obtained with sodium contents x = 0, 0.4, 0.44, 0.7, and 1 in Na_xMnO_2. [36] The two structures with lower sodium content, $Na_{0.4}MnO_2$ and $Na_{0.44}MnO_2$, are three-dimensional structures composed of edge-sharing and also corner-sharing MnO_6 octahedra. The other two materials with higher sodium contents are layered structures made of edge-sharing MnO_6 octahedra. $Na_{0.7}MnO_2$ has P2 structure, an isostructure of the P2 phase $Na_{0.7}CoO_2$. Two different structures, α- and β- phases are identified with $NaMnO_2$, where α has a O'3 structure and β is composed of a double stack of edge-sharing MnO_6 octahedra sheets. $Na_{0.4}MnO_2$ and $Na_{0.7}MnO_2$ are able to intercalate sodium reversibly from x = 0.3 to x = 0.58 and from x = 0.45 to x = 0.85, respectively, and the two $NaMnO_2$ phases intercalate only limited amounts of sodium. [36] Interestingly, $Na_{0.44}MnO_2$ has been shown to have the best performance among these materials. [37,38] It was thought this material would not undergo reversible intercalation because sodium hopping was considered difficult within this structure. To the contrary, $Na_{0.44}MnO_2$ is able to intercalate sodium reversibly from x = 0.2 to x = 0.75, the largest range among these manganese oxides, at a current density of 0.1 mA/cm^2 at 85°C, corresponding a stoichiometric energy density of 440 Wh/kg. More than 60 cycles were obtained before the capacity dropped to 40% of its initial value.

Besides the thermodynamically stable phases, a three-dimensional spinel structure, prepared by the "chimie douce" method at room temperature, has been studied for sodium intercalation. [39] This structure undergoes an immediate phase transition to an unknown structure upon sodium intercalation. But more than 0.6 sodium ions per

formula unit can be intercalated into the structure in spite of the phase transition. The reversibility of this system, however, was not satisfactory. [40]

Molybdenum oxide, $Na_xMo_2O_4$, was tested in liquid electrolyte cells and was able to intercalate sodium in the composition range of $0.55 < x < 1.9$. [41] The parent oxide is a layered structure made of MoO_6 octahedra, but molybdenum atoms are off the centers of their coordination, forming Mo double-chains. Upon electrochemical intercalation, a series of five phase transitions was identified within the above composition range. The stoichiometric energy density of this material is 270 Wh/kg, with an average cell potential of 2 V. Cycling data on this material are not available.

Amorphous molybdenum sulfide, MoS_3, was shown to be able to intercalate 1.4 sodium ions per formula initially in a polymer electrolyte cell, but the capacity decreased to 0.4 sodium ions in the following cycle and then dropped to zero after only 30 cycles. [42]

Some ternary host materials such as KV_3O_8 and KCr_3O_8 with layered structures have also been investigated for sodium intercalation. KV_3O_8 was able to intercalate 2 sodium atoms per formula unit at 80°C, [43] giving a stoichiometric energy density of 310 Wh/kg. It became amorphous during cycling but was able to be cycled 20 times with high electrode utilization before capacity rapidly dropped. [20] KCr_3O_8 was able to intercalate only 1 sodium (175 Wh/kg) and had poor reversibility. [44]

As indicated above, the P2 phase sodium cobalt oxide exhibited the best performance reported so far for sodium intercalation. Some general conclusions may be drawn from the systems that have been studied. Layered structures are attractive for sodium intercalation since the larger size of sodium (compared to lithium) can be easily accommodated between the layers by the inter-space change without strongly perturbing

the host structure. Particularly, structures that are relatively stable upon sodium intercalation without phase transition, such as the P2 phase Na_xCoO_2, are more attractive for their better reversibility. Problems associated with three-dimensional network structures for sodium intercalation may be minimized by choosing more rigid structures with large tunnels for guest species such as the orthorhombic $Na_{0.44}MnO_2$, so that the host structures do not easily transform. Furthermore, the performance of the intercalation materials is sensitive to the synthesis methods, indicating that the intercalation process is influenced by the fine structures obtained with different fabrication routes. These fine structures may include anisotropy of materials [33,34] and lattice defects, [45,46] which would affect the electronic conductivity of the material and also the diffusion coefficient of the guest species.

Limited by the scope of the present work, lithium intercalation systems have not been discussed. In general, intercalation host materials tend to take in less sodium ions than lithium due to the larger size of the former. But with proper choice of the host material this difference can be reduced. The rate capability of the sodium system is comparable to lithium systems. Diffusion of sodium ion in structures such as the P2 phase Na_xCoO_2 ($D = 10^{-8}$ cm^2/s [45]) is not a limiting factor with fine particle sizes (*e.g.*, 1 μ). The major disadvantage of sodium cells is their lower theoretical specific energy due to their lower cell potential and lower charge capacity density. On the other hand, highly oxidizing materials such as Li_xCoO_2 (4.7 V at $x = 0.07$) have the disadvantage of decomposing the electrolyte or corroding the underlying metal support. These materials, therefore, can not be used with polymer electrolytes that are usually not stable above 4V.

47

2.4 Conclusions

$Na_xCoO_2/PEO_8NaCF_3SO_3/Na$ and $Na_{15}Pb_4$ cells have been evaluated in terms of discharge characteristics, rate capability, cycle life, and energy and power densities. The P2 phase Na_xCoO_2 can reversibly intercalate sodium in the range of $x = 0.3$ to 0.9, giving a theoretical specific energy of 440 Wh/kg and energy density of 1600 Wh/l. One hundred cycles to 60% depth of discharge have been obtained at 0.5 mA/cm^2 and two hundred shallower cycles at the same rate. Experiments in which positive/positive cells were cycled suggest that the Na/PEO interface is not the limiting factor to cell cycle life, but x-ray diffraction experiments failed to reveal any structural changes in the sodium cobalt bronze itself. Four-probe DC experiments also show that the Na/PEO interface is stable and makes only minor contributions to the cell resistance. Mass transfer polarization, disconnection of particles in the cathode, and chemical or structural changes in the sodium cobalt bronze are suggested as factors contributing to eventual cell failure. In terms of cycle life, theoretical energy density, and rate capability, these are the best results obtained on a sodium/polymer electrolyte system to date. Furthermore, energy and power density calculations show that Na_xCoO_2/PEO/Na batteries are promising and may meet the requirements for electric vehicle use. The low cost of sodium relative to lithium makes sodium polymer batteries an attractive alternative for these and other applications.

Chapter 3 $Na_{0.7}CoO_2$ Composite Electrodes

3.1 Introduction

The composite electrodes used in the present study contain the electroactive $Na_{0.7}CoO_2$ particles, electronic conducting carbon black, and ionic conductive polymer phase. The advantage of using composite electrodes is that a greater rate capability can be achieved because they provide greater electrode/electrolyte interfacial area and also have improved electronic conductivity contributed by the highly conductive carbons. The draw back of a composite electrode configuration is that the energy density is reduced by the nonelectroactive filling materials. Therefore, properly choosing the fraction of electronic conductive phase and ionically conductive polymer electrolyte phase is important. The electronic conductivity of various transition metal oxides differs greatly for different materials. For example, $Na_{0.7}CoO_2$ has a much higher electronic conductivity than $Na_{0.7}MnO_2$ (10^2 to10^3 S/cm *vs.* 10^{-5} S/cm at room temperature [46,48]) even though they have the same P2 phase structure. Furthermore, $Na_{0.7}CoO_2$ has metallic conduction characteristics, the conductivity of which slightly decreases with increasing temperature. In contrast, the conductivity of $Na_{0.7}MnO_2$ increases with increasing temperature, a typical semiconductor behavior. Five to twenty percent of carbon black are reported in the composite electrodes in the literature, [2,3,11,31,43] but there has been no report on how carbon content affects the electrode performance. Considering the good electronic conductivity of $Na_{0.7}CoO_2$, the necessity of adding carbon in the composite

electrodes is investigated in the present study. This is done by determining the effect of the carbon additive on electrode conductivity and also on cell performance.

3.2 Experimental

The P2 phase sodium cobalt bronze $Na_{0.7}CoO_2$ was prepared by glycine nitrate process. [49] A mixture of sodium nitrate, cobalt nitrate, and glycine in the desired stoichiometric ratio in distilled water was heated to 180°C in a stainless steel container that was covered by a fine stainless steel mesh. A dramatic combustion of the chemicals occurred when the solution dried, resulting in sodium cobalt oxide. The powders then were heated to 750°C for 10 hours to complete the reaction and also convert the material to the P2 phase. The particles were very fine in size, about 1 μm in diameter, as determined by scanning electron microscopy.

Sodium cobalt oxide composite cathodes were made by mixing the electroactive material, carbon black, poly(ethylene oxide) and sodium trifluoromethanesulfonate in the ratio of 20 ethylene oxide units per sodium, and a carbon dispersant (brij) in acetonitrile and then cast into free standing films as described in chapter 2. Two series of electrodes were made for conductivity measurements, one set has 30 w/o of $Na_{0.7}CoO_2$ and 0 to 20 w/o of carbon black, and the other has 50 w/o of $Na_{0.7}CoO_2$ and 0 to 20 w/o of carbon black, but the electrode films with 50 w/o $Na_{0.7}CoO_2$ and 20 w/o carbon could not be successfully made without cracking. The conductivity of these electrodes were measured to assess the effect of carbon black.

Electrodes were also made and tested in $Na/PEO_{20}NaCF_3SO_3/Na_xCoO_2$ cells to determine the effect of carbons on cell performance. Two sets of electrodes are designed to have the same total volume fraction (30 v/o) of solid phases, but one with 10 v/o (11 w/o) of carbon and the other without. Another electrode that has a greater volume fraction (40 v/o or 74 w/o) of $Na_{0.7}CoO_2$ but no carbon was also made and tested to probe the carbon effect further.

Sodium (Alfa products) was purified prior to use in cells using the method described previously in chapter 2. The metal was melted, filtered through coarse stainless steel wool, and then heated to 400°C with small amounts of titanium sponge. The purified sodium was rolled between sheets of polyethylene to form thin foil electrodes.

Electrode conductivity measurements were done in air at room temperature. Electrodes were 1 cm^2 in area and 60 μm to 170 μm in thickness. The electrode films were placed between two platinum plates and connected to the PAR 371 potentiostat/galvanostat and a voltmeter. The potential drop was monitored when current (5 mA and 10 mA) was passed to the electrodes. The conductivity of the electrode was calculated from the ohmic resistance (the ratio of the potential drop over the current) and the film dimension.

The conductivity of the pure $Na_{0.7}CoO_2$ was also measured from a $Na_{0.7}CoO_2$ pellet. The pellet was made by pressing the powders into a 0.5 in. (1.27 cm) diameter die with 350 MPa load and then put into a hydrostatic press filled with oil that applied 140 MPa pressure to the sample. The resulting disk was 86% dense, calculated from the theoretical density of the material.

Electrochemical cells were assembled in a helium-filled glove box with oxygen level below 1 ppm, and tested at 85°C. Galvanostatic charges and discharges were performed on the $Na/PEO_{20}NaCF_3SO_3/Na_{0.7}CoO_2$ cell using a computer controlled PAR 371 potentiostat/galvanostat.

3.3 Conductivity of the $Na_{0.7}CoO_2$ Composite Electrodes

The electronic conductivity of the composite $Na_{0.7}CoO_2$ electrodes as a function of volume fraction of the carbon is shown in Figure 3-1 (a). The conductivity increases dramatically when a small amount of carbon is added to these electrodes, and then increases less significantly when more carbon is added. 10 v/o of carbon can effectively increase the electrode conductivity from 10^{-7} to 10^{-1} S/cm. The two sets of electrodes that have 30 w/o (9.3 v/o) and 50 w/o (19.3 v/o) of $Na_{0.7}CoO_2$ show very similar electronic conductivity values at the same carbon content, indicating that the electrode conductivity is dominated by the volume fraction of carbon. This effect can be further seen in Figure 3-1 (b). The volume fractions of the phases in the composite electrodes are calculated from the densities of each component, where the density of the polymer phase is measured with the method that will be described in the Experimental section in Chapter 4. These calculated values could be larger than the actual volume fractions since the electrodes could contain small voids (though not visible). Nevertheless, the relative effect of the carbon additive and $Na_{0.7}CoO_2$ on the electrode conductivity would not be affected by this.

The electronic conductivity of the pure $Na_{0.7}CoO_2$ pellet (86% volume) made from hydrostatic compression is $8.7x10^{-4}$ S/cm. It is higher than the two more porous electrodes that contain 9.3 v/o $Na_{0.7}CoO_2$ and 90.7 v/o polymer, or 19.3 v/o $Na_{0.7}CoO2$ and 80.7 v/o polymer, but is much less than the values from electrodes with some carbon black additive. Also, this conductivity value is considerably lower than the one reported for $Na_{0.7}CoO_2$ in the literature, [48] in which the sample was sintered at high temperature. The difference indicates that the interfacial resistance between the $Na_{0.7}CoO_2$ particles is high. Though the synthesis condition of $Na_{0.7}CoO_2$ powders could contribute some to the conductivity difference, the interfacial impedance likely dominates. It is then interesting to note that there is something special about the carbon additive. These extremely fine powders seem to have better connections to each other and also to $Na_{0.7}CoO_2$ particles, making the interfacial resistance much less of a problem.

3.4 Charge and Discharge Characteristics

A cell that utilizes an electrode of 10 v/o (11 w/o) of carbon black and 20 v/o (48 w/o) of $Na_{0.7}CoO_2$ was assembled and tested. The cell was first charged to 3.7 V and then discharged to 1.7 V as shown in Figure 3-2. The characteristics of the curves are very similar to the charge and discharge curves that were observed with the cells in chapter 2, for which the electrodes have 16 v/o (20 w/o) of carbon black and 11.5 v/o (30 w/o) of $Na_{0.7}CoO_2$. The separation between the charge curve and discharge curve is very small, indicating a fairly small overpotential across the cell. This cell has been cycled and discharged at various current densities (Figure 3-3). A good rate capability similar to

that of the cell in Figure 2-5 is observed, although less electrode capacity is obtained from this cell. The difference in capacity utilization may be attributed mainly to the different $Na_{0.7}CoO_2$ synthesis methods (a high temperature reaction was used for the cell shown in Figure 2-5, and the glycine nitrate process was used for the present). Operating at lower temperature (85°C *vs.* 90°C) and no current interruption during discharges, and thus less mass transport relaxation time, also contribute to some of the utilization differences.

The cell with the electrode that contains the same volume fraction of solid phase (30 v/o of $Na_{0.7}CoO_2$ but no carbon additive) exhibits quite different charge and discharge characteristics (Figure 3-4). The separation between the charge and discharge curves is much greater, although the cell has a similar cell configuration as the other (the electrolyte and electrode thickness are shown in the figures) and was tested at the same current density (0.1 mA/cm^2). This indicates a greater ohmic drop across the cell that resulted mainly from the cathode resistance. Both the charge and discharge curve do not have distinctive plateau characteristics but rather straight lines, resembling the discharge characteristics at higher discharge current for the cell shown in Figure 3-3, where larger ohmic drop was experienced. The capacity utilization of the electrode is only about 40% of the previous cell at the same discharge current density level. This cell was also cycled at 0.1 mA/cm^2, but the cell capacity dropped dramatically in the subsequent cycles. Clearly, the larger overpotential and lower electrode utilization are caused by the lower electronic conductivity of the electrode. The shorter cell cycle life may be attributed to particle isolation caused by Na_xCoO_2 volume changes during intercalation/deintercalation, and hence a reduced electrode capacity. The better

performance for the cell shown in Figures 3-2 and 3-3 indicates that fine carbon black particles not only improve the electrode conductivity, but also likely help to keep $Na_{0.7}CoO_2$ particles connected during intercalation/deintercalation processes. During these processes, $Na_{0.7}CoO_2$ particles may disconnect from each from each other and from carbon particles, as well, due to the volume changes.

The first charge and discharge curves of the electrode that has a bigger solid volume fraction (40 v/o of $Na_{0.7}CoO_2$, but no carbon additive) are shown in Figure 3-5 (the electrode and electrolyte thickness are also indicated in the figure). The utilization of this electrode is less than the electrode that has 20 v/o of $Na_{0.7}CoO_2$ and 10 v/o of carbon (Figure 3-2), but is much better than the cell that has 30 v/o of $Na_{0.7}CoO_2$ and no carbon additive (Figure 3-4). Improved electrode conductivity by adding more $Na_{0.7}CoO_2$ phase is likely responsible for the better electrode performance. But this cell again does not cycle well. This may also be attributed to particle isolation caused by Na_xCoO_2 volume changes upon intercalation and deintercalation.

3.5 Conclusions

The effect of carbon black additive on the composite $Na_{0.7}CoO_2$ electrodes is evaluated in terms of electronic conductivity and cell performance. The electronic conductivity of the electrodes is dominated by the volume fraction of carbon, increasing as carbon content increases. Adding 10 v/o of carbon can effectively raise the electrode conductivity from about $1x10^{-7}$ S/cm to $1x10^{-1}$ S/cm. The conductivity of the $Na_{0.7}CoO_2$ pellet made from hydrostatic compression is much less than the reported value for a

dense sintered material, indicating that a large interfacial impedance exist between $Na_{0.7}CoO_2$ particles. Adding carbon particles can greatly reduce this impedance. Three electrodes with different $Na_{0.7}CoO_2$ content and different carbon content have been charged, discharged, and cycled. The electrode with 10 v/o of carbon exhibits significantly better performance in terms of electrode utilization and cycle life than the ones with the same or larger volume fraction of solid phase ($Na_{0.7}CoO_2$) but no carbon additive. The difference may be explained by the better connection between $Na_{0.7}CoO_2$ particles established by the very fine carbon black additive.

References for Part I

1. M. Gauthier, D. Fauteux, G. Vassort, A. Belanger, M. Duval, P. Ricoux, J.-M. Chabagno, D. Muller, P. Rigaud, M. B. Armand, and D. Deroo, "Assessment of Polymer-Electrolyte Batteries for EV and Ambient Temperature Applications," *J. Electrochem. Soc.*, **132**, 1333-1340 (1985).

2. F. Bonino, M. Ottaviani, and B. Scrosati, "A Polymeric Electrolyte Rechargeable Lithium Battery," *J. Electrochem. Soc.*, **135**, 12-15 (1988).

3. C. Lampe-Onnerud, J. O. Thomas, M. Hardgrave, and S. Yde-Anderson, "The Performance of Single-Phase V_6O_{13} in the Lithium Polymer Electrolyte Battery," *J. Electrochem. Soc.*, **142**, 3648-3651 (1995).

4. K. West, B. Zachau-Christiansen, M. J. L. Ostergard, and T. Jacobsen, "Vanadium Oxides as Electrode Materials for Rechargeable Lithium Cells," *J. Power Sources*, **20**, 165-172 (1987).

5. A. Hooper and J. M. North, "The Fabrication and Performance of All Solid State Polymer-Based Rechargeable Lithium Cells," *Solid State Ionics*, **9&10**, 1161-1166 (1983).

6. M. Z. A. Munshi and B. B. Owens, "Performance of Polymer Electrolyte Cells at +25 to +100°C," *Solid State Ionics*, **26**, 41-46 (1988).

7. J. M. Tarascon, E. Wang, F. K. Shokoohi, W. R. McKinnon, and S. Colson, "The Spinel Phase of $LiMn_2O_4$ as a Cathode in Secondary Lithium Cells," *J. Electrochem. Soc.*, **138**, 2859 (1991).

8. M. M. Thackeray, A. de Kock, M. H. Rossouw, D. Liles, R. Bittihn, and D. Hoge, "Spinel Electrodes from the Li-Mn-O System for Rechargeable Lithium Battery Applications," *J. Electrochem. Soc.*, **139**, 363 (1992).

9. J. M. Tarascon and D Guyomard, "Li Metal-Free Rechargeable Batteries Bassed on $Li_{1+x}Mn_2O_4$ Cathodes ($0 \leq x \leq 1$) and Carbon Anodes," *J. Electrochem. Soc.*, **138**, 2864 (1991).

10. D. Guyomard and J. M. Tarascon, "Li Metal-Free Rechargeable $LiMn_2O_4$/Carbon Cells: Their Understanding and Optimization," *J. Electrochem. Soc.*, **139**-948 (1992).

11. Q. Xu and G. Wan, "Rechargeable $Li/LiMn_2O_4$ Batteries with a Polymeric Solid Electrolyte," *J. Power Sources*, **41**, 315-320 (1993).

12. M. M. Tackeray, M. H. Rossouw, A. de Kock, A. P. de la Harpe, R. J. Gummow, K. pearce, and D. C. Liles, "The Versatility of MnO_2 for Lithium Battery Applications," *J. Power Sources*, **43-44**, 289 (1993).

13. T. Ohzuku and A Ueda, "Solid-State Redox Reactions of $LiCoO_2$ (R3-m) for 4 Volt Secondary Lithium Cells," *J. Electrochem. Soc.*, **141**, 2972 (1994).

14. E. Plichta, S. Slane, M. Uchiyama, M. Salomon, O. Chua, W. B. Ebner, and H. W. Lin, " An Improved Li/Li_xCoO_2 Rechargeable Cell," *J. Electrochem. Soc.*, **136**, 1865-1869 (1989).

15. C. Delmas and I. Saadoune, "Electrochemical and Physical Properties of the $Li_xNi_{1-y}CoO_2$ Phases," *Solid State Ionics*, **53-56**, 370 (1992).

16. J. R. Dahn, U. von Sacken, M. W. Juzkow, and H. Al-Janaby, "Rechargeable $LiNiO_2$/Carbon Cells," *J. Electrochem. Soc.*, **138**, 2207 (1991).

17. A. Ueda and T. Ohzuku, "Solid State Redox Reactions of $LiNi_{1/2}Co_{1/2}O_2$ (R-3m) for 4 Volt Secondary Lithium Cells," *J. Electrochem. Soc.*, **141**, 2010 (1994).

18. J. Desilvestro and O. Haas, "Metal Oxide Cathode Materials for Electrochemical Energy Storage: A Review," *J. Electrochem. Soc.*, **137**, 5C-21C (1990).

19. K. M. Abraham, "Intercalation Positive Electrodes for Rechargeble Sodium Cells," *Solid State Ionics*, **7**, 199-212 (1982).

20. K. West, "Solid-State Sodium Batteries," in *Lithium Batteries – New materials, Developments and Perspecties*, Ed. G. Pistoia, Elsevier, 1994.

21. T. Ohzuku, A. Ueda, "Why Transition Metal (Di)oxides are the Most Attractive Materials for Batteries," *Solid State Ionic*, **69**, 201-211 (1994).

22. C. Delmas, C. Fouassier, and P. Hagenmuller, "Structural Classification and Properties of the Layered Oxides," *Physica*, **99B**, 81-85 (1980).

23. C. Delmas, J-J Braconnier, C. Fouassier, and P. Hagenmuller, "Electrochemical Intercalation of Sodium in Na_xCoO_2 Bronzes," *Solid State Ionics*, **3/4**, 165-169 (1981).

24. L. W. Shacklette, T. R. Jow, and L. Townsend, "Rechargeable Electrodes from Sodium Cobalt Bronzes," *J. Electrochem. Soc.*, **135**, 2669-2674 (1988).

25. Y. Ma, M. M. Doeff, S. J. Visco, and L. C. De Jonghe, "Rechargeable Na/Na_xCoO_2 and $Na_{15}Pb_4/Na_xCoO_2$ Polymer Electrolyte Cells," *J. Electrochem. Soc.*, **140**, 2726-2733 (1993).

26. T. R. Jow, L. W. Shacklette, M. Maxfield, and D. Vernick, "The Role of Conductive Polymer in Alkali-Metal Secondary Electrodes," *J. Electrochem. Soc.*, **134**, 1730 (1987).

27. T. R. Jow and L. W. Shacklette, "A Rechargeable Cell Based on a Conductive Polymer/Metal Alloy Composite Electrode," *J. Electrochem. Soc.*, **136**, 1-6 (1989).

28. M. Liu, S. J. Visco, and L. C. De Jonghe, "Four Probe Polarization Techniques and the Application to Investigations of Solid-State Electrochemical Devices," *Electrochim Acta*, **38**, 1289-1300 (1993).

29. R. Koksbang, I. I. Olsen, P. E. Tonder, N. Knudsen, and D Fauteux, "Polymer Electrolyte Lithium Batteries Rechargeability and Positive Electrode Degradation - An AC Impedance Study," *J. Appl. Electrochem.*, **21**, 301 (1991).

30. K. West, B. Zachau-Christiansen, T. Jacobsen, E. Miort-Lorenzen, and S. Skaarup, "Poly(ethylene Oxide)-Sodium Perchlorate Electrolytes in Solid-State Sodium Cells," *British Polymer Journal*, **20**, 243-246 (1988).

31. S. Skaarup, K. West, B. Zachau-Cristiansen, and T. Jacobsen, "Solid State Sodium Batteries," *Proceedings of the International Seminar on Solid State Ionic Devices*, eds., B. V. R. Chowdari and S. Radhakrishna, Singapore, 75-86 (1988).

32. K. West, B. Zachau-Christiansen, T. Jacobsen, and S Skaarup, "Sodium Insertion in Vanadium Oxides," *Solid State Ionics*, **28-30**, 1128-1131 (1988).

33. J. P. Pereira-Ramos, R. Messina, S. Bach, and N. Baffier, "Influence of the Synthesis via a Sol-Gel Process on the Electrochemical Lithium and Sodium Insertion in β-$Na_{0.33}V_2O_5$," *Solid State Ionics*, **40/41**, 970-973 (1990).

34. S. Bach, N. Baffier, J. P. Pereira-Ramos, and R. Messina, "Electrochemical Sodium Intercalation in $Na_{0.33}V_2O_5$ Bronze Synthesized by a So-Gel Process," *Solid State Ionics*, **37**, 41-49 (1989).

35. M. Z. A. Munshi, A. Gilmour, W. H. Smyrl, and B. B. Owens, "Sodium/V_6O_{13} Polymer Electrolyte Cells," *J. Electrochem. Soc.*, **136**, 1847-1848 (1989).

36. A. Mendiboure, C. Delmas, and P. Hagenmuller, "Electrochemical Intercalation and Deintercalation of Na_xMnO_2 Bronzes," *J. Solid State Chemistry*, **57**, 323-331 (1985).

37. M. M. Doeff, M. Y. Peng, Y. Ma, and L. C. De Jonghe, "Orthorhombic Na_xMnO_2 as a Cathode Material for Secondary Sodium and Lithium Polymer Batteries," *J. Electrochem. Soc.*, **141**, L145-147 (1994).

38. M. M. Doeff, L. Ding, and L. C. De Jonghe, "Electrochemical Characterization of Orthorhombic Na_xMnO_2 for Alkali Metal Polymer Batteries," *Mat. Res. Soc. Symp. Proc.*, **393**, 107-112 (1995).

39. J. M. Tarascon, D. G. Guyomard, and B. Wilkens, "Chemical and Electrochemical Insertion of Na into the Spinel λ-MnO_2 Phase," *Solid State Ionics*, **57**, 113-120 (1992).

40. M. M. Doeff, Y. Ma, M. Peng, S. J. Visco, and L. C. De Jonghe, "Solid Sodium Polymer Electrolyte Batteries," Proceedings of the *28th Intersociety Energy Conversion Engineering Conference*, # 93039, Atlanta, GA, 1993.

41. J. M. Tarascon and G. W. Hull, "Sodium Intercalation into the Layer Oxides $Na_xMo_2O_4$," *Solid State Ionics*, **22**, 85-96 (1986).

42. K. West, B. Zachau-Christiansen, T. Jacobsen, and S Atlung, "A Rechargeable All-Solid-State Sodium Cell with Polymer Electrolyte," *J. Electrochem. Soc.*, **132**, 3061-3062 (1985).

43. K. West, B. Zachau-Christiansen, T. Jacobsen, and S. Skaarup, "Layered Potassium Vanadium Oxides as Host Materials for Lithium and Sodium Insertion," *Solid State Ionics*, **40/41**, 585-588 (1990).

44. R. Kosbang, S. Yde-Andersen, K. West, B. Zachau-Christiansen, and S. Skaarup, "Lithium and Sodium Insertion in Ternary Chromium Oxides," *Solid State Ionics*, **28-30**, 868-872 (1988).

45. A. Stoklosa, J. Molenda, and D. Than, "Structure of Ionic and Electronic Deffects in Cobalt Bronze Na_xCoO_2," *Solid State Ionics*, **15**, 211-216 (1985).

46. J. Molenda, C. Delmas, P. Dordor, and A. Stoklosa, "Transport Properties of Na_xCoO_{2-y}," *Solid State Ionics*, **12**, 473-477 (1989).

47. C. A. C. Sequeira, J. M. North, and A. Hooper, "Stability Domain of a Complexed Lithium Salt-Poly(Ethylene Oxide) Polymer Electrolyte," *Solid State Ionics*, **13**, 175-179 (1984).

48. J. Molenda, "Correlation Between Electronic and Electrochemical Properties of A_xMO_2-Type Electrode Materials. Electronic Criterion," *Solid State Ionics*, **21**, 263-272, (1986).

49. L. A. Chick, L. R. Pederson, G. D. Maupin, J. L. Bates, L. E. Thomas, and G. J. Exarhos, "Glycine-Nitrate Combustion Synthesis of Oxide Ceramic Powders," *Materials Letters*, **10**, 6-12 (1990).

Figure Captions: Chapter 2

Figure 2-1. Solid-state thin-film Na(or $Na_{15}Pb_4$)/$PEO_nNaCF_3SO_3$/$Na_{0.7}CoO_2$ cells.

Figure 2-2. The four-probe cell configuration with two sodium reference electrodes.

Figure 2-3. Cell potential *vs.* x in Na_xCoO_2 in (a) a cell with a sodium anode at 90°C, and (b) a cell with $Na_{15}Pb_4$ anode at 100°C. The current density was 0.5 mA/cm^2 for both charge and discharge.

Figure 2-4. Overcharge of an $Na_{15}Pb_4$/$PEO_8NaCF_3SO_3$/Na_xCoO_2 cell (cutoff potential 4.0 V). The subsequent discharge showed reduced capacity. The charge current was 0.1 mA/cm^2, and the discharge current was 0.2 mA/cm^2.

Figure 2-5. Discharge curves at various current densities up to 2.5 mA/cm^2 for a Na/$PEO_8NaCF_3SO_3$/Na_xCoO_2 cell at 90°C. For this experiment, the current was periodically interrupted to estimate open-circuit potentials.

Figure 2-6. Capacity as a function of cycle number for the Na/$PEO_8NaCF_3SO_3$/Na_xCoO_2 cell in Figure 2-3(a). The current density was 0.5 mA/cm^2 for both charge and discharge, and the temperature was 90°C.

Figure 2-7. Charge efficiency for the cell in Figure 2-6, defined as the ratio of coulombs passed during discharge to that passed during charge.

Figure 2-8. Discharge curves as a function of cycle number for the Na/$PEO_8NaCF_3SO_3$/Na_xCoO_2 cell from Figure 2-6 and 2-7. The theoretical capacity of 3.2 C corresponds to $\Delta x = 0.6$ in Na_xCoO_2.

Figure 2-9. Capacity as a function of cycle number for a $Na_{15}Pb_4$/$PEO_8NaCF_3SO_3$/Na_xCoO_2 cell at 100°C. Various discharge and charge rates

were used for the first ten cycles (these are not shown), and the cell was overcharged during the second cycle, leading to reduced capacity. A discharge and charge current density of 0.5 mA/cm^2 was used for the subsequent cycles, except as noted. The effect of various potential limits is also shown. The capacity of the first cycle corresponded Δx = 0.6 in Na_xCoO_2 (100% utilization).

Figure 2-10. Charge efficiency for the cell in Figure 2-9, defined as the ratio of coulombs passed during discharge to that passed during charge.

Figure 2-11. Capacity as a function of cycle number for a $Na_{0.7}CoO_2/PEO_8NaCF_3SO_3/Na_xCoO_2$ cell at 90°C. The cell was cycled between -2 to +2 V at 0.5 mA/cm^2 for both charge and discharge.

Figure 2-12. Overpotentials of cell components and interfaces on the application of sequential bipolar square wave pulses to a four-probe cell after the second cycle at 90°C. The cell area was 3 cm^2. The time for each pulse was 50 ms. Only the discharge response is shown for clarity.

Figure 2-13. The change in resistance of the polymer electrolyte and at the sodium electrode in a four-probe cell undergoing galvanostatic discharge at 0.33 mA/cm^2. The cell area was 3 cm^2. The cathode resistance as a function of time is not shown, but exactly follows that of the cell as a whole.

Figure 2-14. Change in resistance of components in a four-probe cell as a function of cycle number, obtained from sequential square wave pulse data similar to that shown in Figure 2-12. Cell area was 3 cm^2. The values obtained after discharge are plotted on the positive axis, and those obtained after charge are plotted on the negative axis for clarity.

Figure 2-15. Practical energy density as a function of loading level and capacity in the sodium cobalt bronze electrode. These calculations assume a cell attaining the

theoretical capacity,, metallized plastic current collectors 5 μm thick, and a twofold excess of sodium in the anode.

Figure 2-16. Practical power density for $Na_xCoO_2/PEO_8NaCF_3SO_3/$ Na cells with 5 μm thick metallized plastic current collectors, 10 μm thick polymer electrolyte separators, and a twofold excess of sodium in the anodes. The loading level in the cathode is assumed to be 45 w/o electroactive material. The graph shows the amount of time that the corresponding currents can be sustained as well as the depth of discharge (DOD) based on the data shown in Figure 2-5.

Figure 2-17. Ragone plot for $Na_xCoO_2/PEO_8NaCF_3SO_3/Na$ cells, using the calculations shown in Figure 2-16. The cell dimensions are the same as in Figure 2-15, and the loading level in the cathode is assumed to be 45 w/o. The zero power density point corresponds to the energy density of a cell with capacity of 3 C/cm^2 in the cathode.

Figure Captions: Chapter 3

Figure 3-1. The electronic conductivity of composite $Na_{0.7}CoO_2$ electrodes as a function of (a) volumetric fraction of carbon black in the electrodes, and (b) total volume fraction of both $Na_{0.7}CoO_2$ and carbon black at room temperature. Two series of electrodes that have 30 w/o and 50 w/o $Na_{0.7}CoO_2$ are shown.

Figure 3-2. The first charge and discharge curve of a $Na/PEO_{20}NaCF_3SO_3/Na_xCoO_2$ cell at 85°C. The composite positive electrode contains 20 v/o (48 w/o) of $Na_{0.7}CoO_2$ and 10 v/o (11 w/o) of carbon black. The current density was 0.1 mA/cm^2 for both charge and discharge.

Figure 3-3. Discharge curves at various current densities for the $Na/PEO_{20}NaCF_3SO_3/Na_xCoO_2$ cell in Figure 3-2 at 85°C.

Figure 3-4. The first charge and discharge curve of a $Na/PEO_{20}NaCF_3SO_3/Na_xCoO_2$ cell at 85°C. The composite positive electrode contains 30 v/o (64 w/o) of $Na_{0.7}CoO_2$ but no carbon black additive. The current density was 0.1 mA/cm^2 for both charge and discharge.

Figure 3-5. The first charge and discharge curves of a $Na/PEO_{20}NaCF_3SO_3/Na_xCoO_2$ cell at 85°C. The composite positive electrode contains 40 v/o (74 w/o) of $Na_{0.7}CoO_2$ but no carbon black additive. The current density was 0.1 mA/cm^2 for both charge and discharge.

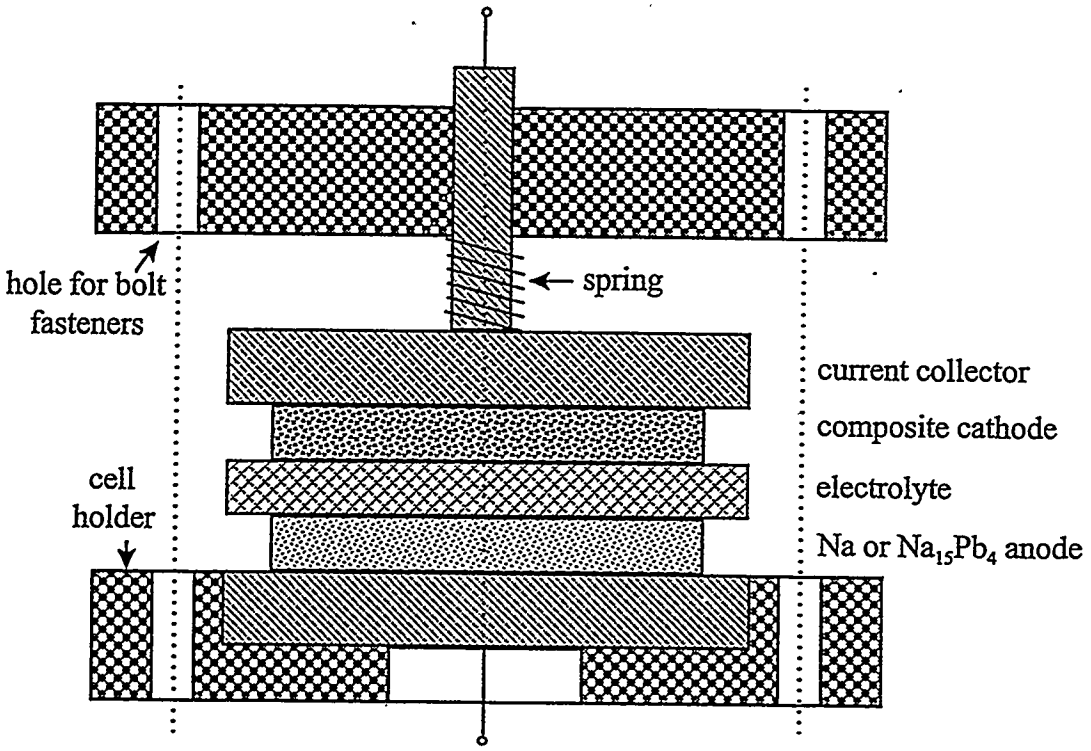

Figure 2-1. Solid-state thin-film Na(or $Na_{15}Pb_4$)/$PEO_nNaCF_3SO_3$/$Na_{0.7}CoO_2$ cells.

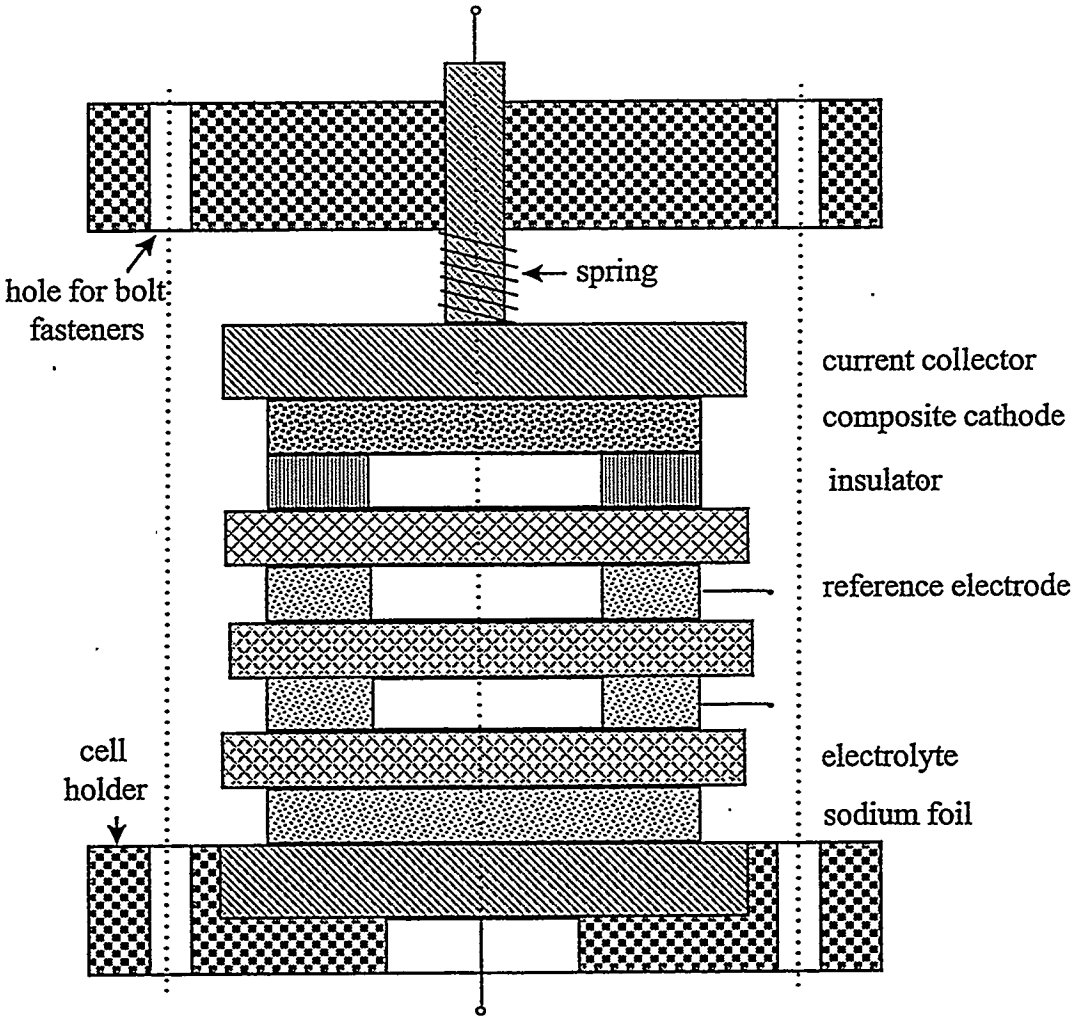

Figure 2-2. The four-probe cell configuration with two sodium reference electrodes.

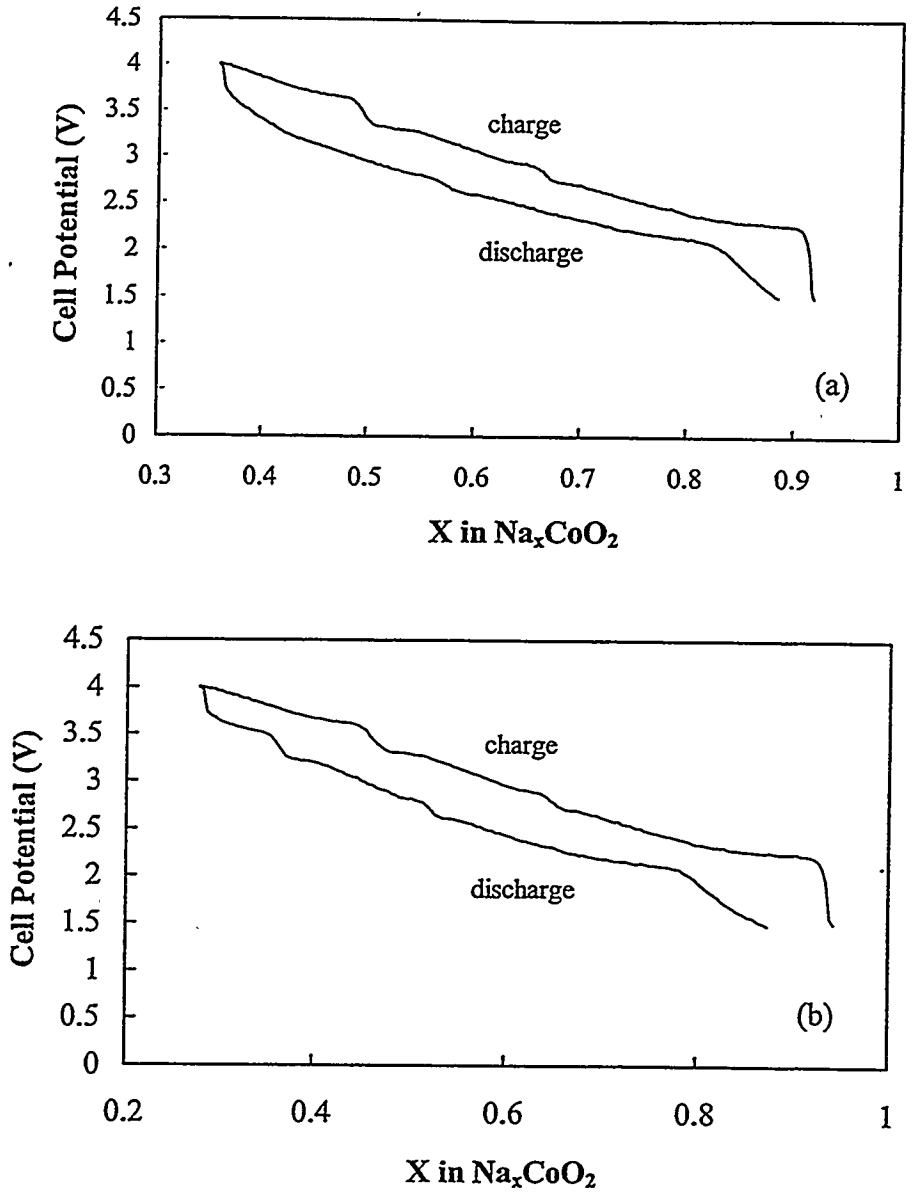

Figure 2-3. Cell potential *vs.* x in Na_xCoO_2 in (a) a cell with a sodium anode at 90°C, and (b) a cell with $Na_{15}Pb_4$ anode at 100°C. The current density was 0.5 mA/cm^2 for both charge and discharge.

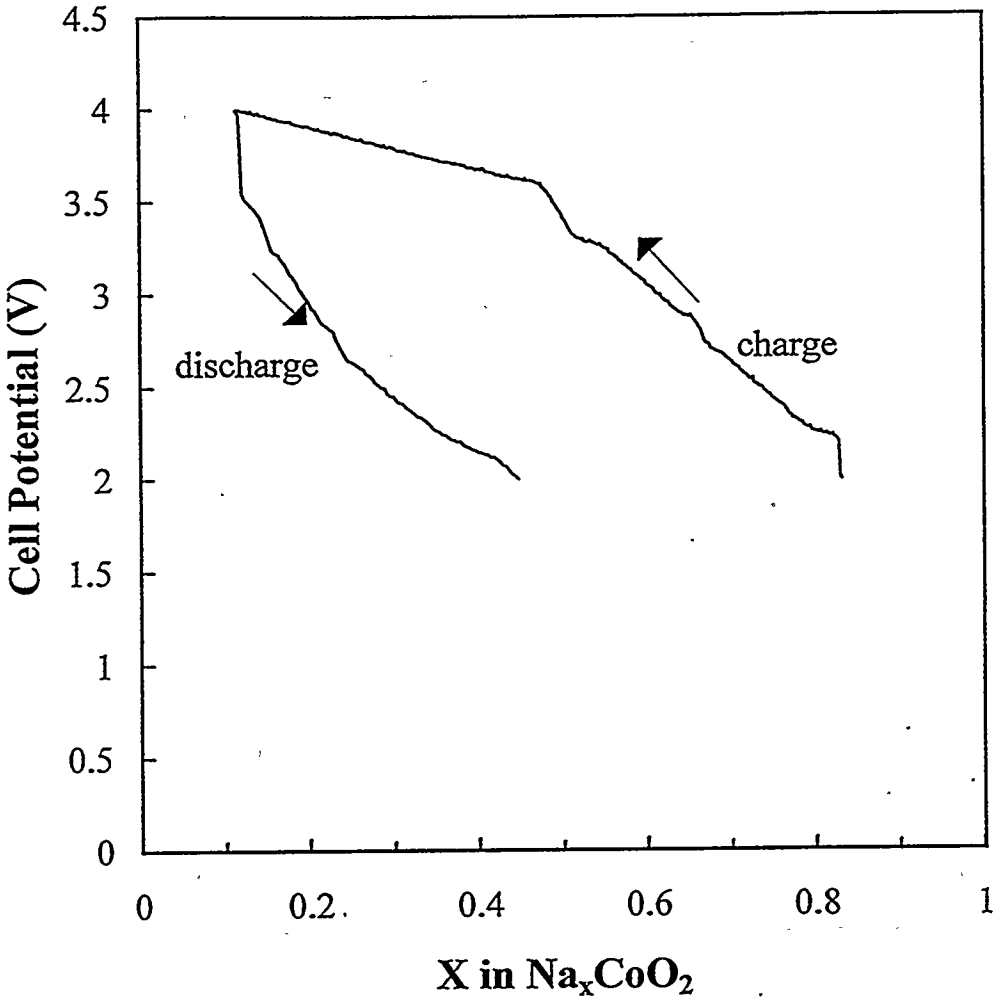

Figure 2-4. Overcharge of an $Na_{15}Pb_4/PEO_8NaCF_3SO_3/Na_xCoO_2$ cell (cutoff potential 4.0 V). The subsequent discharge showed reduced capacity. The charge current was 0.1 mA/cm^2, and the discharge current was 0.2 mA/cm^2.

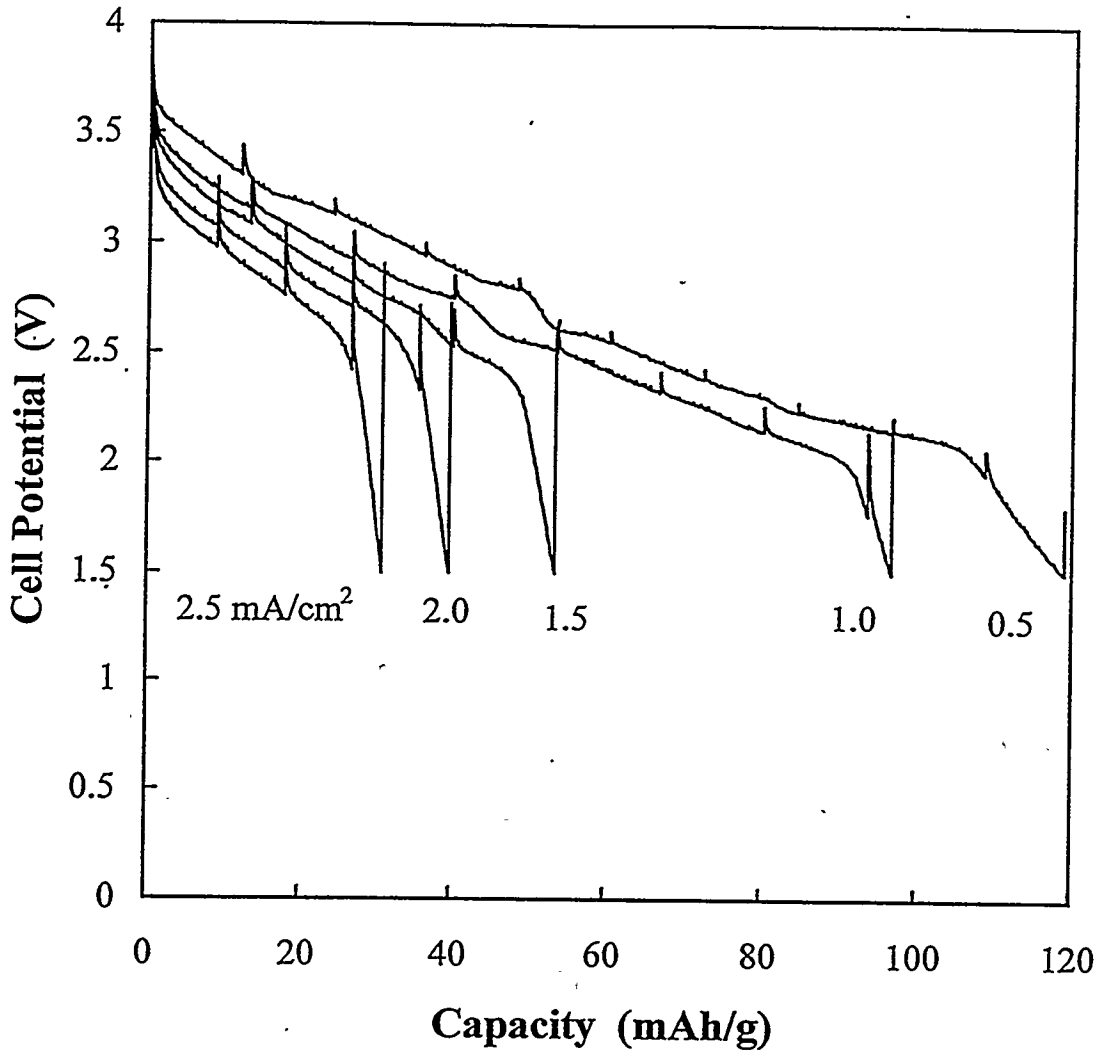

Figure 2-5. Discharge curves at various current densities up to 2.5 mA/cm^2 for $Na/PEO_8NaCF_3SO_3/Na_xCoO_2$ cells at 90°C. For this experiment, the current was periodically interrupted to estimate open-circuit potentials.

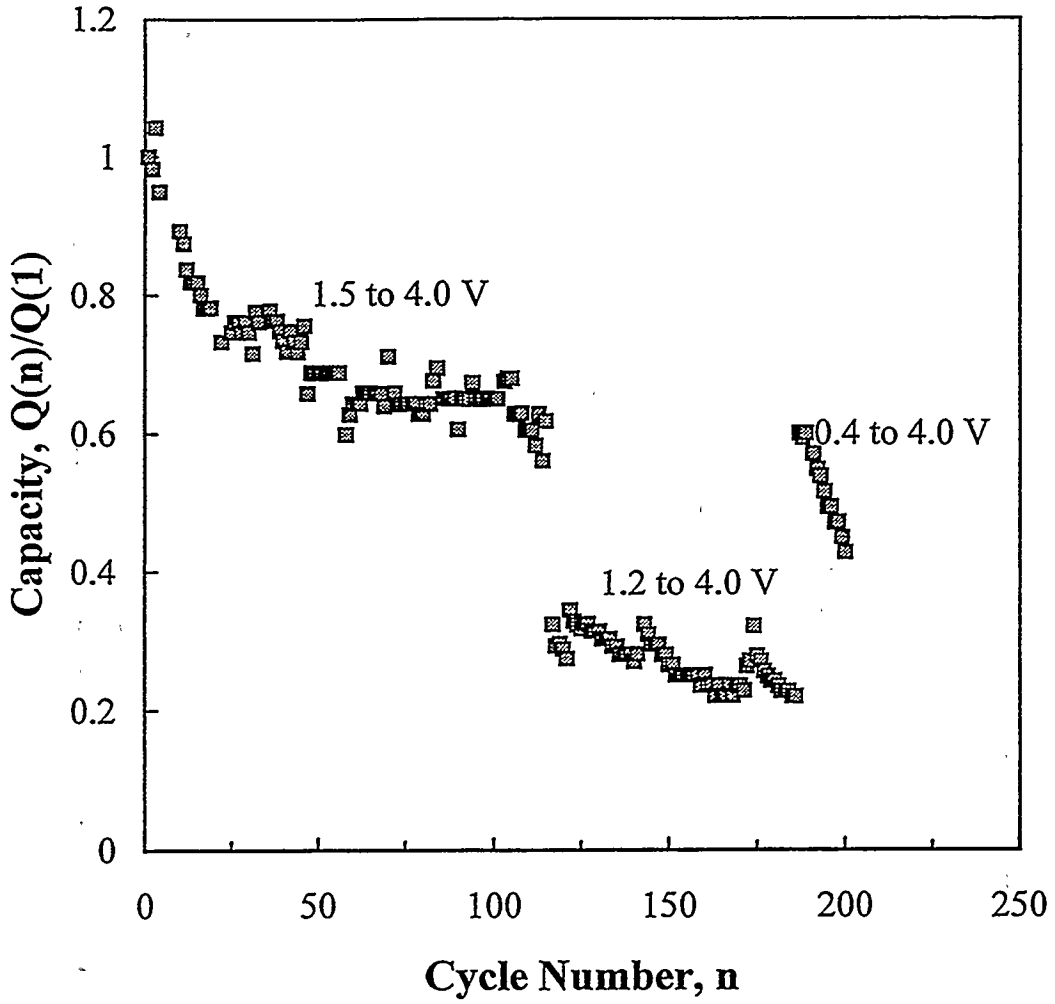

Figure 2-6. Capacity as a function of cycle number for the $Na/PEO_8NaCF_3SO_3/Na_xCoO_2$ cell in Figure 2-3(a). The current density was 0.5 mA/cm^2 for both charge and discharge, and the temperature was 90°C.

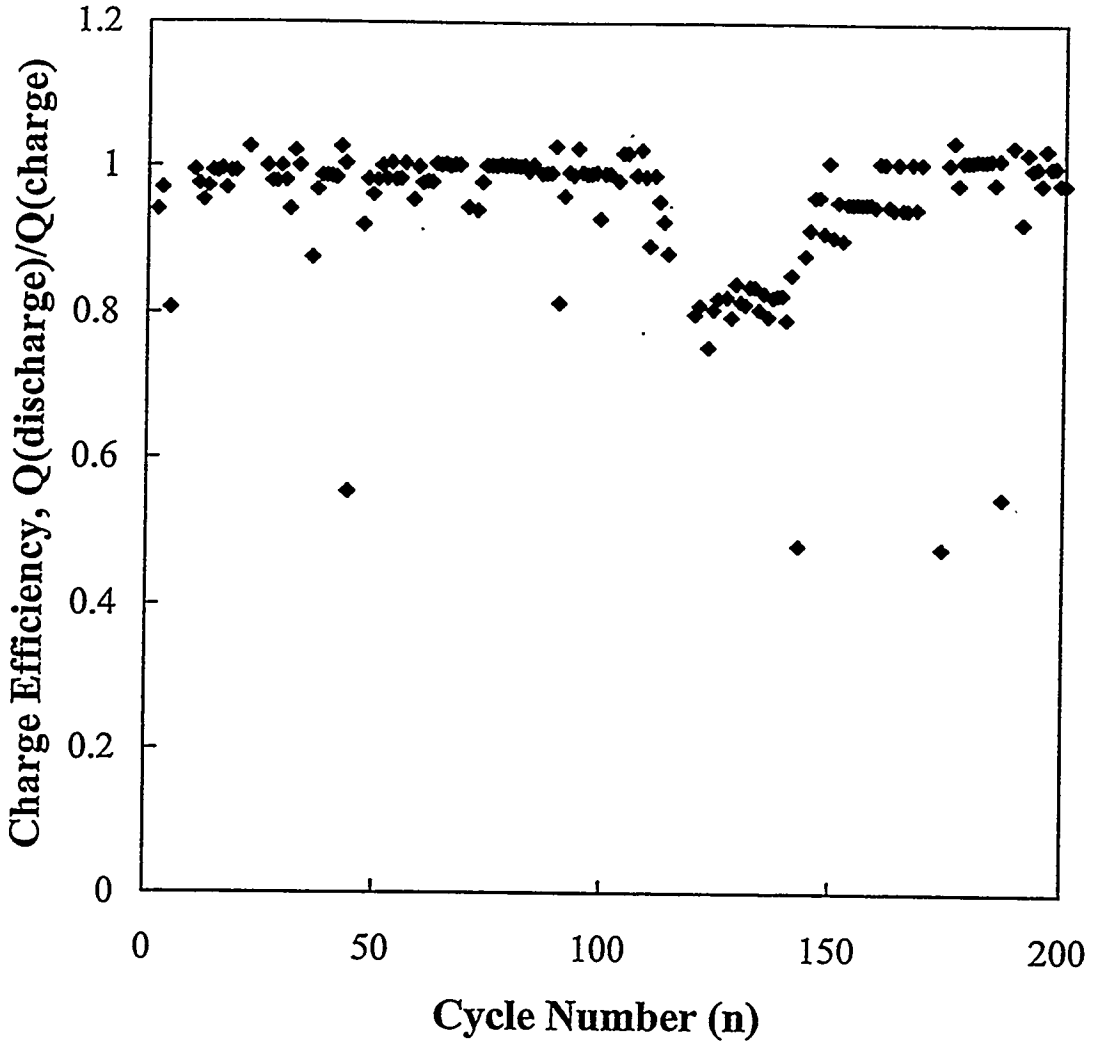

Figure 2-7. Charge efficiency for the cell in Figure 2-6, defined as the ratio of coulombs passed during discharge to that passed during charge.

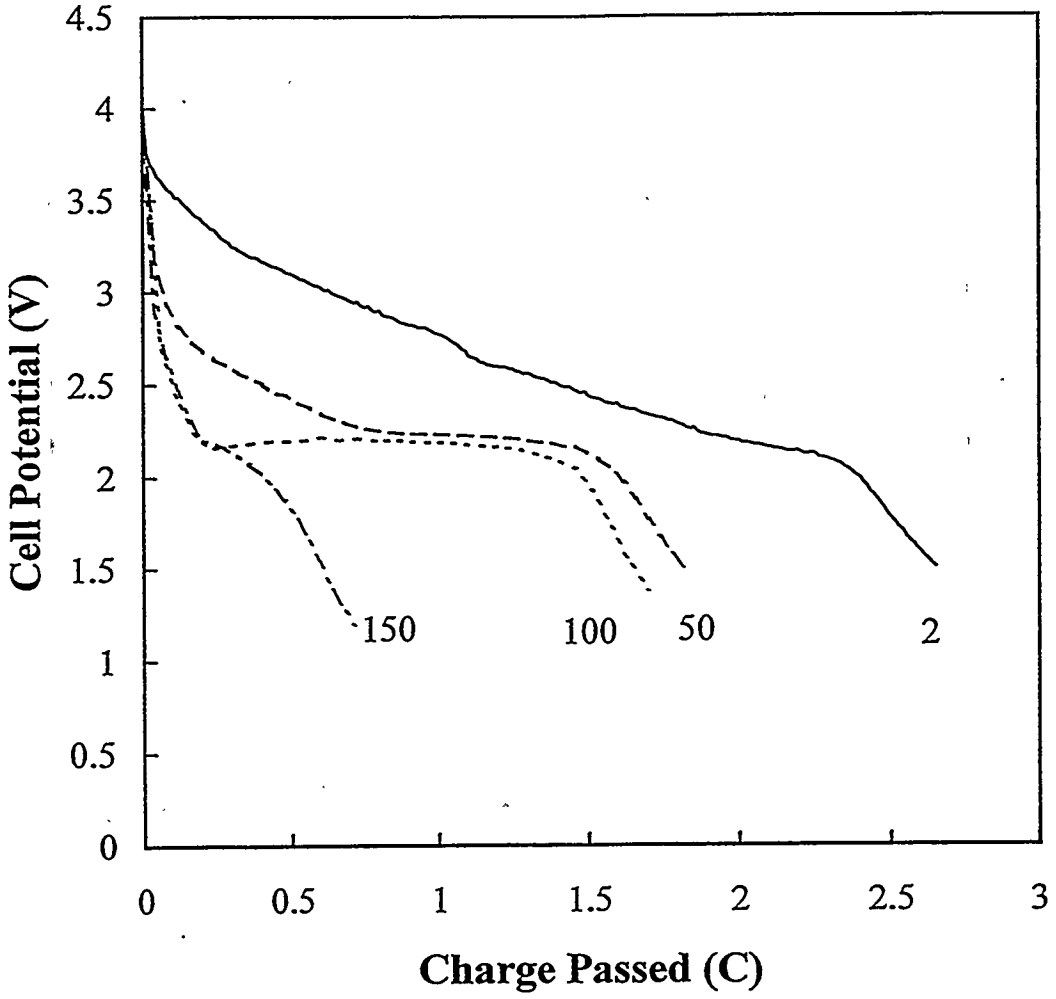

Figure 2-8. Discharge curves as a function of cycle number for the $Na/PEO_8NaCF_3SO_3/Na_xCoO_2$ cell from Figure 2-6 and 2-7. The theoretical capacity of 3.2 C corresponds to $\Delta x = 0.6$ in Na_xCoO_2.

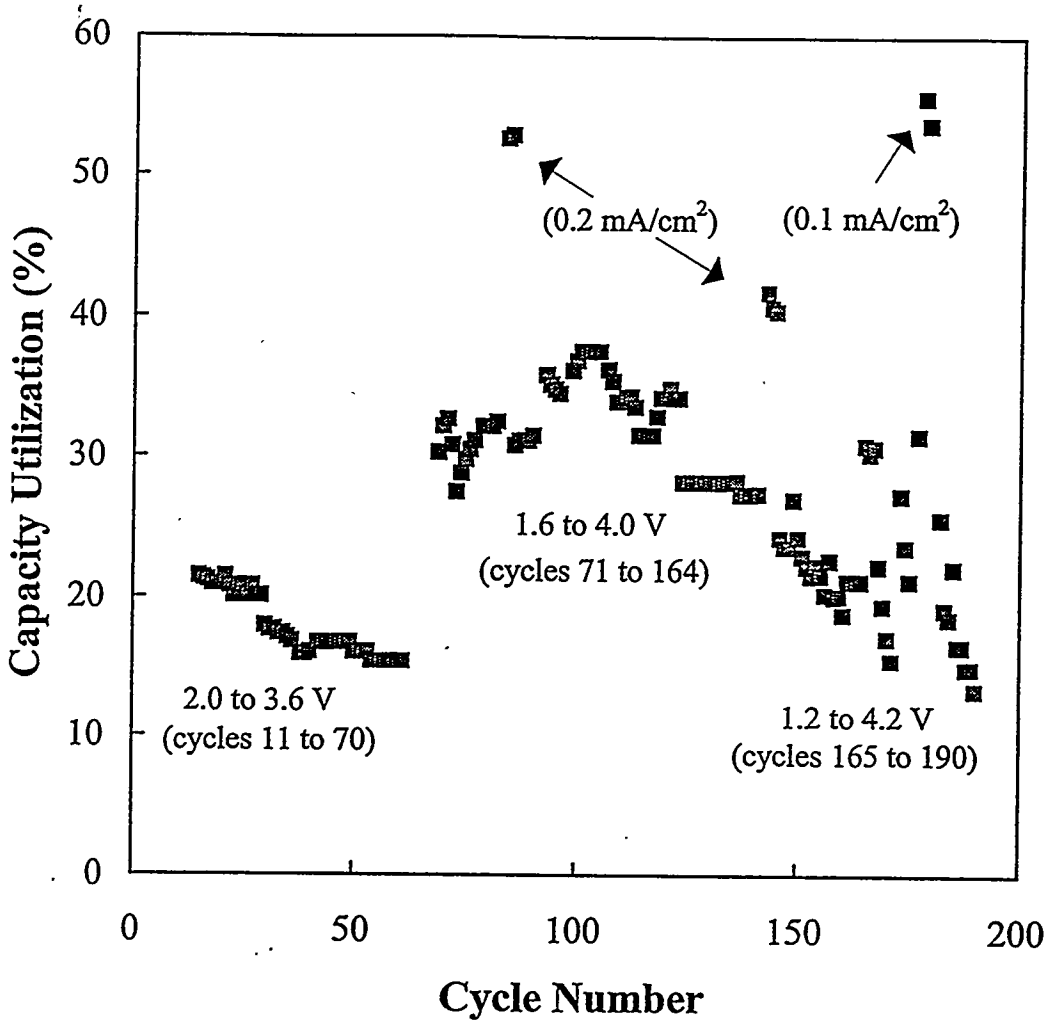

Figure 2-9. Capacity as a function of cycle number for a $Na_{15}Pb_4/PEO_8NaCF_3SO_3/Na_xCoO_2$ cell at 100°C. Various discharge and charge rates were used for the first ten cycles (these are not shown), and the cell was overcharged during the second cycle, leading to reduced capacity. A discharge and charge current density of 0.5 mA/cm^2 was used for the subsequent cycles, except as noted. The effect of various potential limits is also shown. The capacity of the first cycle corresponded $\Delta x = 0.6$ in Na_xCoO_2 (100% utilization).

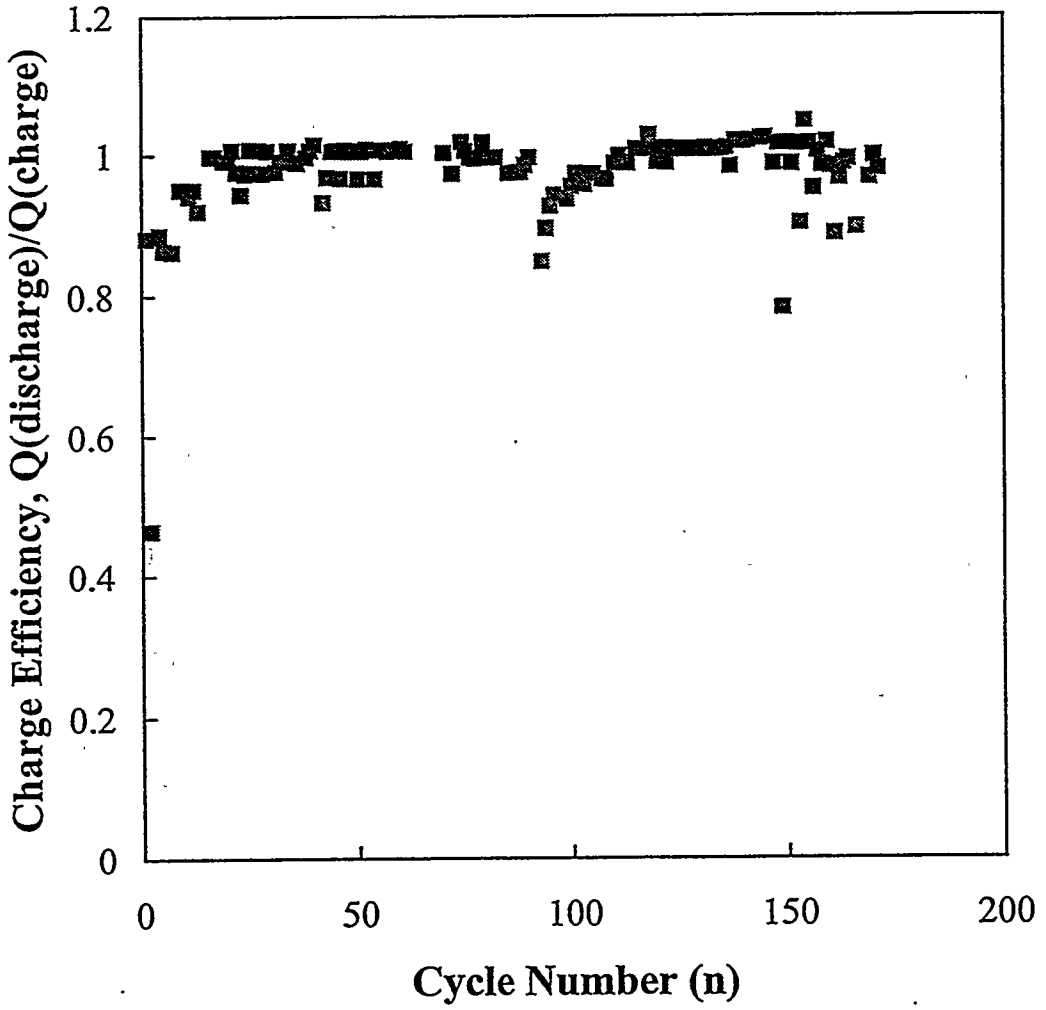

Figure 2-10. Charge efficiency for the cell in Figure 2-9, defined as the ratio of coulombs passed during discharge to that passed during charge.

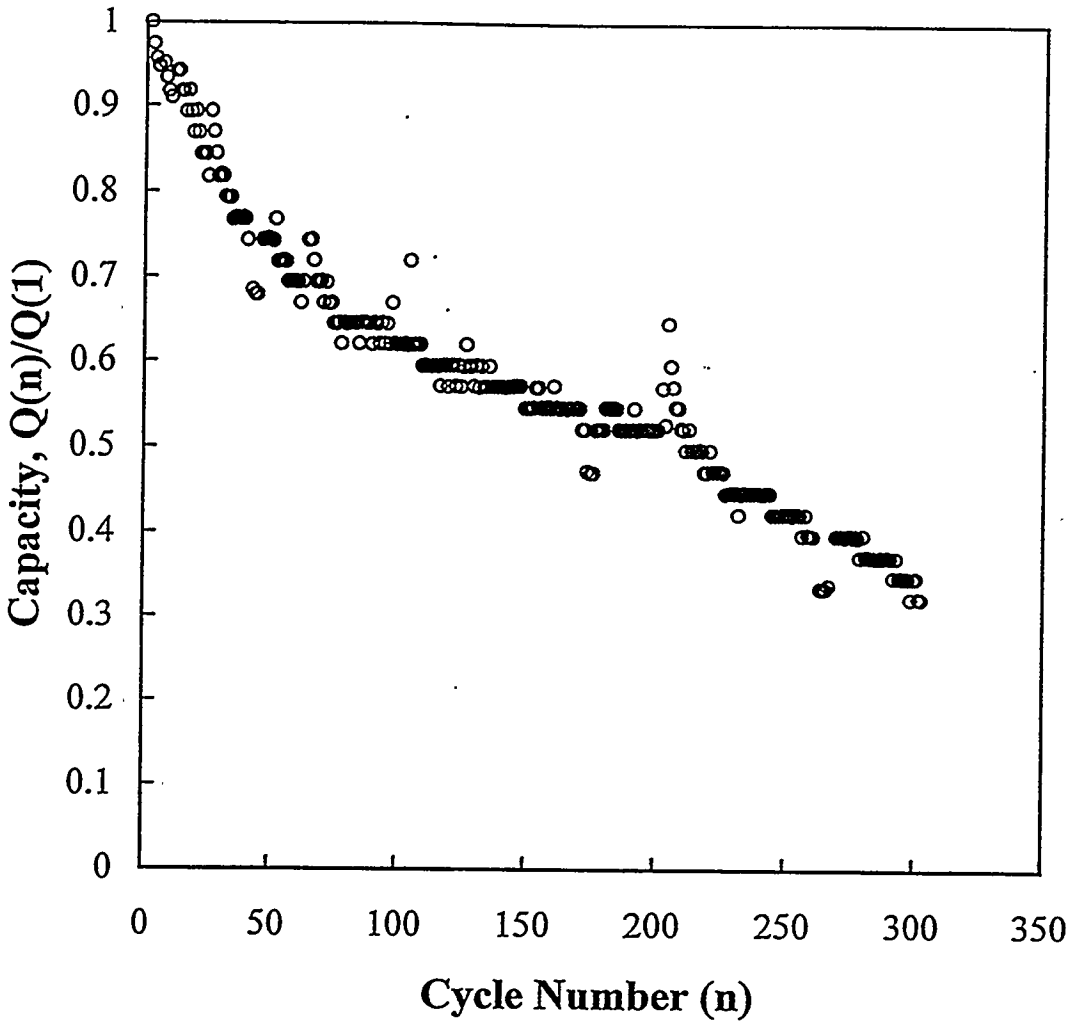

Figure 2-11. Capacity as a function of cycle number for a $Na_{0.7}CoO_2/PEO_8NaCF_3SO_3/Na_xCoO_2$ cell at 90°C. The cell was cycled between -2 V and +2 V at 0.5 mA/cm^2 for both charge and discharge.

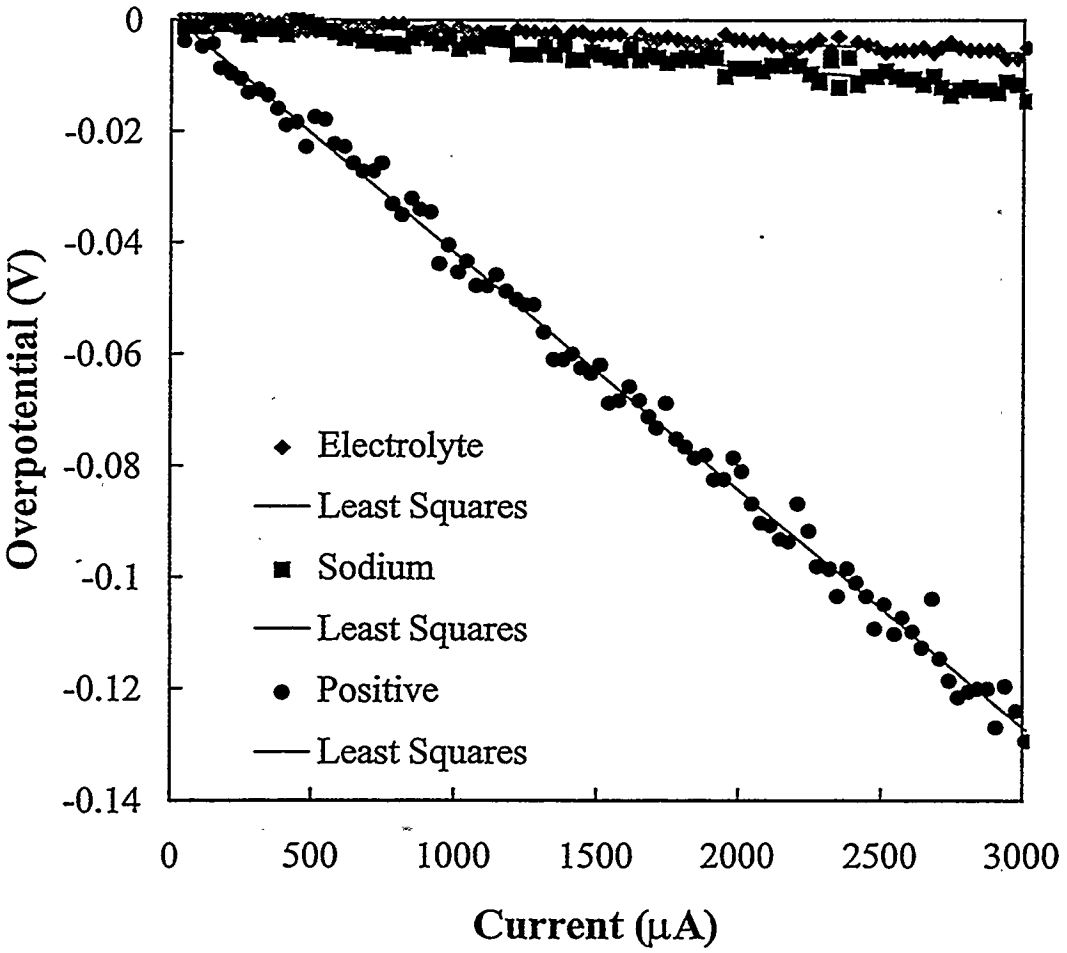

Figure 2-12. Overpotentials of cell components and interfaces on the application of sequential bipolar square wave pulses to a four-probe cell after the second cycle at 90°C. The cell area was 3 cm^2. The time for each pulse was 50 ms. Only the discharge response is shown for clarity.

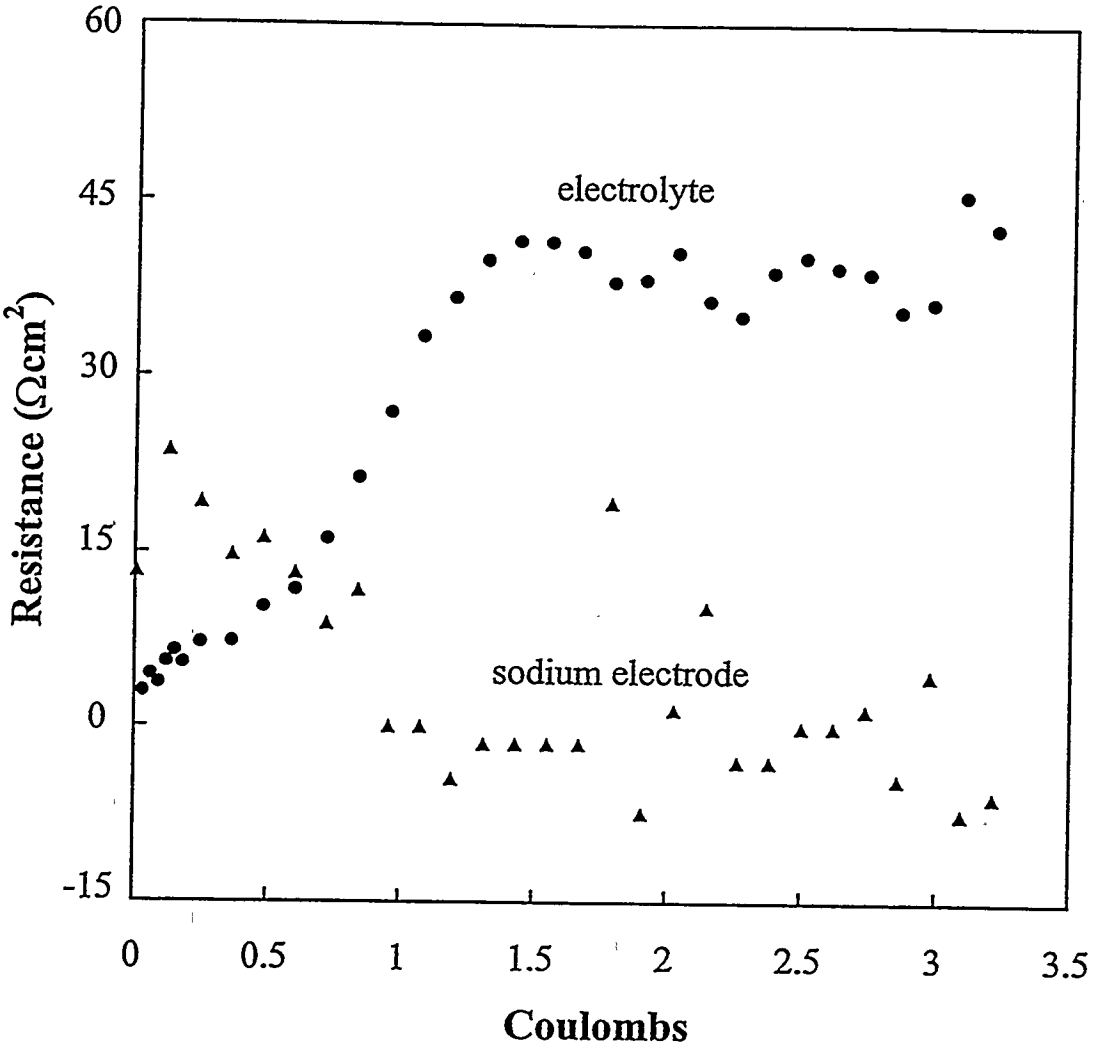

Figure 2-13. The change in resistance of the polymer electrolyte and at the sodium electrode in a four-probe cell undergoing galvanostatic discharge at 0.33 mA/cm^2. The cell area was 3 cm^2. The cathode resistance as a function of time is not shown, but exactly follows that of the cell as a whole.

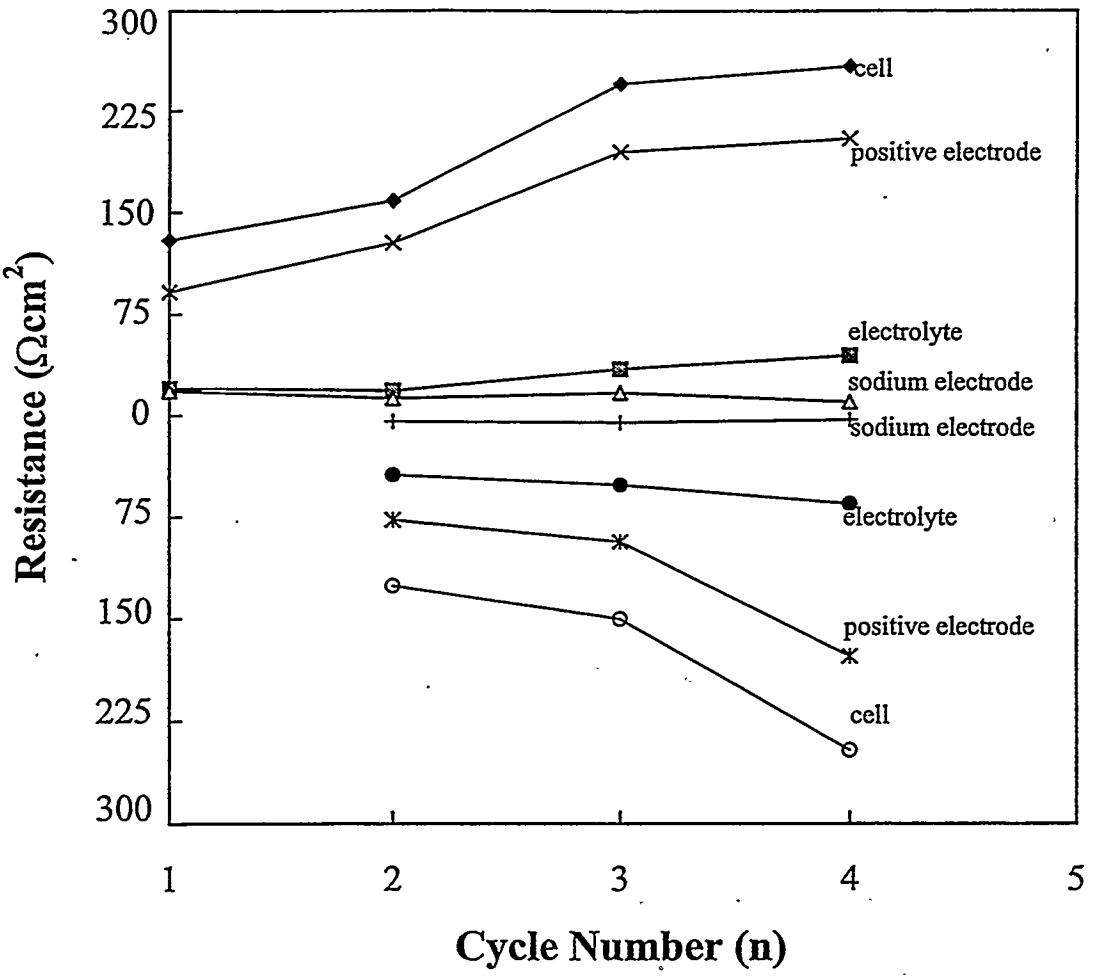

Figure 2-14. Change in resistance of components in a four-probe cell as a function of cycle number, obtained from sequential square wave pulse data similar to that shown in Figure 2-12. Cell area was 3 cm^2. The values obtained after discharge are plotted on the positive axis, and those obtained after charge are plotted on the negative axis for clarity.

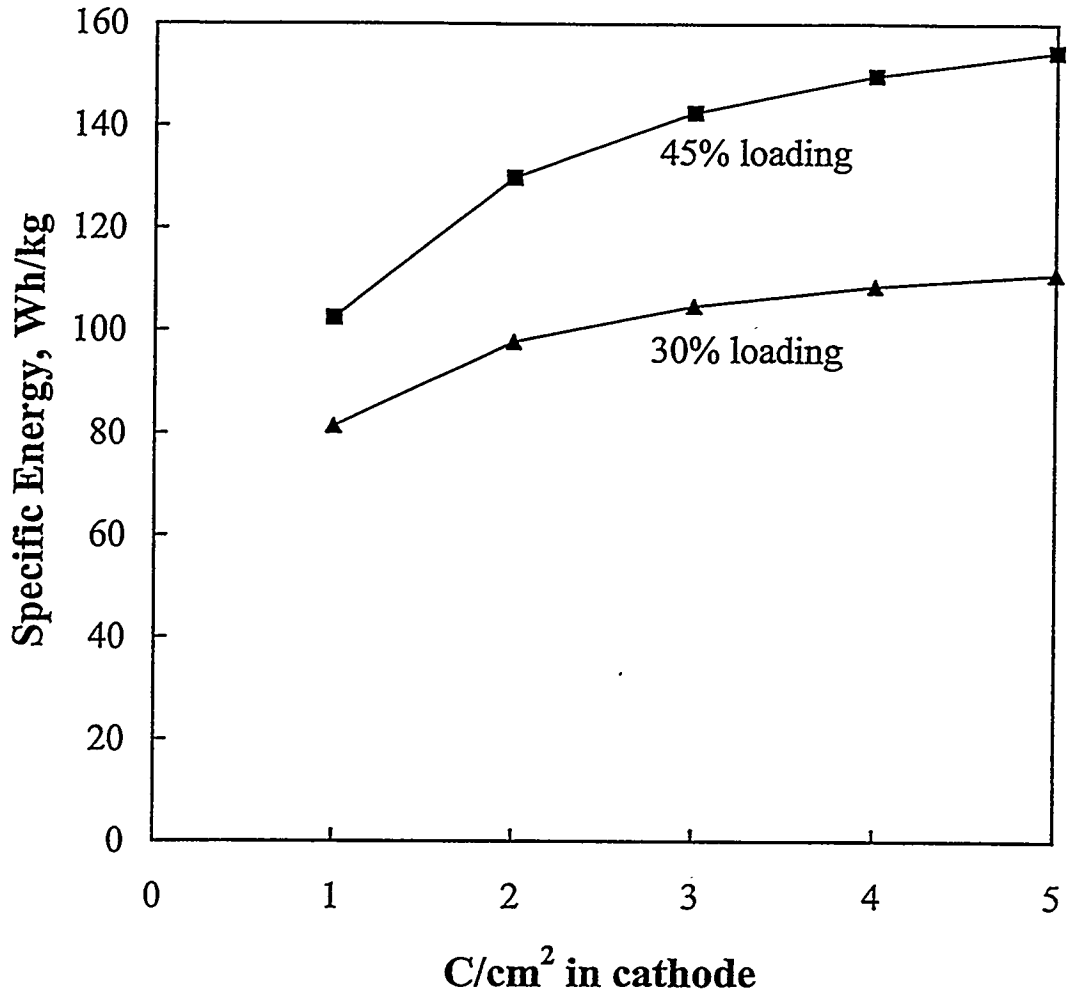

Figure 2-15. Practical energy density as a function of loading level and capacity in the sodium cobalt bronze electrode. These calculations assume a cell attaining the theoretical capacity, metallized plastic current collectors 5 μm thick, and a twofold excess of sodium in the anode.

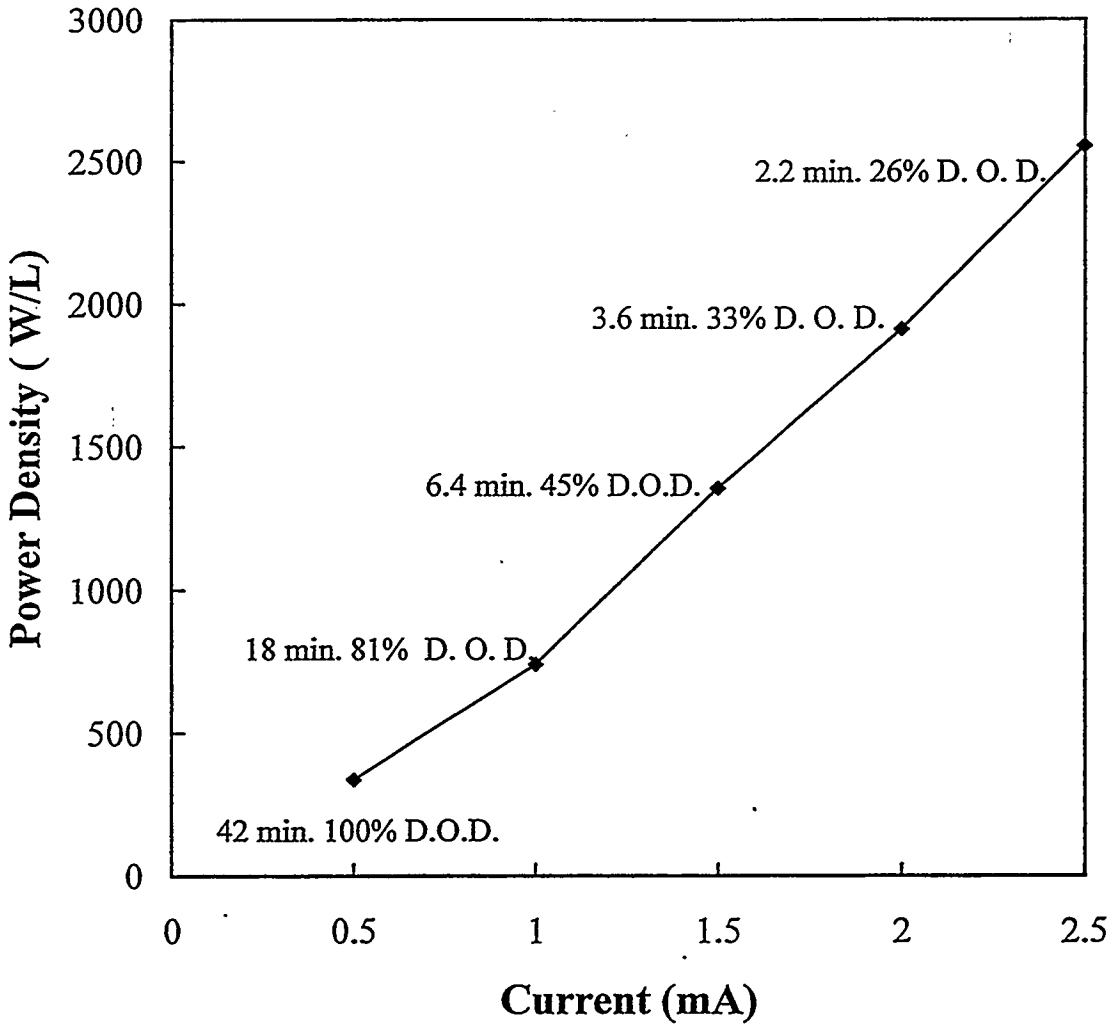

Figure 2-16. Practical power density for $Na_xCoO_2/PEO_8NaCF_3SO_3/$ Na cells with 5 μm thick metallized plastic current collectors, 10 μm thick polymer electrolyte separators, and a twofold excess of sodium in the anodes. The loading level in the cathode i assumed to be 45 w/o electroactive material. The graph shows the amount of time that the corresponding currents can be sustained as well as the depth of discharge (DOD) based on the data shown in Figure 2-5.

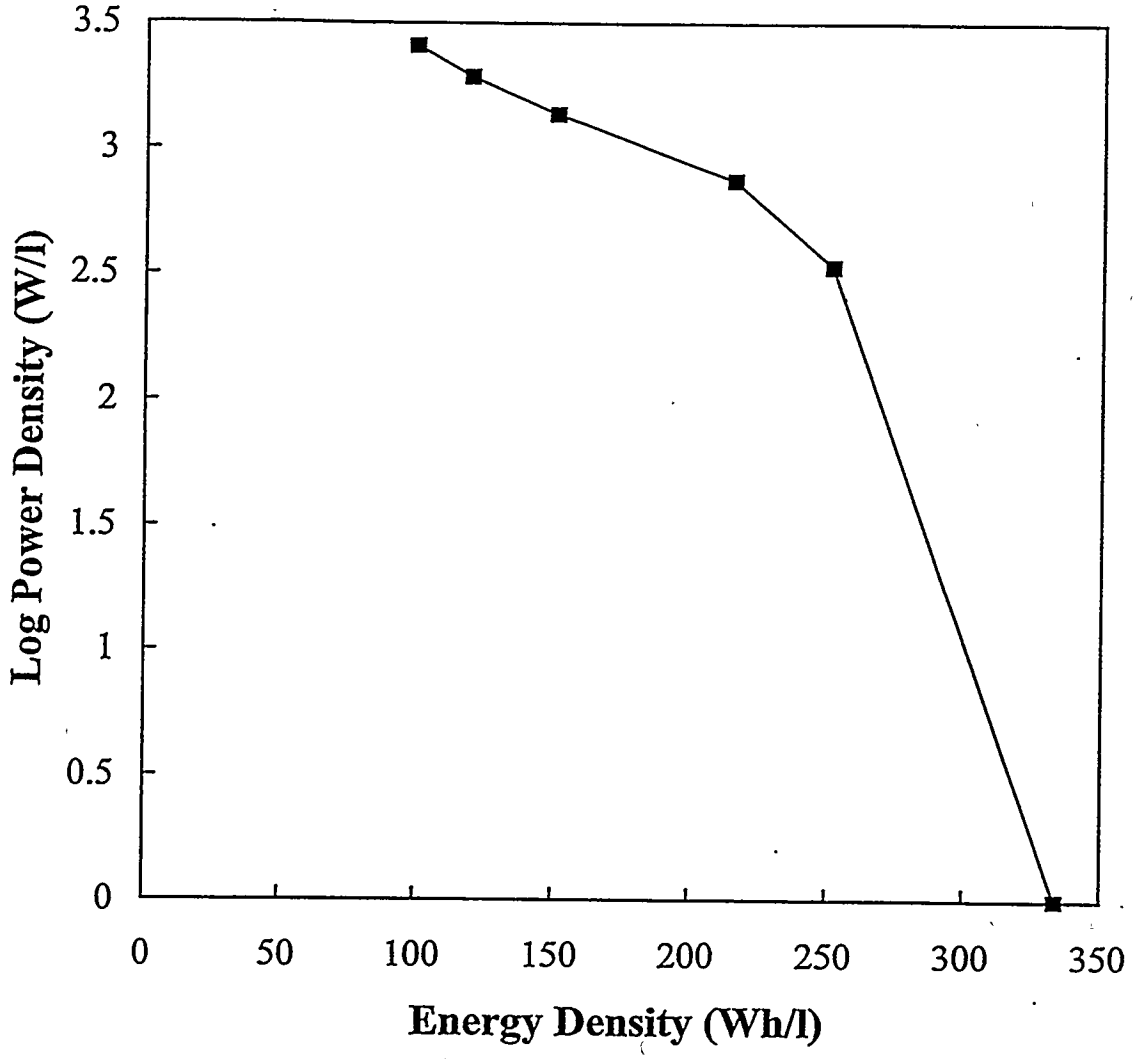

Figure 2-17. Ragone plot for $Na_xCoO_2/PEO_8NaCF_3SO_3/Na$ cells, using the calculations shown in Figure 2-16. The cell dimensions are the same as in Figure 2-15, and the loading level in the cathode is assumed to be 45 w/o. The zero power density point corresponds to the energy density of a cell with capacity of 3 C/cm^2 in the cathode.

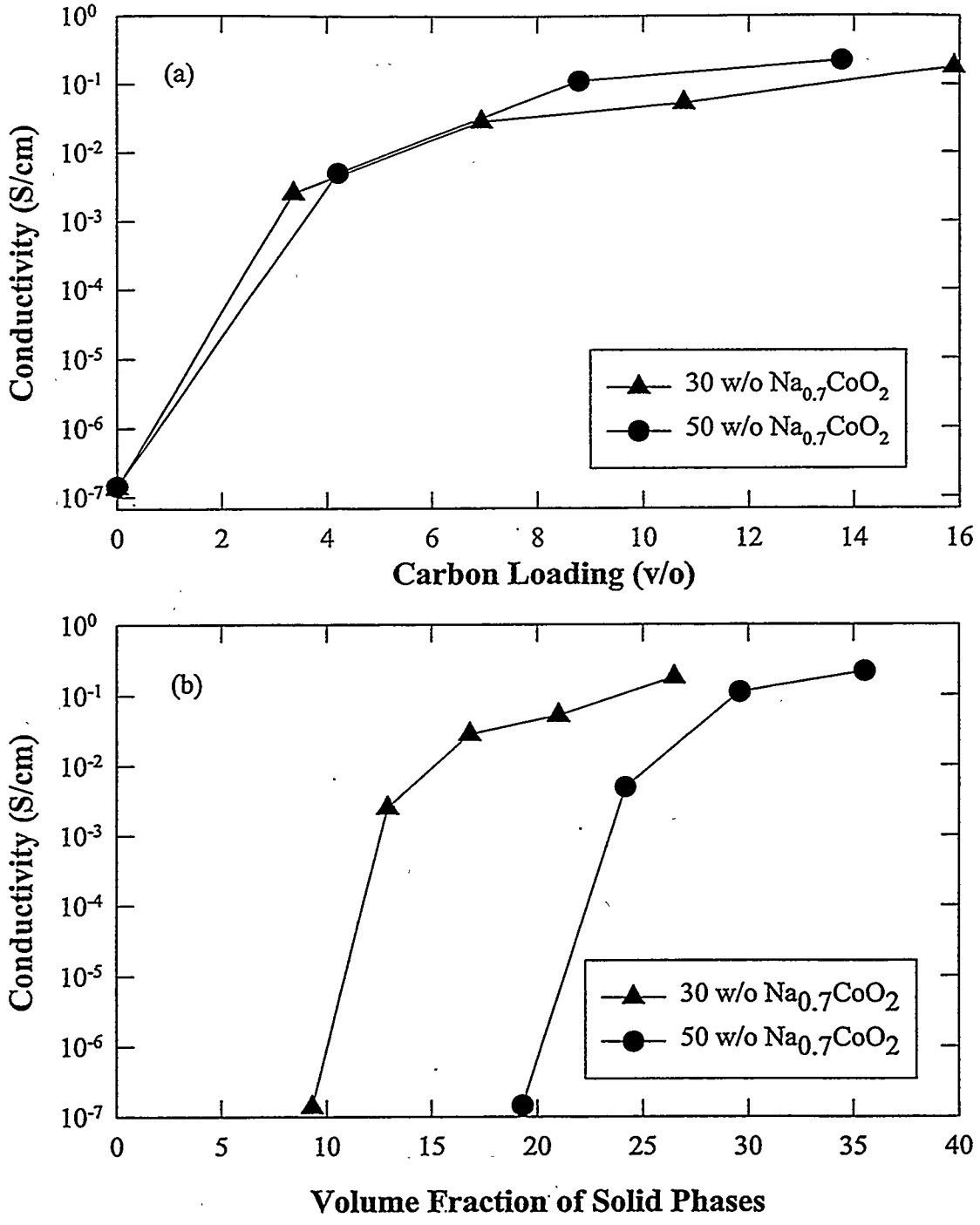

Figure 3-1. The electronic conductivity of composite $Na_{0.7}CoO_2$ electrodes as a function of (a) volume fraction of carbon black in the electrodes, and (b) total volume fraction of both $Na_{0.7}CoO_2$ and carbon black at room temperature.

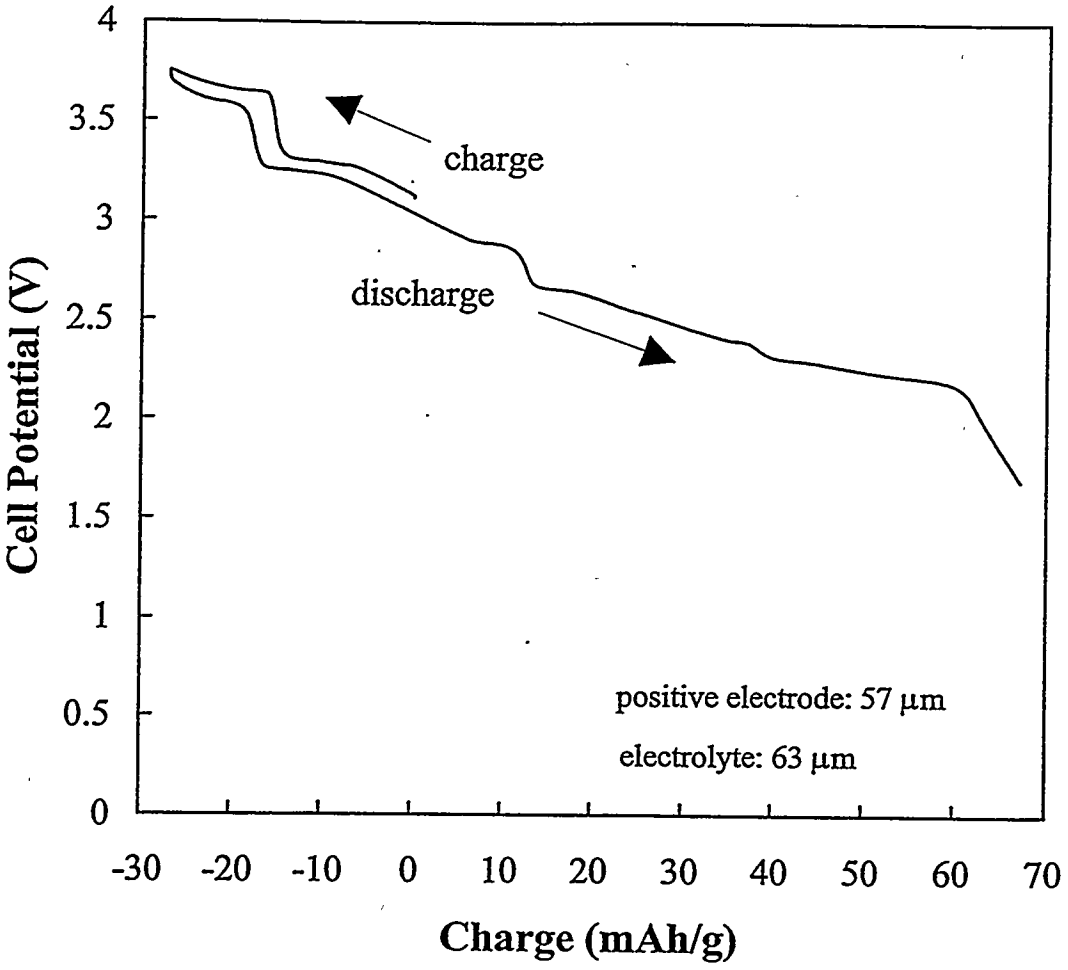

Figure 3-2. The first charge and discharge curve of a Na/$PEO_{20}NaCF_3SO_3$/Na_xCoO_2 cell at 85°C. The composite positive electrode contains 20 v/o (48 w/o) of $Na_{0.7}CoO_2$ and 10 v/o (11 w/o) of carbon black. The current density was 0.1 mA/cm^2 for both charge and discharge.

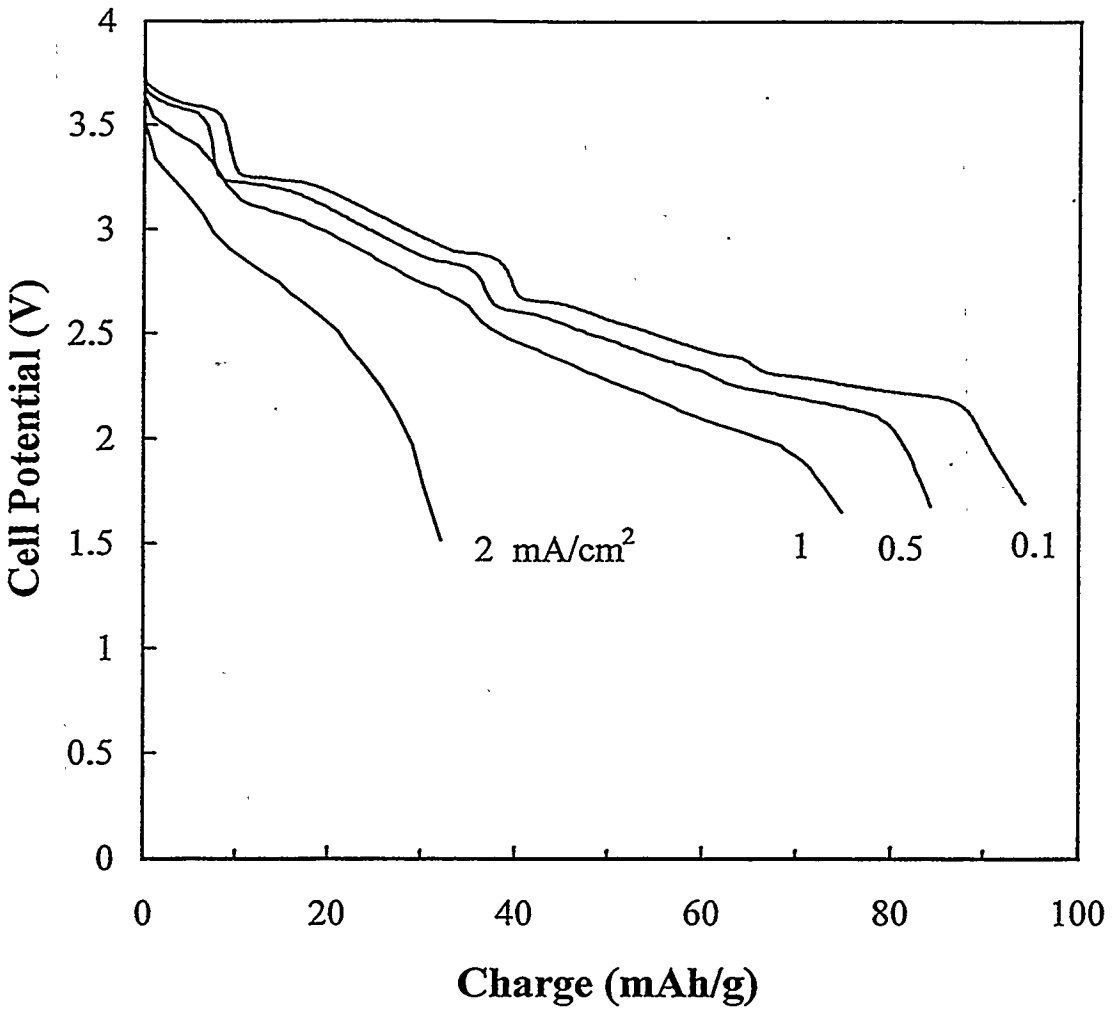

Figure 3-3. Discharge curves at various current densities for the $Na/PEO_{20}NaCF_3SO_3/Na_xCoO_2$ cell in Figure 3-2 at 85°C.

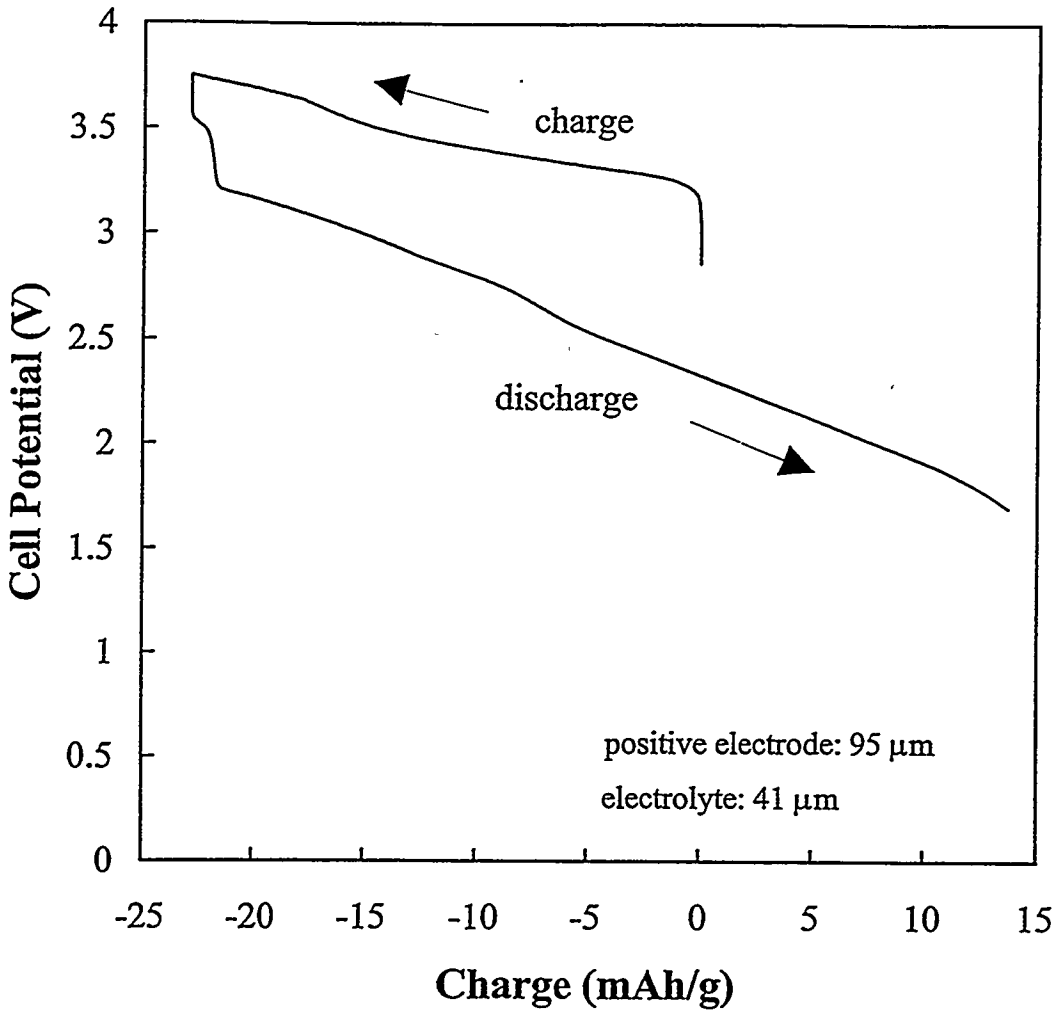

Figure 3-4. The first charge and discharge curve of a $Na/PEO_{20}NaCF_3SO_3/Na_xCoO_2$ cell at 85°C. The composite positive electrode contains 30 v/o (64 w/o) of $Na_{0.7}CoO_2$ but no carbon black additive. The current density was 0.1 mA/cm^2 for both charge and discharge.

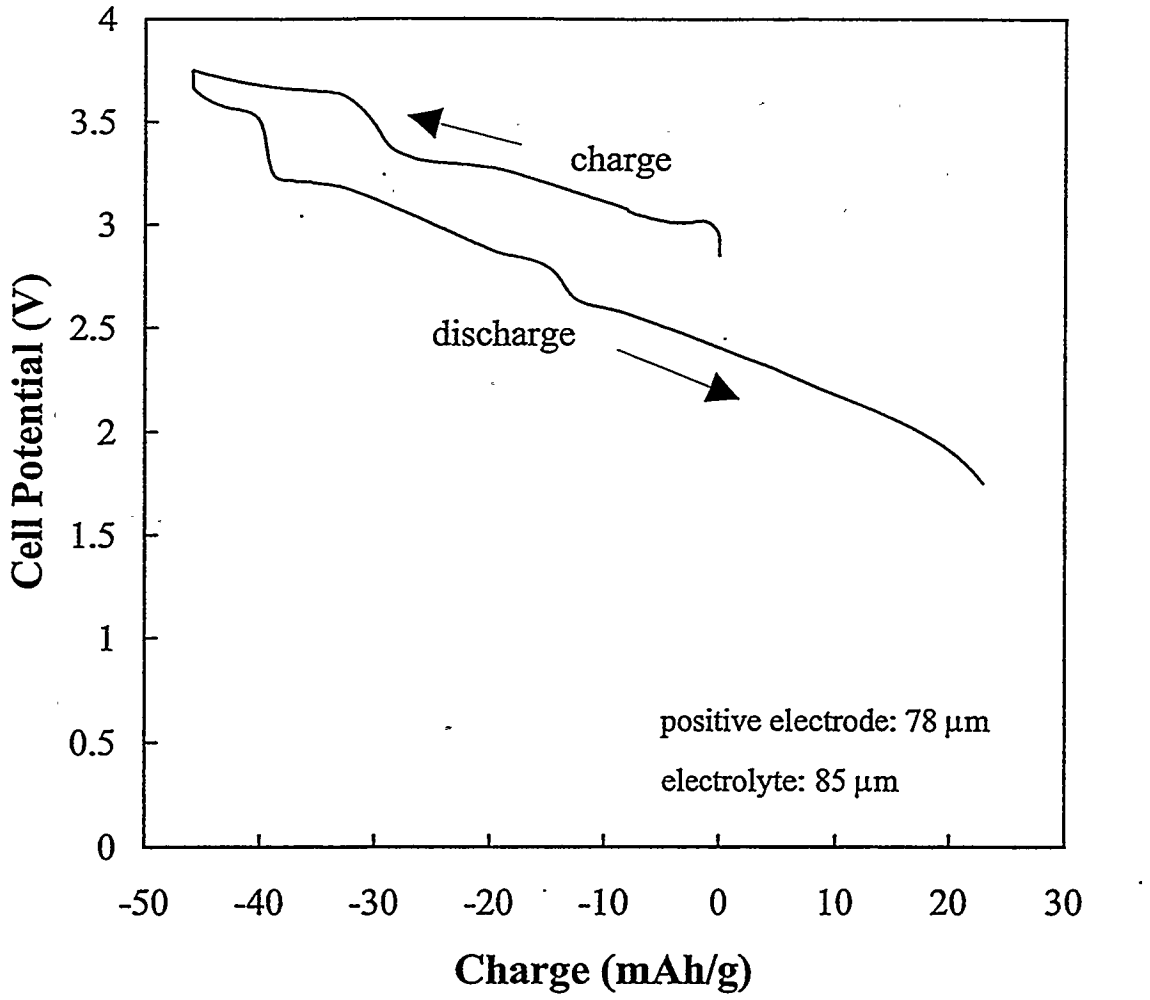

Figure 3-5. The first charge and discharge curves of a $Na/PEO_{20}NaCF_3SO_3/Na_xCoO_2$ cell at 85°C. The composite positive electrode contains 40 v/o (74 w/o) of $Na_{0.7}CoO_2$ but no carbon black additive. The current density was 0.1 mA/cm^2 for both charge and discharge.

PART II SOLID STATE POLYMER ELECTROLYTES

Chapter 4 Transport Properties of Solid State Polymer Electrolytes

4.1 Introduction

Polymer electrolytes are formed by the dissolution of salts in ion-coordinating macromolecules. [1] These molecules contain atoms or groups that have electron-donor power to form coordination bonds with cations. A suitable distance between coordinating centers is required to avoid the formation of intrapolymer ion bonds that lead to a reduced ionic mobility. Low barriers to bond rotation are also necessary to allow ease of polymer segmental motion.

The mechanism of ion transport in polymer electrolytes is distinct from the processes occurring in liquid solutions, molten salts and crystalline solids. Ionic movement in polymer electrolytes is facilitated by local structural relaxation processes, but in a different manner from what occurs in liquid electrolytes. It is suggested that the structural relaxation provides time-dependent pathways or opportunities for ions to move between suitable sites, and also provides a mechanism of short-range transport of ions temporarily attached to the polymer chains. [2]

The transport mechanisms in polymer electrolytes are complicated by significant ion association resulting from the low dielectric constants of the hosts. The existence of ion association in polymer electrolytes is demonstrated from studies of activity coefficients, [3] ion-paring, [4,5] and the concentration dependence of ionic conductivities. [6,7] For these electrolytes, formed by dissolving a binary salt in a polymer solvent, all three

pair-wise interaction parameters (between cation and solvent, between anion and solvent, and between cation and anion) need to be considered when describing the transport processes in the solution. In practice, macroscopic transport properties, namely ionic conductivity (κ), salt diffusion coefficient (D), and ion transference number (t_+^o) are used. These quantities are related to the pair-wise interaction parameters (D_{+-}) through the following relations [8]

$$\frac{1}{\kappa} = \frac{-RT}{c_T z_+ z_- F^2}\left(\frac{1}{D_{+-}} - \frac{c_0 z_-}{c_+\left(z_+ D_{0+} - z_- D_{0-}\right)}\right) \qquad [1]$$

$$D = \frac{c_T}{c_0}\left(1 + \frac{d\ln\gamma_\pm}{d\ln m}\right)\cdot\left(\frac{D_{0+}D_{0-}\left(z_+ - z_-\right)}{z_+ D_{0+} - z_- D_{0-}}\right) \qquad [2]$$

$$t_+^o = 1 - t_-^o = \frac{z_+ D_{0+}}{z_+ D_{0+} - z_- D_{0-}} \qquad [3]$$

The most commonly reported property of polymer electrolytes is the conductivity. [1,9,10]. The value reflect the cumulative mobility of all ionic species present. Ion transference numbers, on the other hand, allow the evaluation of the mobility of individual ionic species such as the one of prime interest. By definition, a transference number of one ion is the fraction of current carried by that ion in the absence of concentration gradients. It should be noted that a transference number is the overall response of species containing the ion of interest. Transference numbers are useful quantities in evaluating the interaction of an ionic constituent with the solvent and the degree of aggregation of ion species.

The transport properties are crucial in determining how fast a cell can be

discharged while still utilizing most of the electrode capacity. The effects of these properties on cell performance have been described and modeled in liquid electrolyte systems, [11] and in lithium/polymer electrolyte and lithium-ion batteries. [12,13] A low electrolyte conductivity would lead to a large ohmic loss and hence a small cell potential. The ohmic loss also increases over the course of discharge as the reaction front propagates into the back of the cathode, requiring a longer pathway for lithium ions to travel to reach the reaction front. [14] This would cause an early drop-off of cell potential, and also an increasingly sloping discharge curve, which is not desired in many applications. A low cation transference number, coupled with a low diffusion coefficient, would adversely affect cell performance by forming a large concentration polarization, leading to depletion of the electrolyte or solubility limitations.

It is generally believed that the anion is more mobile than the cation in lithium polymer electrolytes (lithium ion transference numbers less than 0.5). Efforts have been made to increase the lithium ion transference number. These include fixing the anion onto the backbone of the polymer chain [15,16] and use of large, and hence relative immobile, anions. However, these approaches resulted in dramatic decreases of ionic conductivities, implying that anion conduction is significant in these solutions.

Various techniques have been used to measure the transference numbers in polymer electrolytes, especially in poly(ethylene oxide) systems. These include the steady-state current technique (potentiostatic polarization technique), [17,18,19,20] ac impedance techniques, [21] pulse-field gradient NMR techniques, [22,23,24] radio-tracer diffusion experiments, [25] EMF measurements on concentration cells, [3] Hittorf method, [26] and others.

[27,28] There has been a lot of discussion on the validity of these methods for electrolytes experiencing ion association. The results derived from these techniques have also appeared to be in conflict. The discrepancies can probably be explained by invalid assumptions made in the analyses, including not accounting for the concentration dependence of transport properties or the assumption of an ideal solution. Detailed critiques on the steady-state current [29] and the ac impedance methods [30] have appeared in the literature. These and other methods will be discussed in more detail in the Discussion section.

In the present study, a novel method to measure the transference number is developed. [31] This method is derived from concentrated solution theory and is rigorous for any binary electrolyte. A complete set of transport properties for one particular polymer/sodium salt electrolyte system is measured. The solution is sodium trifluoromethanesulfonate ($NaCF_3SO_3$) in poly(ethylene oxide) (PEO), which is the sodium analog to the well-known $PEO_nLiCF_3SO_3$. The $PEO_nNaCF_3SO_3$ system has been studied by several authors [32,33] and has been used successfully in cells using sodium negative electrodes and cobalt oxide positive electrodes as have been shown in chapter 2. All three transport properties, as well as the mean molar activity coefficient of the salt, are measured over a wide range of concentrations. These properties will be used in chapter 5 to analyze and optimize the electrolytes.

4.2 A Novel Method to Measure the Transference Number

Polymer electrolytes usually need to be heated above the glass transition temperature in order to be conductive. Studies on polymer electrolyte systems reveal that complicated equilibria exist in polymer electrolytes. Eutectic-type phase diagrams are reported for several PEO based lithium salt electrolytes. [6,34] One such an example is $PEO_nLiCF_3SO_3$. However, this electrolyte system exhibits a complicated response dependent of the electrolyte concentration. Interpreting these results using the phase diagram certainly is not sufficient. Polymer electrolytes are also very thermal-history dependent and exhibit aging effects, indicating that these electrolytes usually are not in their equilibrium states. Considering the complexity of polymer systems and also the lack of phase equilibrium information, the $PEO_nNaCF_3SO_3$ system is treated as a homogeneous phase at the cell operation temperature (85°C) in the present study.

In spite of ion association, there are three independent species in a binary electrolyte, as long as ion exchange and aggregation reactions are fast enough to be in equilibrium. These are chosen to be Na^+, $CF_3SO_3^-$, and PEO for $PEO_nNaCF_3SO_3$ solutions, without regard for microscopic speciation. The concentrations of the other species can be related through equilibrium expressions.

Measurement of the transference number is complicated by the nonideality of the solution, which necessitates knowledge of the thermodynamic factor. Assuming electroneutrality, the concentrated binary electrolyte is described by the three equations [35]

$$\frac{\partial c}{\partial t} + v \cdot (D\nabla c) = \nabla(D\nabla c) - \frac{c_o \overline{V_o}}{F}(i \cdot \nabla t_+^o) \qquad [4]$$

$$\nabla \cdot v = \frac{\overline{V_e}}{F}\left(i \cdot \nabla t_+^o\right) \qquad [5]$$

where v^0 is the volume average velocity, and

$$i = -\kappa\nabla\Phi + \frac{2\kappa RT}{F}\left(1+\frac{d\ln f_{\pm}}{d\ln c}\right)\left(1-t_+^0\right)\nabla\ln c \qquad [6]$$

The potential in Eq. 6 is that measured with respect to a lithium reference electrode in the solution. The reference velocity used is the volume-average velocity, and the partial molar volume of the salt is set to be constant. From Eq. 6, the expression for the potential of a concentration cell can be found by setting $i = 0$

$$\nabla\Phi = \frac{2RT}{F}\left(1+\frac{d\ln f_{\pm}}{d\ln c}\right)\left(1-t_+^0\right)\nabla\ln c \qquad [7]$$

The potential of this cell can be used to determine t_+^0 if the thermodynamic factor, $(1+d\ln f_{\pm}/d\ln c)$, is known.

Unfortunately, a reliable method of determining the mean molar activity coefficient for solid polymer electrolytes without knowledge of t_+^0 has not been developed. Theoretically, by employing a cell configuration

$$M/PEO_nMX/X$$

comprised of cation electrode and anion electrode, and measuring the cell potential as a function of electrolyte concentration, it is possible to determine the activity coefficient through

$$dE/d\ln c = (2RT/F)(1+d\ln f_{\pm}/d\ln c) \qquad [8]$$

However, the anion electrode is difficult to develop due to the unusual anion species commonly used in polymer electrolytes (*e.g.*, $CF_3SO_3^-$, $N(CF_3SO_2)_2^-$). Other methods such as vapor pressure measurements used for low molecular weight solvents can not be

used in solid polymer electrolytes. Knowledge of the transference number is, therefore, essential to determine the activity coefficient for these electrolytes.

In fact, both the transference number and the activity coefficient can be determined simultaneously by using two similar yet orthogonal experiments. The first experiment is the standard concentration cell measurements using a cell configuration

$$Na/PEO_nNaCF_3SO_3/PEO_mNaCF_3SO_3/Na$$

The cell potential as a function of n and m, U_{mn}, is determined according to Eq. 7, by the values of both the transference number and the activity coefficient. These results are then tabulated or plotted as U_{mn} *vs.* n (fixed m) and used in the second experiment.

The second experiment involves passing a constant current through the cell

$$Na/PEO_nNaCF_3SO_3/Na$$

for a short amount of time, t_i. The time should be sufficient to establish concentration gradients at the electrode surfaces, but not long enough for the concentration boundary layers to propagate to the center of the cell ($t_i << L^2/D$). Under these conditions, the experiment can be modeled as a semi-infinite diffusion problem. The excess salt on one side of the cell (or depleted salt on the other side) is directly proportional to the transference number.

Figure 4-1 provides a diagram of the cell under consideration. Initially the cell is polarized by passing a constant current I through the cell for some time t_i. In the case of constant physical properties, Eq. 4 in one-dimension is [36]

$$\frac{\partial c}{\partial t} = D\left(\frac{\partial^2 c}{\partial x^2}\right) \qquad [9]$$

with boundary conditions

$$\frac{\partial c}{\partial x}(x=0) = -\frac{I\left(1-t_+^o\right)}{FD} \qquad [10]$$

and

$$c(x=0 \text{ and } x=\infty) = c_\infty \qquad [11]$$

The first boundary condition above assumes that a charge-transfer reaction of the form

$$Na \Leftrightarrow Na^+ + e^-$$

occurs at the electrode/solution boundary, which is consistent with the species chosen to exist in the solution under the macroscopic model. The last boundary condition implies a thick cell such that $L >> (Dt_i)^{1/2}$. The solution to this problem is [37]

$$c(x=0) = c_\infty + \frac{2t_-^o}{F(\pi D)^{1/2}}\left(It_i^{1/2}\right). \qquad [12]$$

$[c(x=0)-c_\infty]$ will be referred to as Δc, the concentration difference across the half-cell to which the electrode responds. Note that there are two of these regions in the cell, one adjacent to each electrode, and thus the values of Δc given in Eq. 12 must be multiplied by two to give the full-cell concentration difference. Equation 12 provides an expression for the concentration existing adjacent to one electrode after constant-current polarization for a given amount of time.

Equation 12 predicts a linear dependence of Δc on the quantity $(It_i^{1/2})$, which fails at large values due to the concentration dependence of the transport properties. However, at small enough values of the quantity $(It_i^{1/2})$, the linear dependence of Eq. 12 will hold even for concentrated solutions.

The transference number, evaluated at the bulk concentration c_∞, can be determined from Eq. 12, if the size of the concentration difference is known. A similar situation exists in the Hittorf method, where at this point the two ends of the cell would be separated and an analytical technique would be utilized to determine the average concentration at either end. Instead, an indirect method that takes advantage of the results from the previous concentration-cell experiments is used in this study.

After passing the current I through the cell for time t_i, the current is interrupted, and the potential monitored. The value of the potential just after current interruption, *i.e.*, after double-layer discharging but before the concentration gradients have had time to relax, is recorded. In this way a plot of $\Delta\Phi$ *vs.* $(It_i^{1/2})$ is generated for each bulk concentration. The potential, $\Delta\Phi$, can be related to the concentration variation by concentration-cell experiments through Eq. 7, when Δc is small relative to its bulk concentration

$$\Delta\Phi = \frac{1}{c_\infty}\left(\frac{dU}{d\ln c}\right)\Delta c \qquad [13]$$

and U(c) represents the concentration cell data. The potential across the galvanostatic polarization cell is then found to be:

$$\Delta\Phi = \frac{4t_-^\circ}{c_\infty F(\pi D)^{1/2}}\left(\frac{dU}{d\ln c}\right)\cdot\left(It_i^{1/2}\right) \qquad [14]$$

If the slope of a plot of $\Delta\Phi$ *vs.* $(It_i^{1/2})$ is referred as m, then the transference number of the anion is

$$t_-^o = \frac{mc_\infty F(\pi D)^{1/2}}{4} \Big/ \left(\frac{dU}{d\ln c}\right) \qquad [15]$$

The quantity dU/dlnc is the slope of the concentration cell data. The transference number calculated corresponds to the bulk value at the concentration c_∞.

A disadvantage of this method, when compared to classical methods of measuring t_+^o, is that it relies on three separate experimental quantities (m, D, and dU/dlnc) and is thus highly susceptible to experimental error. But, considering the simplicity of the method and the lack of unwarranted assumptions, it is worthwhile to pursue this approach. A more detailed comparison of various methods of measuring the transference number follows in the Discussion section.

Once the transference number is known, the mean molar activity coefficient of the salt can be extracted from concentration cell results. This is calculated from

$$\left(1+\frac{d\ln f_\pm}{d\ln c}\right) = \frac{F}{2RTt_-^o}\left(\frac{dU}{d\ln c}\right) \qquad [16]$$

and must also be evaluated at each bulk concentration.

4.3 Experimental

Electrolytes of different concentrations, $PEO_nNaCF_3SO_3$, were made by a solvent evaporation method. Poly(ethylene oxide) (PEO) (average MW = 5,000,000 g/mol, Aldrich) and sodium trifluoromethanesulfonate ($NaCF_3SO_3$) in the desired ratio in acetonitrile (Aldrich, HPLC grade) were well mixed and cast onto a Teflon-coated plate.

Upon completion of solvent evaporation, electrolytes were dried in vacuum for at least three days before use. Films used were generally 100 μm thick and very uniform. Thicker films were formed by stacking and heating several films together.

The salt concentration was calculated from the salt mass fraction (ω_e) using the formula

$$c = \frac{\rho \omega_e}{M_e} \qquad [17]$$

Assuming the molar volume of the salt is constant, the density of the electrolyte is

$$\rho = M_e c_e + M_o c_o$$

Since the sum of the salt fraction volume and the polymer volume fraction is unity:

$$c_e \overline{V_e} + c_o \overline{V_o} = 1$$

the density can be further expressed in terms of the salt mass fraction ω_e and the polymer density ρ^o_{PEO} ($\rho^o_{PEO} = M_o / \overline{V_o}$):

$$\frac{1}{\rho} = \frac{1}{\rho^o_{PEO}} + \omega_e \left(\frac{\overline{V_e}}{M_e} - \frac{1}{\rho^o_{PEO}} \right) \qquad [18]$$

The molar volume of the salt ($\overline{V_e}$) was obtained from a linear fitting of density data measured for salt-free PEO and $PEO_8NaCF_3SO_3$ samples.

Salt-free PEO films and $PEO_8NaCF_3SO_3$ films were cast as described above. They were weighed using a Mettler AE 163 balance with a precision of 0.01 mg, and the thickness of the films was measured using a Mitutoyo micrometer with a precision of 1 μm. Films used were in the range of 150 to 450 μm in thickness and have an area of 0.9 cm^2. PEO films give a density of 1.01 g/cm^3, averaged from three samples, with a

standard deviation of 0.020, and $PEO_8NaCF_3SO_3$ films give a density of 1.31 g/cm^3, averaged also from three samples, with a standard deviation of 0.017. The partial molar volume of the salt was found to be 36 cm^3/mol from Eq. 18 using these values.

Sodium electrodes were made as described previously in chapter 2. Experimental cells, $Na/PEO_nNaCF_3SO_3/Na$, were assembled in a helium-filled glove box with an oxygen level less than 1 ppm. Cells were heated to 85°C for at least 5 hours prior to testing. A convection oven with a Eurotherm temperature controller was used as the heating source. Temperature variation was less than ±1°C during cell operation.

The restricted-diffusion method [35,38] was used to measure the diffusion coefficient of $NaCF_3SO_3$ in PEO (the principle of this method is described in the Results and Discussion section). Measurements were carried out entirely in the helium-filled glove box. Cells were polarized in galvanostatic mode using a computer-driven EG&G Princeton Applied Research 371 potentiostat/galvanostat and software developed in this laboratory. Usually 10 to 15 min of polarization time at 0.1 to 0.3 mA/cm^2 were used to establish concentration gradients for the diffusion coefficient measurements, although for the very dilute solutions smaller currents and times were required. The cells had a working area of 0.9 cm^2 and thickness of about 300 to 400 μm.

An identical procedure was used for assembling cells for the transference number measurements. Thick films (300 to 400 μm) were used so that semi-infinite diffusion conditions applied for a sufficient amount of time upon passage of current. The current densities employed were similar to those used above, but the polarization times were much shorter (about 1 min). The time elapsed to record the potential data after current

interruption was 0.5 s. The double-layer capacity is presumably discharged completely during this period, and mass transfer polarization hasn't change.

Conductivities were measured using the standard ac impedance technique with a Solartron SI 1286 electrochemical interface and a 1254 four-channel frequency response analyzer. The cells were assembled as above for the restricted diffusion experiments and then transferred into an external convection oven. Strict temperature control was maintained, including using the same thermal history for each sample to ensure that the pseudo-equilibrium state of each polymer film was identical. The working area of the cells was 0.9 cm^2 for all experiments.

For the concentration-cell experiments, it is necessary to assemble the cell, heat it to the temperature of interest, and then measure the potential, without allowing the concentration gradient to relax to the electrode surfaces. A slightly different cell configuration was used for this experiment. Instead of being placed face to face, the two films were overlaped edgewise and connected to sodium electrodes on the two ends. This gives a diffusion length of several centimeters and diffusion time on the order of days. The large distance between the electrodes is possible because no current is flowing. The potential difference was measured across the concentration cell with a Keithley 642 electrometer.

All measurements were performed over the range of concentrations: $0.14 \leq c(mol/l) \leq 2.58$, corresponding to $160 \geq n \geq 8$ in $PEO_nNaCF_3SO_3$. The concentration cell data were taken over a larger range of concentrations: $0.05 < c(mol/l) < 4.71$, to improve the accuracy in the differentiation of the data.

4.4 Results and Discussion

4.4.1 Ionic Conductivity

The conductivity measurements were conducted using the standard ac impedance method. The impedance response of a $Na/PEO_nNaCF_3SO_3/Na$ cell with frequency was recorded in a complex-plane plot. An example of these plots is shown in Fig. 4-2. The ohmic resistance of the electrolyte is taken to be the high-frequency intercept on the real axis, or an extrapolation to the real axis if necessary. The conductivity of the electrolyte is the reciprocal of resistance multiplied by the thickness and divided by the area of the sample. These values as a function of concentration at 85°C are plotted in Figure 4-3. This curve is complicated, with a maximum at a concentration of 1.09 mol/l ($PEO_{20}NaCF_3SO_3$). As might be expected, the shape of this curve is very similar to that found for the conductivity of $PEO_nLiCF_3SO_3$ solutions at a similar temperature, although somewhat higher in magnitude. [39] The conductivity of the lithium system also exhibits a maximum at approximately the same concentration (n = 18 in $PEO_nLiCF_3SO_3$), although it has a second maximum at a very low concentrations (n = 100) that was not seen here. The conductivity of the sodium salt electrolyte decreases at both low and high concentrations. The decrease at low concentrations is presumably due to a decrease in charge carriers, and the decrease at high concentrations due to a decrease in carrier mobility. When more salt is added to an electrolyte, transient cross linking by ionic species and consequently chain entanglement increase, leading to an effective decrease in

carrier mobility.

4.4.2 Salt Diffusion Coefficient

Salt diffusion coefficients are obtained using the restricted method. [35,38] A constant current was passed through a $Na/PEO_nNaCF_3SO_3/Na$ cell to establish a concentration gradient in the electrolyte. The potential signal, which is proportional to the concentration variation when the variation is relatively small, was monitored after the current was interrupted. The linear relationship between the potential signal and concentration variation can be seen later in the concentration-cell experiments. It has been shown that the electrolyte concentration at the electrode interface relaxes exponentially with time

$$\Delta c = \text{constant} + \exp(-\pi^2 Dt/L^2) \qquad [19]$$

when Δc is small. Since the concentration variation is proportional to potential, the salt diffusion coefficient can be calculated from the slope of a plot of $\ln(\Delta\Phi)$ *vs.* time

$$d\ln(\Delta\Phi)/dt = -\pi^2 D/L^2 \qquad [20]$$

An example of this plot is given in Figures 4-4 for an electrolyte $PEO_{55}NaCF_3SO_3$, where (a) shows the experimental data (potential *vs.* time) and (b) is the semi-logarithmic plot of (a). The slope must be taken after sufficient time has elapsed for linear behavior (on the lower plot) to be observed.

The results of these measurements are compiled as a plot of D *vs.* c in Figure 4-5. The diffusion coefficient decreases with concentration at all data points except for a local

minimum at 0.28 mol/l (n = 80). The values found here for the diffusion coefficient of sodium triflate are similar to those reported for lithium triflate ($D = 7.5 \times 10^{-8}$ cm^2/s at n = 45). [3] The steady decrease in the salt diffusion coefficient at high salt concentrations suggests a mechanism similar to that seen in the conductivity data, *i.e.*, increasing salt concentration is leading to increased chain entanglement and decreased ion mobility.

The scattering of the calculated diffusion coefficient values resulting from the experimental errors in thickness measurements and in slope fitting (relaxation time constant) was estimated for one electrolyte, $PEO_{55}NaCF_3SO_3$, as an example. The experimental data of the membrane was shown in Figure 4-4. The film thickness was measured at five different spots on the sample, giving an average value of 400 μm with a standard deviation of 2.44 μm. There was also some variation in the relaxation time constant fitting, depending on the time windows used to fit the curve. The period from 40 to 80 min in Figure 4-4 was used to obtain the slope for this sample. The variation in this quantity within this time range was checked by determining the fitting for four different time windows, namely the 40 min to 50 min time period, the next 10 min period, and so forth. These fittings gave a standard deviation of 0.0016/min with an average slope value of 0.0374/min. The error of diffusion values can then be estimated from

$$\left(\frac{\sigma_D}{D}\right)^2 = \left(\frac{2\sigma_L}{L}\right)^2 + \left(\frac{\sigma_s}{s}\right)^2 \qquad [21]$$

where σ_D and σ_s are the standard deviations of film thickness measurements and relaxation time constant fitting, respectively. The error is 4.4% for the measured membrane. The scattering of the diffusion coefficients measured from two different measurements on the

same sample was also checked for all the electrolytes with different concentrations. The deviations from the average values are all less than 5%.

4.4.3 Ion Transference Number and Thermodynamic Factor

The ion transference number is measured using the novel method developed in this work. This method, as described previously, combines two experiments: concentration cell measurements and galvanostatic polarization measurements. Concentration cells of the form $Na/PEO_nCF_3SO_3/PEO_mNaCF_3SO_3/Na$ where m = 8 and n varies from 4 to 500 were prepared as described in the Experimental section. In Figure 4-6, the potential differences of these cells are presented as a function of the natural logarithm of the concentration; the markers represent data points, and the solid line is a curve fit discussed in the next paragraph. Data points in Figure 4-6 represent the average value of two to five experiments for each concentration difference. It should be pointed out that negative values of the concentration-cell data (-dU/dlnc) need to be used in Eq. 15 according to the way the data was plotted (positive values for cells with $n < 8$).

Although there was about a 1 to 4 mV standard deviation in the concentration cell data, an accurate fit to the data points with a six-parameter function is used instead of an approximate fit with a simpler function. This choice is made because of the extreme sensitivity of the calculated transference numbers to the differentiation of this data fit. The data were fit by the equation

$$U = \nu(0) + \nu(1)c + \nu(2)\exp[-\nu(3)c + \nu(4)\exp[-\nu(5)c] \qquad [22]$$

with the fitting parameters

$$\nu(0) = 3.2807,$$

$$\nu(1) = -0.0020545,$$

$$\nu(2) = 62.521$$

$$\nu(3) = 0.0018733,$$

$$\nu(4) = 130.33,$$

$$\nu(5) = 0.028355$$

where U is in mV and c is in mol/l. The slope of Eq. 22 is the important quantity for evaluation of the transference number and thermodynamic factor.

Galvanostatic polarization of cells of $Na/PEO_nNaCF_3SO_3/Na$ cells provides a second experiment needed to extract the transference number and thermodynamic factor separately from the concentration-cell data. The potential difference across the cell as a function of the quantity $(It_i^{1/2})$ for several values of n in $PEO_nNaCF_3SO_3$ is plotted in Figure 4-7. These plots are linear for small values of $(It_i^{1/2})$, as predicted in the theoretical development (Eq. 14), and then deviate upwards at larger values. Deviations of these plots from linearity are possibly due to the concentration dependence of the transference number (discussion on this will be given later). The slope of this plot near the origin, *i.e.*, as $(It_i^{1/2})$ approaches zero, which is referred to as m, is the important experimental quantity. The predicted linear dependence is seen over the whole range of concentrations used here, *i.e.*, from n = 8 to n = 500. Figure 4-8 gives the experimental data for the slopes m as a function of the bulk salt concentration. Bear in mind that Figure 4-7 can be extrapolated rigorously into the third quadrant because the two electrodes are symmetric

and the curves are odd in ($It_i^{1/2}$); *i.e.*, the same results would result when a current of opposite direction is applied.

The transference number of the sodium ion *vs.* concentration, calculated using Eq. 15, is presented in Figure 4-9. At the higher concentrations, these transference numbers are lower than any of the values reported for lithium triflate in PEO, which tend to range from 0 to 0.5. The transference number decreases from its maximum value of 0.31 in the most dilute solution (0.05 mol/l) to a minimum of -4.4 in the most concentrated (2.58 mol/l). The transference number steadily decreases above the concentration of 0.56 mol/l (n = 40), where it goes through a local maximum of 0.09, and is negative over a large range of salt concentrations. A negative transference number has been seen for other systems, and has been explained in terms of complexation (formation of mobile triplets consisting of two anions and one cation). [40] However, considering the complexity of the results in Figure 4-9, it is unlikely that any simple speciation model would accurately describe this system.

The practical significance of these results is that large concentration gradients must develop in the polymer electrolyte in order to sustain current flow, a detrimental situation for battery performance. It is possible for a polymer electrolyte battery with a cationic transference number of zero or even less than zero to operate successfully. However, on discharge this cell will develop large salt concentration gradients; the magnitude of the concentration difference can be estimated from the steady-state value

$$\Delta c = \frac{I\left(1 - t_+^0\right)L}{FD} \qquad [23]$$

The large salt concentration gradient may lead to salt depletion or to salt solubility problems, depending on several factors such as the cell design and other physical properties.

Now that the transference number is known, the thermodynamic factor (1 + $d\ln f_{\pm}/d\ln c$) can be calculated from Eq. 16. The calculated value is given in Figure 4-10 as a function of the salt concentration. The thermodynamic factor generally decreases with increasing concentration from its dilute value, 0.64 at 0.11 mol/l, leveling off to 0.02 at 2:58 mol/l. The data have a local maximum at n = 40, similar to both the transference number and the diffusion coefficient data. For the most dilute concentrations, the thermodynamic factor seems to be approaching unity, which is the ideal-solution result. These activity coefficient results are a verification of the strong nonideality of the solid polymer electrolyte solutions. It is easy to show that, with such small values for the thermodynamic factor, making the erroneous assumption that this polymer electrolyte is an ideal solution would lead to large errors in the calculated transference numbers.

It should be stressed here that the calculated transference number and thermodynamic factor are sensitive to the differentiation of the concentration cell data. This is especially true for the most dilute data points because the slope $dU/d\ln c$ is largest in this region. Taking as many data points as possible from the concentration cell experiment is recommended, including points well outside of the range of concentration being studied, to assure the highest possible accuracy in the calculated values.

To justify using Eq. 15 to determine the transference number, which applies for constant transport properties, Eq. 4 and 6 can be solved simultaneously with all three of

the concentration-dependent transport properties presently measured, to compare to the experimental results. Before doing this, it is instructive to examine a limiting case that illustrates the effect of the variable transport properties on the galvanostatic polarization experiments without the complication of a numerical solution. The results given in Figures 4-4 and 4-5 demonstrate that the assumptions of a constant diffusion coefficient is valid over small ranges of the concentration. The poorest assumption is that of a constant transference number; from Figure 4-9 it is apparent that this condition does not hold even over very small ranges of concentration. If a linear relationship of the transference number as a function of concentration is assumed instead, the concentration difference across the cell after a constant-current polarization would be [36]

$$\Delta c = \frac{2t_-^o}{FD^{1/2}}\left(It_i^{1/2}\right)\left(\frac{1}{\pi^{1/2}} - \frac{\zeta}{8} + \frac{\zeta^2}{12\pi^{1/2}} + O\left(\zeta^4\right)\right) \qquad [24]$$

where the perturbation parameter ζ is

$$\zeta = \frac{2c_\infty}{FD^{1/2}}\left(\frac{dt_+^o}{d\ln c}\right)\left(It_i^{1/2}\right). \qquad [25]$$

The parameter ζ is proportional to the slope of Figure 4-9, *i.e.* $dt_+^o / d\ln c$. One can show that $\zeta < 0.1$ over the range of concentrations covered in this work. This leads to the following potential difference across the cell

$$\Delta\Phi = \frac{4t_-^o}{c_\infty FD^{1/2}}\left(\frac{dU}{d\ln c}\right)\left(It_i^{1/2}\right)\left(\frac{1}{\pi^{1/2}} + \frac{\zeta^2}{12\pi^{1/2}} + O\left(\zeta^4\right)\right) \qquad [26]$$

Notice that the first correction term in Eq. 26 is of $O(\zeta^2)$ because the terms of $O(\zeta)$ from either side of the cell in Eq. 24 cancel one another, a fortuitous situation. Equation 26

allows the simulation of the polarization experiment up to larger values of ($It_i^{1/2}$) where the linear dependence of $\Delta\Phi$ on ($It_i^{1/2}$) no longer holds. However, with the small values of ζ used in the present experiments, Eq. 26 confirms that linear behavior should always be observed.

With all necessary properties known, it is possible to use the numerical solution of the governing equations to simulate the experimental method. This can be used to support the validity of the experiments as well as provide more detailed information about the concentration profiles during the experiments. It is especially interesting to examine the time required to reach a limiting current, as well as the effect of using too thin a membrane so that semi-infinite diffusion conditions no longer apply. Either of these situations should be avoided in measurements.

Figure 4-11 demonstrates some of the comparisons between the theoretical simulations and the experimental data out to larger values of $It_i^{1/2}$. Each simulation curve uses the same parameters and cell specifications as in the experimental work, as well as all of the variable physical properties. Equations 4 and 6 are solved by converting them into finite-difference equations which are subsequently linearized and solved using BAND. [8] The effect of the fluid motion, generated by the flow of current, on the concentration profiles is ignored here. Because all of the action is confined to the region near the surface of the electrodes, a savings in computational effort is obtained by using either a variable mesh spacing or scaling the equation (with $x/t^{1/2}$) to recognize this fact.

The agreement near the origin for the data shown in Figure 4-11 is always good, and at larger values the agreement is also reasonable. The simulation results all exhibit the

same deviation upwards from linearity on these plots at larger values of $It_i^{1/2}$, as suggested by Eq. 26 and seen in the experimental data.

Interestingly, by using the simulations to explore the use of different values of the experimental parameters, it is found that a deviation upwards from linearity on Figure 4-11 is not the only possible result. Instead, this depends on the details of the experimental conditions, in particular the membrane thickness being used. For example, once semi-infinite diffusion conditions no longer apply, the potential difference across the cell begins to level off with $It_i^{1/2}$. On the other hand, if a limiting current is reached, then the curve does have a positive deviation from linearity.

4.4.4 Comparison of the Novel Method to Other Methods

It should be possible to compare the utility of this method of measuring the transference number to other known methods. The problems involved in measuring the transference number in a solid polymer electrolyte have been discussed already in the Introduction section. The results given above also support the fact that assumptions of constant transport properties or of ideality fail even at the most dilute concentrations used in the present work. For this reason, methods that are derived from dilute solution theory are not recommended for polymer electrolytes.

The steady-state current method is one of the most widely used. It measures the current response of a $Na/PEO_nNaCF_3SO_3/Na$ cell upon applying small potential. A steady-state current is obtained once migration of anions is balanced by diffusion in the

opposite direction. The ratio of the steady-state current over the initial current, after correcting for the interface impedance, was believed to be the cation transference number,

$$\frac{I_{ss}(\Delta V - I_i R_i)}{I_i(\Delta V - I_{ss} R_{ss})} = t_+^o \qquad [27]$$

This method has recently been analyzed by Doyle and Newman from the concentrated solution theory point of view, and the following relationship is found [29]

$$\frac{I_{ss}(\Delta V - I_i R_i)}{I_i(\Delta V - I_{ss} R_{ss})} = \frac{1}{1 + \frac{2RT\kappa}{F^2 D c_\infty}\left(1 + \frac{d\ln f_\pm}{d\ln c}\right)(1 - t_+^o)^2} \qquad [28]$$

The quantity on the left of Eq. 28, which was believed to be the transference number from steady state current method, is theoretically related to all three transport properties as well as the thermodynamic factor. To obtain the transference number, it is neccessary to know these values in addition to the initial and steady-state current and the interfacial impedances required in steady-state current measurements. When, as treated in dilute solution theory, the thermodynamic factor and ion-ion interaction are ignored, the expression indeed reduces to Eq. 27.

A large error could be introduced using the conventional steady state current method for a concentrated solution. This may be demonstrated with a highly concentrated polymer solution $PEO_8NaCF_3SO_3$. The ionic conductivity, salt diffusion coefficient, sodium transference number, and the thermodynamic factor of the $PEO_8NaCF_3SO_3$ solution are

$\kappa = 1.54 \times 10^{-4}$ S/cm

$D = 1.47 \times 10^{-8}$ cm^2/s

$$t_+^o = -4.38$$

and

$$(1 + d\ln f_\pm / d\ln c) = 0.023$$

Pluging these values to the right side of Eq. 28 gives a value of 0.37. This value would be erroneously taken to be the sodium ion transference number with the steady state current method.

AC impedance techniques have also been used to measure the transference number in polymer electrolytes. The low frequency Warburg impedance loop of electrolyte is related to the cation transference number by

$$t_+^o = \frac{1}{1+[R_e / Z_\varpi(0)]} \qquad [29]$$

where $Z_\varpi(0)$ is the width of the low-frequency impedance loop and R_e is the electrolyte resistance. Pollard and Comte [30] have analyzed this method from the standpoint of concentrated solution theory, and found that for a monovalent binary solution the cation transference number is related to more parameters than is shown in Eq. 29,

$$t_+^o = \left(\frac{F^2 D c_\infty Z_\varpi(0) A}{2RTc_o \overline{V_o} L\left(1+d\ln f_\pm / d\ln c\right)} \right)^{1/2} \qquad [30]$$

In order to obtain the transference number, knowledge of the salt diffusion coefficient and the thermodynamic factor is needed.

The most direct measurement of the transference number from a theoretical perspective comes from the Hittorf method. This method is very similar to the galvanostatic method that is developed in the present work. As discussed earlier, the

electrolyte concentration changes upon passage of current as a result of non-unity sodium ion transference number. The concentration change at the electrode interface can be measured to determine how many anions have been transferred to the electrode, and then the anion transference number can be calculated. In the Hittorf method the total amount of anions (Δm) transferred across the electrolyte upon passing a total amount of charge across the cell (Q) is measured by employing elemental analysis techniques. The ion transference number can be extracted from this quantity through

$$t_-^o = 1 - t_+^o = \frac{F\Delta m}{Q} \qquad [31]$$

This measurement has been made successfully by one group on a PEO-based system, but only one salt at a single concentration was studied. It is interesting that this measurement gave one of the lowest values for t_+^o yet reported (0.06). The difficulty lies in the fact that the polymer must be sectioned and analyzed after the passage of current. This leads to problems of separating the polymer electrolyte from the electrode surfaces, which motivated researchers to use either lithium alloy or lead electrodes from which separation is easier. Also, longer diffusion lengths (perhaps 1 to 2 cm) become necessary in order to section the polymer easily; however, these longer diffusion lengths make passing current difficult for poorly conducting polymer electrolytes.

Radio-tracer and pulse-field gradient nuclear-magnetic-resonance (NMR) measurements are the other methods that have been used to measure the transference number. [23,24] Radioactive isotopes are used in the radio tracer technique and aligned nuclear spins are created in the NMR measurements. The diffusion coefficients of the

labeled nuclei are determined to calculate the ion transference number through

$$t_+^o = \frac{D_+}{D_+ + D_-} \qquad [32]$$

The mobility of the ions has been reported to be accessible in the presence of an electric current. In this case the transference number can be found from

$$t_+^o = \frac{c_o u_+ AF}{I}. \qquad [33]$$

It is recognized that such methods are valid only for dilute solutions in which the salt is completely dissociated. When other species such as ion pairs exist in the solution due to association, the measured diffusion coefficients and ionic mobilities are not the ones sought, but contributed to by all the species containing the ion of interest in the solution. Interpretation of the results on the measurements could be very difficult or even impossible.

Based on the above analysis, it is concluded that no single method of measuring the transference number in solid polymer electrolyte solutions is clearly the best method. At the present time, there appears to be a trade-off between the experimental difficulty and the theoretical simplicity of the various methods that are available. The Hittorf method, which is difficult experimentally, is the most direct from a theoretical perspective. Although the method presented in this paper has the advantage of experimental simplicity, the result is sensitive to the values of several other experimental quantities such as the salt diffusion coefficient and the concentration cell data. Considering this state of affairs, it seems likely that future research will lead to the development of even more novel methods of measuring either the transference number or the salt activity coefficient in solid polymer

electrolyte solutions.

4.5 Speciation

It is useful to discuss the issue of speciation in order to elucidate some of the effects of ion-ion interactions on the macroscopic transport parameters. Consider, for example, a case where the three independent species in the solution are Na^+, $Na(CF_3SO_3)_2^-$, and the polymer. For convenience, the sodium cation is referred as species 1 and the sodium triflate anion as species 2. The fluxes of the species in the absence of concentration gradients are

$$N_1^* = -u_1 F c_1 \nabla \Phi \qquad [34]$$

$$N_2^* = u_2 F c_2 \nabla \Phi \qquad [35]$$

where the superscript * denotes the actual species in solution. As any practical experiment or device will be able to determine only the net amount of sodium transported across the cell, the apparent fluxes need to be used

$$N_{Na^+} = N_1^* + N_2^* \qquad [36]$$

$$N_{CF3SO3^-} = 2N_2^* \qquad [37]$$

The current flow in the solution is

$$i = F(N_1^* - N_2^*) \qquad [38]$$

This allows us to calculate the experimentally accessible transference number as

$$t^o_{Na^+} = \frac{FN_{Na^+}}{i} = \frac{u_1 - u_2}{u_1 + u_2} \qquad [39]$$

Even from this simple model it is possible to justify a negative transference number when $u_2 > u_1$, *i.e.*, when more mobile negative triplet ions exist. Also, one should note that the existence of ion pairs does not affect the value of the macroscopic transference number because the transference number is defined in the absence of concentration gradients. Even if an equilibrium is allowed to exist between the above species and a neutral ion pair, the same result for Eq. 39 would be found.

To explore more complicated models of the microscopic speciation, equilibrium constants for the various ion-exchange processes have to be included. [36] For example, consider the case when there are the following species in solution: Na^+, $CF_3SO_3^-$, $Na(CF_3SO_3)_i^{(i-1)-}$, and the polymer, where i runs from 1 to n. These species are referred to with the subscripts 0 through N (N = n + 3), where 0 represents the polymer, 1 represents the sodium ion, 2 represents the triflate ion, 3 represents the ion pair, 4 represents the triplet, *etc.* As there are (n + 3) species and 3 of these are independent, n expressions of reaction equilibrium of the form exist

$$K_i = c_i/(c_1 c_2^{i-2}) \qquad [40]$$

In addition, the electroneutrality condition holds for the solution

$$c_1 = c_2 + 0 \cdot c_3 + 1 \cdot c_4 + \cdots\cdots + (N-3) \cdot c_N \qquad [41]$$

Combination of this with the n equilibrium expressions gives

$$c_1 = c_2/(1 - 1 \cdot K_4 c_2^2 - \cdots\cdots - (N-3) \cdot K_N c_2^{n-2}) \qquad [42]$$

Following the same procedure outlined previously, an expression for the apparent flux of sodium can be writen in terms of the actual flux of each species

$$N_{Na+} = N_1^* - N_4^* - \cdots\cdots - N_N^* \qquad [43]$$

The total current flow is

$$i = F(N_1^* + N_2^* + N_4^* + \cdots\cdots + N_N^*) \qquad [44]$$

The sodium ion transference number is then

$$t_+^o = \frac{FN_{Na^+}}{i} \qquad [45]$$

or

$$t_+^o = \frac{u_1 - u_4K_4c_2^2 - \cdots\cdots - u_NK_Nc_2^{N-2}}{u_1 + u_2\frac{c_2}{c_1} + u_4K_4c_2^2 + \cdots\cdots + u_NK_Nc_2^{N-2}} \qquad [46]$$

For simplicity, the following quantities are defined

$$A = u_1 - u_4K_4c_2^2 - \cdots\cdots - u_NK_Nc_2^{N-2} \qquad [47]$$

$$B = u_1 + u_4K_1c_2^2 + \cdots\cdots + u_NK_Nc_2^{N-2} \qquad [48]$$

$$C = c_2/c_1 = 1 - 1\cdot K_4c_2^2 - \cdots\cdots - (N-3)\cdot K_Nc_2^{N-2} \qquad [49]$$

Thus, the transference number can be expressed as

$$t_{Na^+}^o = A/(B + u_2C) \qquad [50]$$

An expression of this sort could theoretically be used to describe the concentration dependence of the macroscopic transference number in terms of the presumed constant mobility of the individual species and their equilibrium relationships. However, as these mobilities and equilibrium constants are unlikely to be available, this expression is simply used to explore the possible values of t_+^o. Eq. 50 will provide negative values of t_+^o under certain conditions, although it will never give a value smaller than negative one.

A model of speciation that could provide transference numbers with arbitrarily large negative values would include species of the form: Na^+, $CF_3SO_3^-$, $Na_i(CF_3SO_3)_{(i+1)}^-$,

and the polymer, where i runs from 1 to n. It is easy to see from this model that the negative species carry many more sodium ions than the net current, leading to negative values of $t_+^o < -1$. However, considering the infinite number of combinations of species that may exist in the solution and the lack of quantitative data on these species, the above considerations are not suggested as evidence of the existence of specific species. Again, it must be emphasized that the transport processes in solution are described completely by the three macroscopic, concentration-dependent transport properties, and any further studies surrounding speciation are extraneous. If one's only purpose is to model the performance of an electrochemical device that utilizes a solid polymer electrolyte, the information contained in the three transport properties is sufficient.

Figures 4-12 further illustrates, from the mass transport point of view, that a cell can be discharged regardless of the values of sodium ion transference. Figure 4-12 (a) illustrates the transport process in the electrolyte when the sodium ion transference number is unity. In this case, mass transport across the electrolyte is solely provided by the sodium ions. Once the anion is mobile, a concentration gradient occurs because the anion does not participate the electrode reaction. Anions travel under the electric field toward the anode and accumulate, resulting in increased salt concentration at this side and decreased concentration at the cathode side. A steady state is reached when the migration flux of anions is balanced by the diffusion flux that transport the anions in the opposite direction. It is easy to see then that when the sodium ion transference number is zero, as shown in Figure 4-12 (b), mass transport processes (current) can still be sustained. Although sodium ions don't move under the electric field in this case, they can still be

transported across by diffusion. According to Eq. 3 a sodium ion transference number equal to 0 results when D_{o+} is zero or D_{o-} is much greater than D_{o+}. When D_{o+} has a value of zero, the salt diffusion coefficient is zero according to Eq. 2, and mass transport does not occur. When D_{o-} is much greater than D_{o+}, the diffusion coefficient would have a finite value ($2D_{o+}$ for ideal solutions), and the cation can be transported by diffusion. Similarly, in the case of a negative sodium ion transference number, current can still be sustained, as shown in Figure 4-12 (c).

4.6 Conclusions

A novel method of measuring the transference number was developed in this work based on galvanostatic polarization experiments in combination of concentration-cell experiments. It is theoretically rigorous for any binary electrolytes, yet experimentally simple to carry out.

A complete set of transport properties was measured for one solid-polymer-electrolyte system: sodium trifluoromethanesulfonate ($NaCF_3SO_3$) in poly(ethylene oxide) (PEO) over a wide range of concentration (0.1 to 2.6 mol/l, corresponding to n = 160 to 8 in $PEO_nNaCF_3SO_3$) at 85°C. The conductivity was measured with ac impedance techniques and found to vary with the electrolyte concentration in a manner similar to that of $LiCF_3SO_3$ in PEO: increasing as concentration increases at low concentrations, going through a maximum and then decreasing when more salt is added. The salt diffusion coefficient was measured using the restricted diffusion method. The concentration

difference was extracted from the potential signals from $Na/PEO_nNaCF_3SO_3/Na$ cells. Diffusion coefficients also vary with concentration, decreasing as the electrolyte concentration increases.

The sodium ion transference number was measured using the novel method developed in this work. The transference numbers decrease strongly with electrolyte concentration, going from around 0.31 in the most dilute solution (0.05 mol/l) to -4.37 in the most concentrated solution (2.58 mol/l). Some discussion of the impact of microscopic speciation on the macroscopic transport properties is given to rationalize the large negative transference numbers. The thermodynamic factor was calculated and found to decrease with increasing salt concentration. These values indicate that the polymer-electrolyte solutions are highly nonideal.

Experiment results show that highly concentrated solutions have lower values of transport properties, when compared with moderately concentrated solutions. The effects of these values on cell performance will be investigated in the next chapter.

List of Symbols

A	area, cm^2, or parameter defined in equation 47
B	parameter defined in equation 48
C	parameter defined in equation 49
c	concentration of electrolyte, mol/l
c_i	concentration of species i, mol/l

c_T	total concentration of solution, mol/l
D	diffusion coefficient, cm^2/s
D_{ij}	pair wise interaction parameter between species i and j, cm^2/s
$f_{\pm}$	mean molar activity coefficient
E	cell potential, V
F	Faraday's constant, 96487 C/eq
i	current density, mA/cm^2
I	cell current density, mA/cm^2
L	separator thickness, cm
m	slope of polarization plot, $\Omega \cdot cm^2/s^{1/2}$,
	or concentration of electrolyte, mol/kg
M_e	molecular weight of the salt, g/mol
n	number of electrons involved in electrode reaction
N_i	flux of species i
Q	charge, C
R	universal gas constant, 8.3143 J/mol·K
R_e	resistance of electrolyte, $\Omega \cdot cm^2$
R_i	interfacial resistance at condition i
s	slope of $\ln\Phi$ vs. t plot
t	time, s
t_+^o	transference number of species i
T	temperature

u_i	mobility of species i, $cm^2 \cdot mol/J \cdot s$
U	potential of concentration cell, V
$v^{\square}$	volume-average velocity, cm/s
$\overline{V_e}$	partial molar volume of species i, cm^3/mol
ΔV	potential imposed on a cell, V
x	distance from the negative electrode, cm
z_i	charge number of species i
$Z_\omega(0)$	width of Warburg loop on Nyquist plot, $\Omega \cdot cm^2$
ζ	perturbation parameter defined in equation 24
κ	conductivity of the electrolyte, S/cm
ν	fitting parameters used in equation 21
$\gamma_\pm$	mean molal activity coefficient of an electrolyte
ρ	density of solution, g/cm^3
σ_i	standard deviation of quantity i
Φ	electrical potential, V
ϖ_i	mass fraction of species i

Subscript

0	solvent, or initial condition, or standard condition
+	cation

-	anion
e	electrolyte
ss	steady-state value
∞	infinity (bulk material property)

Superscript

0	with respect to the solvent
*	actual species in solution

Chapter 5 Polymer Electrolyte Optimization

5.1 Introduction

Transport properties of electrolytes are the critical factors to the performance of electrochemical cells. As has been shown in the previous chapter, these properties are very concentration dependent for the $PEO_nNaCF_3SO_3$ system. The choice of the initial salt concentration, therefore, is import to obtain the best rate capability from the system. The optimum initial salt concentration is also an important issue for economic reasons. It is advantageous to minimize the salt concentration to decrease the overall battery cost. For example, reducing the amount of $NaCF_3SO_3$ from 2.58 M ($PEO_8NaCF_3SO_3$) to 1.77 M ($PEO_{20}NaCF_3SO_3$) is significant since $NaCF_3SO_3$ can be one of the most expensive components in the cell.

The transport properties of $PEO_nNaCF_3SO_3$ have been shown decreasing as electrolyte concentration increases. A salt solubility limit, therefore, could be encountered as a result of larger concentration gradients for highly concentrated solutions. On the other hand, if too low a salt concentration is used, the battery's rate capability can also be compromised, as salt depletion in the porous electrode will occur even at low current densities. These phenomena are explored in more detail here as they are less well studied with solid polymer electrolytes and is critical to the optimization process. The performance of $PEO_nNaCF_3SO_3$ electrolytes in $Na/Na_{0.7}CoO_2$ cells is assessed by cell testing and also computer simulations using the differential transport properties measured

in the previous chapter.

5.2 Experimental

The P2 phase sodium cobalt oxide, $Na_{0.7}CoO_2$, was prepared by a glycine nitrate process as described in chapter 3. An aqueous solution of $NaNO_3$, $Co(NO_3)_3$, and glycine in the desired stoichiometric ratio was heated to 180°C in a stainless steel container. A dramatic combustion of the chemicals occurred when the solution dried. The resulting powders were heated to 750°C for 10 hours to complete the reaction, and then were ground with a mortar and pestle to about 1 μm in diameter.

Sodium cobalt oxide composite cathodes were made as described in chapter 2. The electroactive material, Shawinigan carbon balck, poly(ethylene oxide), sodium trifluoromethanesulfonate (in ratios of 8 and 20 ethylene oxide units per sodium, respectively), and a carbon dispersant (brij) were well mixed in acetonitrile and then cast onto Teflon coated glass plates. After air drying, the electrode films were cut to 3 cm^2 and dried in vacuum for a week. Polymer electrolytes of compositions $PEO_8NaCF_3SO_3$ and $PEO_{20}NaCF_3SO_3$ were made in a similar fashion. Salt concentration on a molar scale was calculated from density data and the partial molar volume of the salt. The detailed description of the density measurements was given in chapter 4. Sodium electrodes were made as described in chapter 2.

Cells were assembled in a helium-filled glove box with oxygen level below 1 ppm. All cell testing was done at 85°C. Galvanostatic charges and discharges were performed

at 0.1 to 2.5 mA/cm^2 for the $Na/PEO_8NaCF_3SO_3/Na_{0.7}CoO_2$ cell and the $Na/PEO_{20}NaCF_3SO_3/Na_{0.7}CoO_2$ cell using a computer controlled Princeton Applied Research (PAR) 371 potentiostat/galvanostat and software developed in this laboratory. A current of 0.55 mA/cm^2 was used in a symmetric cell of the form $Na/PEO_8NaCF_3SO_3/Na$ for the salt precipitation study.

5.3 Results and discussion

The discharge curves of the $Na/PEO_8NaCF_3SO_3/Na_{0.7}CoO_2$ cell and the $Na/PEO_{20}NaCF_3SO_3/Na_{0.7}CoO_2$ cell are given in Figure 5-1 (a) and 1 (b), respectively. The two cells were cycled following the same sequence to minimize complications from capacity fading. Cells were charged initially to 3.7 V before cycling since $Na_{0.7}CoO_2$ is in the half charged state. The current density was 0.1 mA/cm^2 for the initial charge, and 0.2 mA/cm^2 for subsequent charges. The discharge cut-off potential was eventually set to 1.8 V, though different values (1.5 V to 2.0 V) were tried for the first three cycles for the $Na/PEO_8NaCF_3SO_3/Na_{0.7}CoO_2$ cell. At 0.1 mA/cm^2, both cells can pass 110 mAh/g during discharge. With increasing discharge current, the charge capacity utilization decreases in both cells, but to a different extent. Larger capacities are obtained for the cell with a lower electrolyte concentration ($PEO_{20}NaCF_3SO_3$) at high current densities. For example, 38 mAh/g can be passed at 2.5 mA/cm^2 in this cell, in contrast to 10 mAh/g passed in the $Na/PEO_8NaCF_3SO_3/Na_{0.7}CoO_2$ cell at the same current level.

The two cells had similar cell configurations (the electrode capacity was 1.147

C/cm^2 for the $PEO_8NaCF_3SO_3$ cell and 0.918 C/cm^2 for the $PEO_{20}NaCF_3SO_3$ cell, based on $\Delta x = 0.6$ in Na_xCoO_2). Therefore, the difference in utilization can most likely be attributed to the difference of electrolytes used in these cells. The study on the transport properties of $PEO_nNaCF_3SO_3$ has revealed that the ionic conductivity, salt diffusion coefficient, and sodium ion transference number of this electrolyte system are very concentration dependent. The moderately concentrated solution, $PEO_{20}NaCF_3SO_3$, has a higher ionic conductivity, a higher salt diffusion coefficient, and also a higher sodium ion transference number when comparing to the highly concentrated $PEO_8NaCF_3SO_3$ solution. All these lead to smaller overpotentials across the electrolyte upon passing current and allow greater capacity utilizations at higher discharge currents. Utilization of electrode capacity is determined by one of the two limiting processes (in cases where the active electrode material is not the limiting factor), depletion of active species at the cathode or exceeding the solubility limit at the anode. Once these limiting conditions are reached, the cell potential will drop steeply. The time for the occurrence of these processes depends strongly on the transport properties. Longer discharge times are desired in order to attain better electrode capacity.

In general, the optimum initial salt concentration will be one which allows the battery to be discharged at the highest rate without reaching a transport-limited current. As the current density is increased, one will either drive the concentration to zero or exceed the salt solubility limit. Predicting which of these will occur, and also optimizing the salt content, is a more difficult task. It is likely that the rate capability of above two cells is limited by salt precipitation processes at the sodium electrode when relatively high

currents are used during discharge. When a lower initial salt concentration with better transport properties is used, the onset of salt precipitation brought on during the discharge is delayed. The development of concentration gradients in the polymer electrolyte is examined by computer simulations using the measured transport properties.

This is done for a $Na/PEO_{12}NaCF_3SO_3/Na$ cell undergoing a galvanostatic discharge. The previously measured transport properties are used to solve equations 4 and 6 in the previous chapter simultaneously. The fluid motion generated by the flow of currents is neglected, as this can be shown to have a very minor effect. [41] For simplicity only this symmetric cell is studied. The processes in the electrolyte phase in cells using composite electrodes is more complicated [12] and has not been investigated in the present study.

The simulation concentration profiles, shown in Figure 5-2, were generated by passing a current of 0.4 mA/cm^2 across a $Na/PEO_{12}NaCF_3SO_3/Na$ cell with the transport properties measured previously (transport properties of $PEO_8NaCF_3SO_3$ are used for solutions with higher concentrations than $PEO_8NaCF_3SO_3$). The impact of the variable physical properties is quite prominent; steeper profiles at the anode and a quicker propagation rate at the cathode are generated. The profiles given in Figure 5-2 are equally spaced in time at thirty-second intervals. As long as semi-infinite diffusion conditions hold, the concentration profiles scale with the value of $It_i^{1/2}$.

The steeper concentration profile at the anode likely leads to the onset of salt precipitation before a limiting current is reached at the cathode. This effect is due to the decrease in the sodium ion transference number and salt diffusion coefficient with

increasing salt concentration. An asymmetrical variation in concentration at the two electrodes can be clearly seen in Figure 5-3 when current I passes across the electrolyte for time t_i. Even at relatively small values of $It_i^{1/2}$, a large concentration variation exists across the cell. At larger values of $It_i^{1/2}$, the concentration difference changes in a complicated manner due to the variable physical properties. It should be noted that the anodic curve becomes linear above a concentration of about 2.58 M because the physical properties were taken to be constant above this value.

It is possible to predict the onset of a limiting current by using the simulated data of the form given in Figure 5-3. To do this, knowledge of the salt solubility limit in the polymer electrolyte is needed. This information, however, has not been found in the literature for $NaCF_3SO_3$ in PEO. Crystalline complexes with a ratio of three polymer to one salt are seen with many other lithium and sodium salts in PEO. [6] If $PEO_3NaCF_3SO_3$ were the highest polymer/salt complex possible, the salt solubility would be 5.94 M. To assess the salt solubility limit, transition-time experiments coupled with an analysis using the theoretical model and known transport properties were performed. This was done by constructing a $Na/PEO_8NaCF_3SO_3/Na$ cell, and discharging the cell at a constant current density of 0.55 mA/cm^2. The cell potential was monitored during the discharge. When the potential changes abruptly, either salt precipitation or a limiting current is assumed to have been reached.[10] The time for this to happen is referred to as the transition time.

Data for several experiments are compared in Figure 5-4. Each experiment was followed by an extended rest period (2 to 64 hours) during which the cell concentration profiles were allowed to relax to their initial values (manifested by a zero cell potential

difference reading). For repeated experiments at the same current density, the transition time is found to vary depending on the relaxation times between cycles. The transition time in a fresh cell occurs at $It_i^{1/2} = 21.4$ $mAs^{1/2}/cm^2$. According to the simulations, this equates to wall concentrations of about 0.10 M and 12.80 M at the cathode and anode, respectively. The concentration at the anode is well above the expected value of 5.94 M for a 3:1 polymer/salt crystalline complex. Later transitions occur at shorter times with the smallest being around $It_i^{1/2} = 11.0$ $mAs^{1/2}/cm^2$.

Relatively high current densities and thick membranes are used in this work such that semi-infinite diffusion conditions apply. This simplifies the theoretical analysis as plots such as Figure 5-3 can be used to determine the final wall concentrations. It should be noted that the predicted value of the maximum salt concentration in the cell will have some error due to the assumption that the transport properties are constant above an electrolyte concentration of 2.58 M. Also, the maximum concentration may be somewhat lower because the transient build-up of a salt film on the electrode is ignored. This causes the measured transition time to be longer than the actual time that it takes the salt to precipitate.

The transition time eventually converges on a steady value as shown in Figure 5-5. Successive transition-time experiments were carried out allowing only sufficient time for concentration profiles to relax before repeating the experiment ($L^2/D \approx 1$ hour). This steady-state value is assumed to resemble a true transition time as the effect of salt dissolution kinetics should be minimized. It is found that the transition time approaches the value of $It_i^{1/2} = 10.5$ $mAs^{1/2}/cm^2$. Simulations show that this corresponds to wall

concentrations of 0.70 at the cathode and 7.83 M at the anode. This anode concentration is still larger than the value of 5.94 M that was earlier rationalized as a possible maximum, but is now significantly less than the initial value from the transition time measured in a fresh cell.

The variation in transition time indicates that the cell history has an effect on the salt precipitation process. The initial precipitation process, with the fresh cell, takes much longer to occur, indicating a larger degree of supersaturation. Later discharges show a more rapid precipitation that is likely assisted by the previous salt precipitation processes perhaps *via* salt nucleation sites. As the wall concentration at the cathode is not zero during the experiments shown in Figures 5-4 and 5-5, a salt precipitation process and not a limiting current is probably occurring in the cell. The salt solubility of $NaCF_3SO_3$ in PEO is close to 7.8 M for the cycled electrolyte after stabilization has occurred. To describe properly the PEO/$NaCF_3SO_3$ system, however, the kinetics of the salt precipitation and dissolution processes needs to be studied in more detail than what has been done here.

It is now possible to analyze the discharge behavior of the Na/$PEO_nNaCF_3SO_3$/Na_xCoO_2 cells. At lower current densities, both cells can be discharged for rather long times (two hours at 0.1 mA/cm^2), attaining similar capacities. As the current density is increased, the attainable capacity for the $PEO_8NaCF_3SO_3$ cell drops off steeply as salt precipitation begins to occur during the discharge. The $PEO_{20}NaCF_3SO_3$ cell also begins to lose capacity at higher rates, although it is more difficult to say whether this cell is experiencing salt precipitation or a true limiting current due to salt depletion. It is believed that moderately concentrated solutions represent the

ideal compromise where both salt precipitation and salt depletion are delayed. Lower concentrations would reach a limiting current due to salt depletion sooner and higher concentrations would reach a current limitation due to salt precipitation.

5.4 Conclusions

The $Na/Na_{0.7}CoO_2$ cell utilizing a moderately concentrated polymer electrolyte, $PEO_{20}NaCF_3SO_3$, has much better rate capability than the one using a more concentrated solution $PEO_8NaCF_3SO_3$. This is attributed to the better transport properties of the $PEO_{20}NaCF_3SO_3$. Contrary to what is generally believed that more concentrated solutions are better electrolytes because there is less tendency for a limiting current to be reached, cells with $PEO/NaCF_3SO_3$ electrolytes have an optimum electrolyte concentration. The optimum is a compromise between avoiding salt depletion and salt precipitation. Knowledge of the transport properties of polymer electrolytes and their dependence on salt concentration is critical to modeling these processes and to designing cells with optimum performance.

The rate-limiting process is believed to be salt precipitation at high discharge currents for highly concentrated electrolytes (salt precipitation occurs at the anode before the salt becomes depleted at the cathode). The precipitation process has been studied by computer simulations and cell testing. Lowering the initial salt concentration to a value closer to 1.0 mol/l ($PEO_{20}NaCF_3SO_3$) is thus advantageous for these polymer electrolyte cells. It is also desirable from economic considerations to use the minimum initial

concentration that still achieves satisfactory (or better) rate capacity.

References for Part II

1. M. Armand, "Current State of PEO-Based Electrolyte," in *Polymer Electrolyte Reviews-1*, Eds., J. R. MacCallum and C. A. Vincent, Elsevier Applied Science, London, pp. 1-22 (1987).

2. P. G. Bruce and C. A. Vincent, "Polymer Electrolytes," *J. Chem. Soc. Faraday Trans.*, **89(17)**, 3187-3203 (1993).

3. A. Bourdiah, F. Dalard, D. Deroo, and M. Armand, "Potentiometric Measurements of Ionic Transport Parameters in Poly(Ethylene Oxide)-LiX Electrolytes," *J. Appl. Electrochem.*, **17**, 625-634 (1987).

4. M. A. Ratner, "Aspects of the Theoretical Treatment of Polymer Solid Electrolytes: Transport Theory and Models," in *Polymer Electrolyte Reviews-1*, Eds., J. R. MacCallum and C. A. Vincent, Elsevier Applied Science, London, pp. 173-236 (1987).

5. P. G. Bruce and C. A. Vincent, "Effects of Ion Association on Transport in Polymer Electrolytes," *Faraday Disc. Chem. Soc.*, **88**, 43 (1989).

6. C. D. Robitaille and D. Fauteux, "Phase Diagrams and Conductivity Characterization of Some PEO-LiX Electrolytes," *J. Electrochem. Soc.*, **133**, 315 (1986).

7. K. West, B. Zachau-Christiansen, T. Jacobsen, E. Hiort-Larenzen, and S. Skaarup, "poly(Ethylene Oxide)-Sodium Perchlorate Electrolytes in Solid-State Sodium Cells," *British Polymer Journal*, **20**, 243-246 (1988).

8. J. Newman, *Electrochemical Systems*, Prentice Hall, Englewood Cliffs, NJ (1991).

9. M. Watanabe and N. Ogata, "Ionic Conductivity of Poly(Propylene Oxide) Electrolytes," in *Polymer Electrolyte Reviews-1*, Eds., J. R. MacCallum and C. A. Vincent, Elsevier Applied Science, London, pp. 39-68 (1987).

10. N. Boden, S. A. Leng, and I. M. Ward, "Ionic Conductivity and Diffusivity in Polyethylene Oxide/Electrolyte Solutions as Models for Polymer Electrolytes," *Solid State Ionics*, **45**, 261-270 (1991).

11. K. West, T. Jacobsen, and S. Atlung, "Modeling of Porous Insertion Electrodes with Liquid Electrolyte," *J. Electrochem. Soc.*, **129**, 1480-1485 (1982).

12. M. Doyle, T. F. Fuller, and J. Newman, "Modeling of Galvanostatic Charge and Discharge of the Lithium/Polymer/Insertion Cell," *J. Electrochem. Soc.*, **140**, 1526-1533 (1993).

13. T. F. Fuller, M. Doyle, and J. Newman, "Simulation and Optimization of the Dual Lithium Ion Insertion Cell," *J. Electrochem. Soc.*, **141**, 1-10 (1994).

14. M. Doyle and J. Newman, "The Importance of the Lithium Ion Transference Number in Lithium/Polymer Cells", *Electrochemica. Acta*, **39**, 2073-2081 (1994).

15. N. Kobayashi, M. Uchiyama, and E. Tsuchida, "Poly[Lithium Methacrylate-CO-Oligo(Oxyethylene)Methacrylate] as a Solid Electrolyte with High Ionic Conductivity," *Solid State Ionics*, **17**, 307-311 (1985).

16. Z. Ogumi, Y. Uchimoto, Z. Takehara, and F. R. Foulkes, "Ionically Conductive Thin Polymer Films Prepared by Plasma Polymerization, III. Preparation and Characterization of Ultrathin Films Having Fixed Sulfonic Acid Groups with Only One Mobile Species," *J. Electrochem. Soc.*, **137**, 29-34 (1990).

17. J. Evans, C. Vincent, and P. Bruce, "Electrochemical Measurement of Transference Numbers in Polymer Electrolytes," *Polymer*, **28**, 2324-2328 (1987).

18. M. Watanabe, S. Nagano, K. Sanui, and N. Ogata, "Estimation of Li^+ Transference Number in Polymer Electrolytes by the Combination of Complex Impedance and Potentiostatic Polarization Measurements," *Solid State Ionics*, **28-30**, 911-917 (1988).

19. P. G. Bruce, J. Evans, and C. A. Vincent, "Conductivity and Transference Number Measurements on Polymer Electrolytes," *Solid State Ionics*, **28-30**, 918-922 (1988).

20. P. M. Blonsky, D. F. Shriver, P. Austin, and H. R. Allock, "Complex Formation and Ionic Conductivity of Polyphosphazene Solid Electrolytes," *Solid State Ionics*, **18/19**, 258-264 (1986).

21 P. R. Sorensen and T. Jacobsen, "Conductivity, Charge Transfer and Transport Number - An A.C. Investigation of the Polymer Electrolyte LiSCN-Poly(Ethylene Oxide)," *Electrochim. Acta*, **27**, 161 (1982).

22. W. Gorecki, R. Andreani, C. Berthier, M. Armand, M. Mali, J. Roos, and D. Brinkmann, "NMR, DSC, and Conductivity Study of a Poly(Ethylene Oxide) Complex

Electrolyte: PEO($LiClO_4$)$_x$," *Solid State Ionics* **18/19**, 295-299 (1986).

23. S. Bhattacharja, S. W. Smoot, and D. H. Whitmore, "Cation and Anion Diffusion in the Amorphous Phase of the Polymer Electrolyte $(PEO)_8LiCF_3SO_3$," *Solid State Ionics*, **18/19**, 306-314 (1986).

24. M. Holz, O. Lucas, and C. Muller, "NMR in the Presence of an Electric Current. Simultaneous Measurements of Ionic Mobilities, Transference Number, and Self Diffusion Coefficients Using an NMR Pulsed-Gradient Experiment," *J. Magnetic Resonance*, **58**, 294-305 (1984).

25. A. V. Chadwick and M. R. Worboys, "NMR, EXAFS and Radiotracer Techniques in the Characterization of Polymer Electrolytes," in *Polymer Electrolyte Reviews-1*, eds. J. R. MacCallum and C. A. Vincent, Elsevier Applied Science, London, pp. 275-313 (1987).

26. P. G. Bruce, M. T. Hardgrave, and C. A. Vincent, "The Determination of Transference Number in Solid Polymer Electrolytes Using the Hittorf Method," *Solid State Ionics*, **53-56**, 1087 (1992).

27. P. R. Sorensen and T. Jacobsen, "Limiting Currents in the Polymer Electrolyte: $PEO_xLiCF_3SO_3$," *Solid State Ionics*, **9&10**, 1147 (1983).

28. M. Watanabe, M. Rikukawa, K. Sanui, and N. Ogata, "Evaluation of Ionic Mobility and Transference Number in a Polymeric Solid Electrolyte by Isothermal Transient Ionic Current Method," *J. Appl. Phys.*, **58(2)**, 736-740 (1985).

29. M. Doyle and J. Newman, "Analysis of Transference Number Measurements Based on the Potentiostatic Polarization of Solid Polymer Electrolytes," *J. Electrochem. Soc.*, **142**, 3465 (1995).

30. R. Pollard and T. Comte, "Determination of Transport Properties for Solid Electrolytes from the Impedance of Thin Layer Cells," *J. Electrochem. Soc.*, **136**, 3734-3748 (1989).

31. Y. Ma, M. Doyle, T. F. Fuller, M. M. Doeff, L. C. De Jonghe and J. Newman, "The Measurement of a Complete Set of Transport Properties for a Concentrated Solid Polymer Electrolyte Solution," *J. Elelectrochem. Soc.*, **142**, 1859 (1995).

32. M. Kakihana, S. Schantz, L. M. Torell, and J. R. Stevens, "Dissociated Ions and

Ion-Ion Interactions in Poly(Ethylene Oxide) Based $NaCF_3SO_3$ Complexes," *Solid State Ionics*, **40/41**, 641-644 (1990).

33. D. Martin-Vosshage and B. V. R. Chowdari, "X-Ray Photoelectron Spectroscopy Studies on Poly(Ethylene Oxide) with Sodium Triflate," *J. Electrochem. Soc.*, **140**, 3531 (1993).

34. P. Ferloni, G. Chiodelli, A. Magistris, and M. Sanesi, "Ion Transport and Thermal Properties of Poly(Ethylene Oxide)-$LiClO_4$ Polymer Electrolytes," *Solid State Ionics*, **18&19**, 265-270 (1986).

35. J. Newman and T. W. Chapman, "Restricted Diffusion in Binary Solutions," *AIChE J.*, **19**, 343 (1973).

36. M. Doyle, Ph.D. Dissertation, University of California, Berkeley (1995).

37. J. Crank, *The Mathematics of Diffusion*, Oxford University Press, London (1956).

38. S. D. Thompson and J. Newman, "Differential Diffusion Coefficients of Sodium Polysulfide Melts," *J. Electrochem. Soc.*, **136**, 3362-3369 (1989).

39. D. Fauteux, J. Prudhomme, and P. E. Harvey, "Electrochemical Stability and Ionic Conductivity of Some Polymer-LiX Based Electrolytes," *Solid State Ionics*, **28-30**, 923-928 (1988).

40. R. A. Robinson and R. H. Stokes, *Electrolyte Solutions*, 2nd ed., Butterworths, London, p. 161 (1959).

41. R. Pollard and J. Newman, "Mathematical Modeling of the Lithium-Aluminum, Iron Sulfide Battery," *J. Electrochem. Soc.*, 128, 491-502 (1981).

Figure Captions: Chapter 4

Figure 4-1. The cell configuration to measure the transference number using the galvanostatic polarization method developed in this work.

Figure 4-2. The Nyquist plot of the $PEO_{20}NaCF_3SO_3$ electrolyte at 85°C. The intercept of the high frequency loop on the real impedance axis (R_e) is the ohmic resistance of the electrolyte membrane.

Figure 4-3. Logarithmic plot of the ionic conductivity of $PEO_nNaCF_3SO_3$ as a function of electrolyte concentration at 85°C.

Figure 4-4. Data from diffusion coefficient measurements for $PEO_{55}NaCF_3SO_3$ at 85°C. (a). A $Na/PEO_{55}NaCF_3SO_3/Na$ cell was first polarized by passing a current through it, and then relaxed to its initial condition after the current was interrupted. (b) Natural logarithm of potential *vs.* time during the relaxation period. Linear behavior is observed in the plot after a sufficient amount of time elapsed.

Figure 4-5. Diffusion coefficients of $NaCF_3SO_3$ in PEO as a function of electrolyte concentration at 85°C. Data were obtained by using the method of restricted diffusion.

Figure 4-6. Data measured from concentration cells of the form: $Na/PEO_nNaCF_3SO_3/PEO_8NaCF_3SO_3/Na$ at 85°C. The scale of the x-axis is the concentration value of the $PEO_nNaCF_3SO_3$ membrane, where n varies from 4 to 500. The solid line is a fit to the data.

Figure 4-7. Data measured from galvanostatic polarization experiments on $Na/PEO_nNaCF_3SO_3/Na$ cells at 85°C. Cells were polarized by passing a constant current of about 0.1 mA/cm^2 to 0.3 mA/cm^2 for a time period on the order of 1 min.

Figure 4-8. Slopes of galvanostatic polarization plots of $Na/PEO_nNaCF_3SO_3/Na$ cells as a function of electrolyte concentration at 85°C. The slope is taken at the origin of the polarization plots.

Figure 4-9. Transference numbers for the sodium ion in $PEO_nNaCF_3SO_3$ at 85°C using the galvanostatic polarization method developed in this work.

Figure 4-10. Semilogarithmic plot of the thermodynamic factor for $NaCF_3SO_3$ in PEO at 85°C as a function of the electrolyte concentration.

Figure 4-11. Comparisons between the galvanostatic polarization data and the results of numerical simulations for various bulk concentrations. The solid lines are the simulation results.

Figure 4-12. Schematics of mass transportation processes in a polymer electrolyte in the case of (a) unity sodium ion transference number, (b) zero sodium ion transference number, and (c) negative sodium ion transference number. These sketches only serve to illustrate that a cell can be discharged regardless of the value of sodium ion transference number.

Figure Captions: Chapter 5

Figure 5-1. Discharge curves for $Na/PEO_nNaCF_3SO_3/Na_xCoO_2$ Cells at 85°C, where (a) n = 8, and (b) n = 20. The two cells were cycled in the same sequence to minimize the electrode capacity fading effect. The current density was in the range of 0.1 mA/cm^2 to 2.5 mA/cm^2.

Figure 5-2. Concentration profiles across a $Na/PEO_{12}NaCF_3SO_3/Na$ cell during a galvanostatic polarization for four minutes at 85°C at 0.4 mA/cm^2. The profiles are equally spaced in time at thirty-seconds intervals. These simulations use the variable physical properties measured in this work.

Figure 5-3. The difference between concentrations of the electrolyte at the electrode and the bulk. This is the theoretical prediction for galvanostatic polarization experiments for a $Na/PEO_{12}NaCF_3SO_3/Na$ cell at 85°C using the physical properties measured in this work.

Figure 5-4. Transition-time experiments for the system $Na/PEO_8NaCF_3SO_3/Na$ at 85°C. A current density of 0.55 mA/cm^2 was used in each of the tests. Different rest times were used between successive experiments.

Figure 5-5. Transition time experiments for the $Na/PEO_8NaCF_3SO_3/Na$ system at 85°C. A current density of 0.55 mA/cm^2 was passed across the cell for all the tests. Each experiment is followed by one-hour rest period.

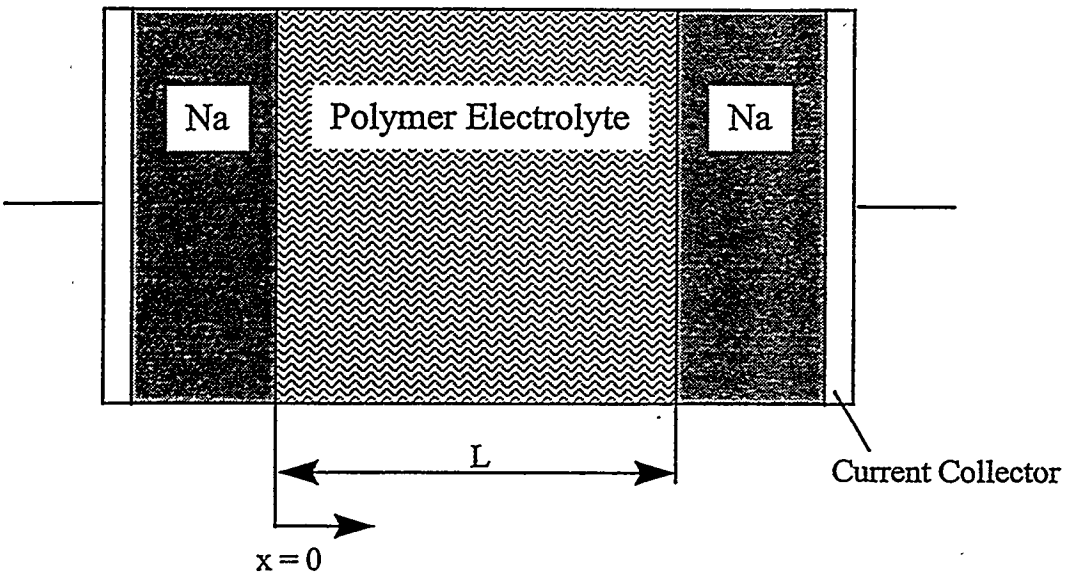

Figure 4-1. The cell configuration to measure the transference number using the galvanostatic polarization method developed in this work.

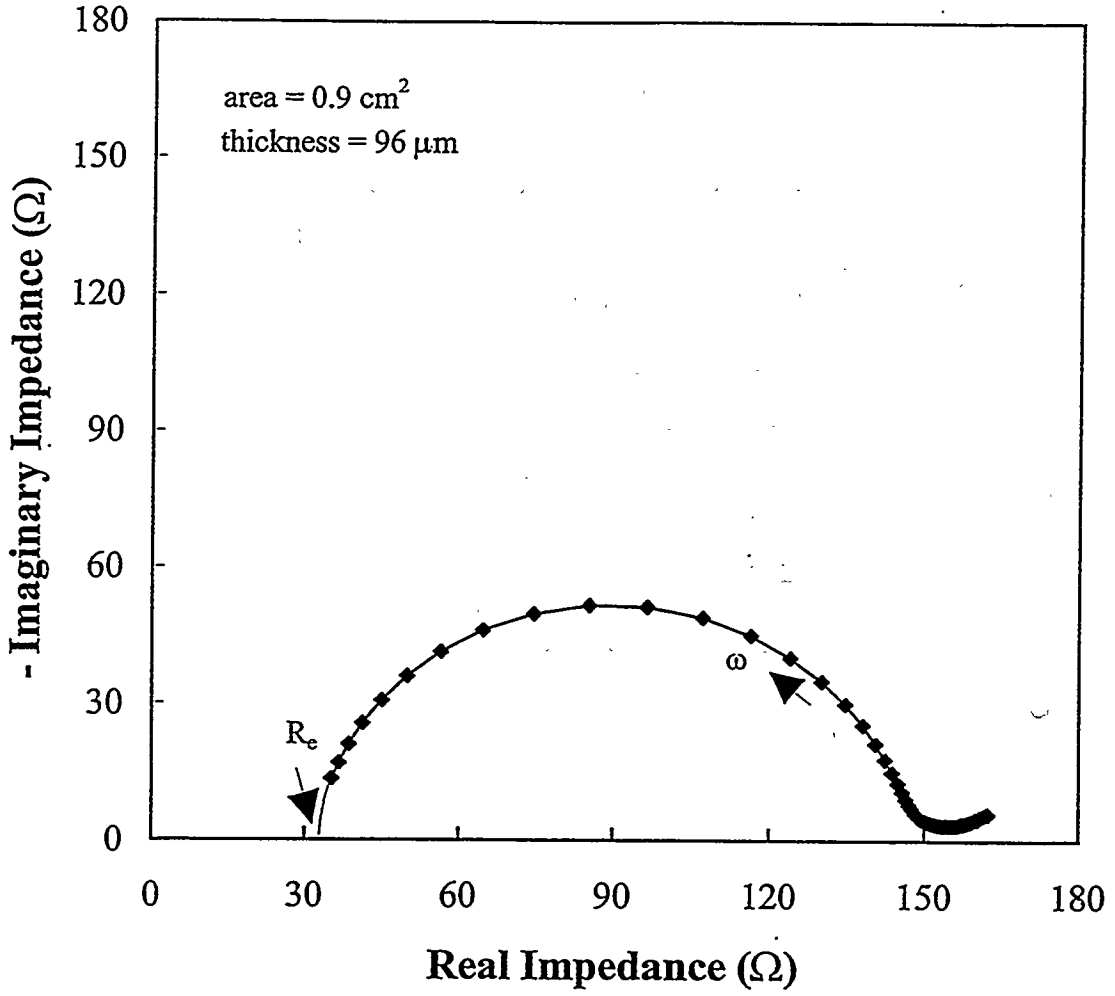

Figure 4-2. The Nyquist plot of the $PEO_{20}NaCF_3SO_3$ electrolyte at 85°C. The intercept of the high frequency loop on the real impedance axis (R_e) is the ohmic resistance of the electrolyte membrane.

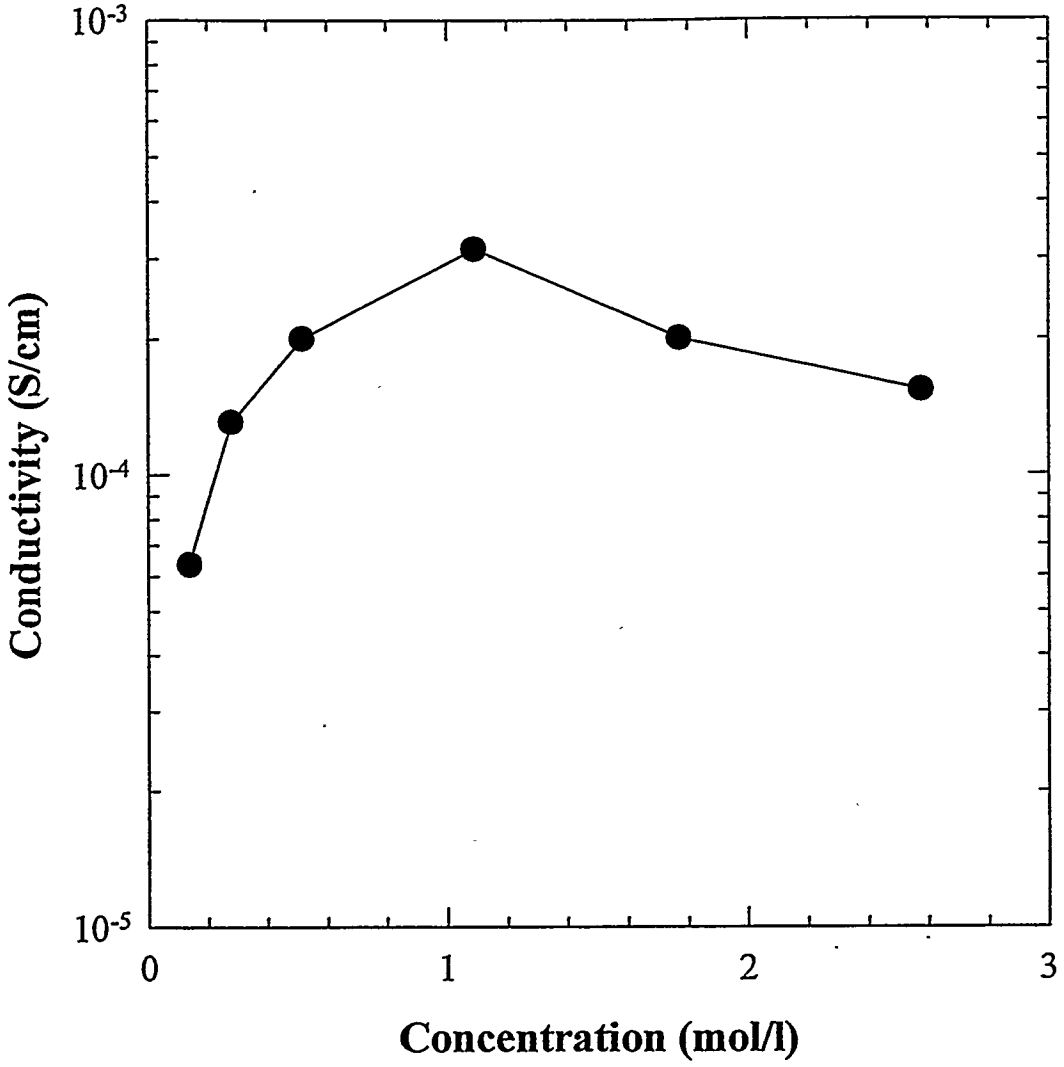

Figure 4-3. Logarithmic plot of the ionic conductivity of $PEO_nNaCF_3SO_3$ as a function of electrolyte concentration at 85°C.

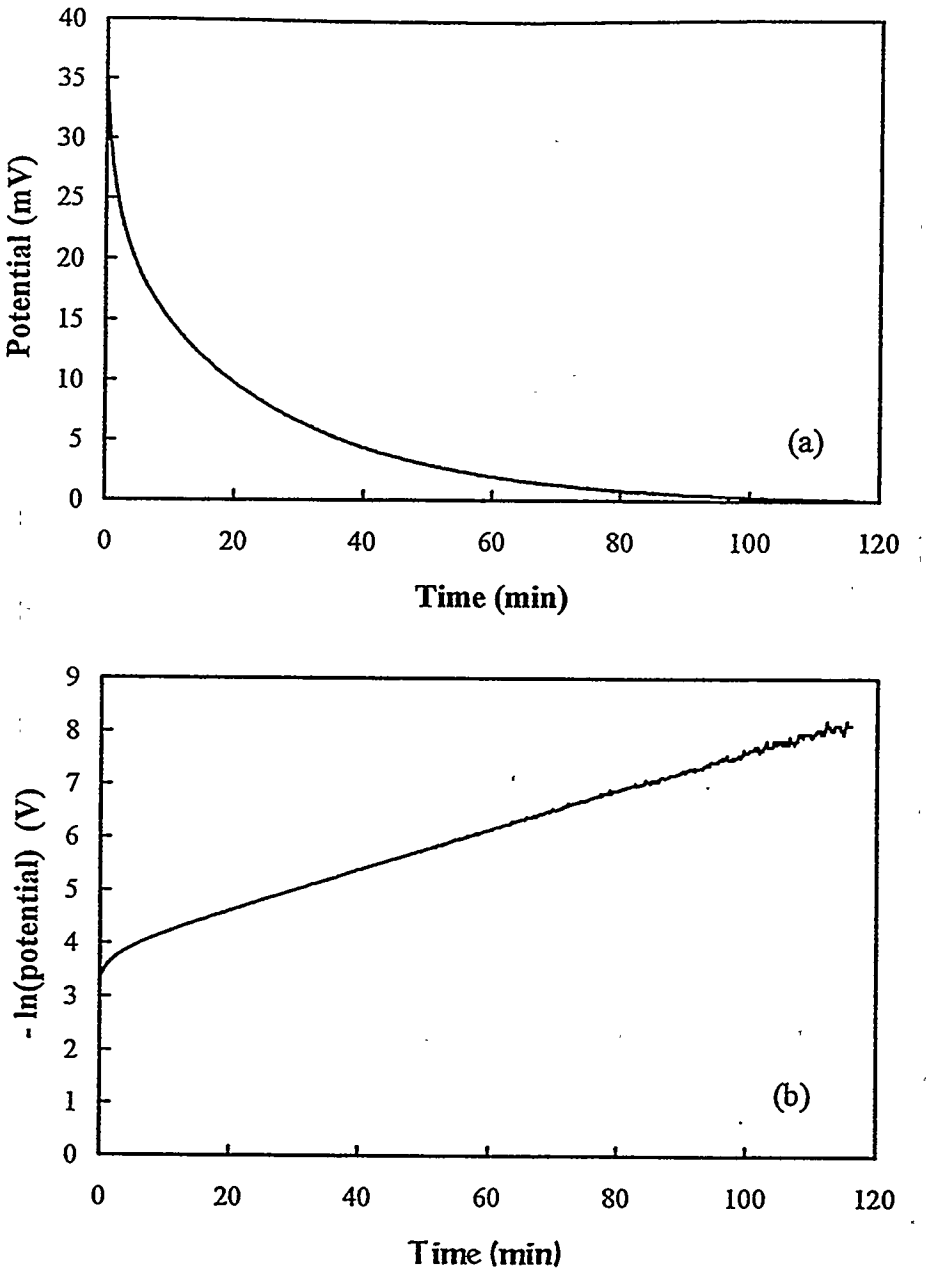

Figure 4-4. Data from diffusion coefficient measurements for $PEO_{55}NaCF_3SO_3$ at 85°C. (a). A Na/$PEO_{55}NaCF_3SO_3$/Na cell was first polarized by passing a current through it, and then relaxed back to its initial condition after the current was interrupted. (b) Natural logarithm of potential *vs.* time during the relaxation period. Linear behavior is observed in the plot after a sufficient amount of time elapsed.

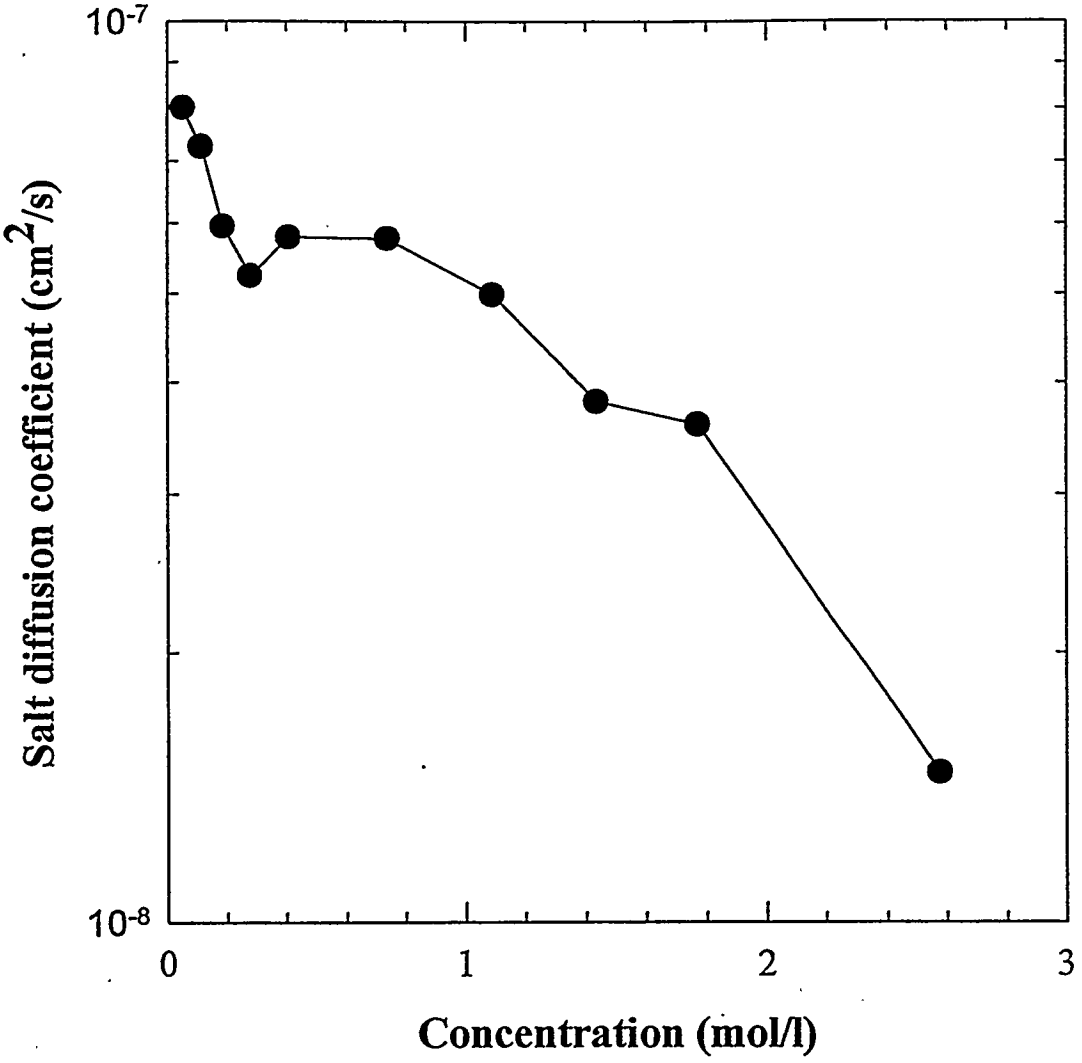

Figure 4-5. Diffusion coefficients of $NaCF_3SO_3$ in PEO as a function of electrolyte concentration at 85°C. Data were obtained by using the method of restricted diffusion.

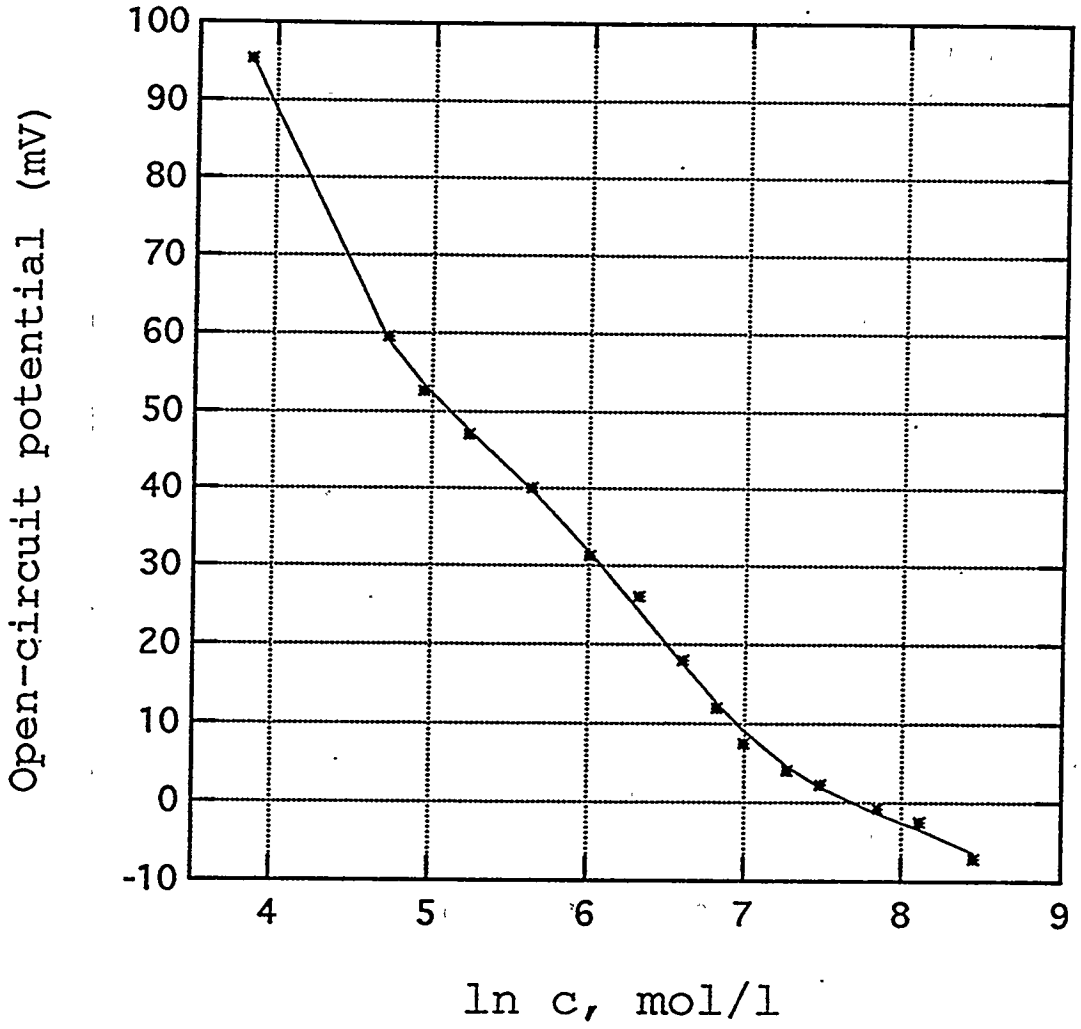

Figure 4-6. Data measured from concentration cells of the form: $Na/PEO_nNaCF_3SO_3/PEO_8NaCF_3SO_3/Na$ at 85°C. The scale of the x-axis is the concentration value of the $PEO_nNaCF_3SO_3$ membrane, where n varies from 4 to 500. The solid line is a fit to the data.

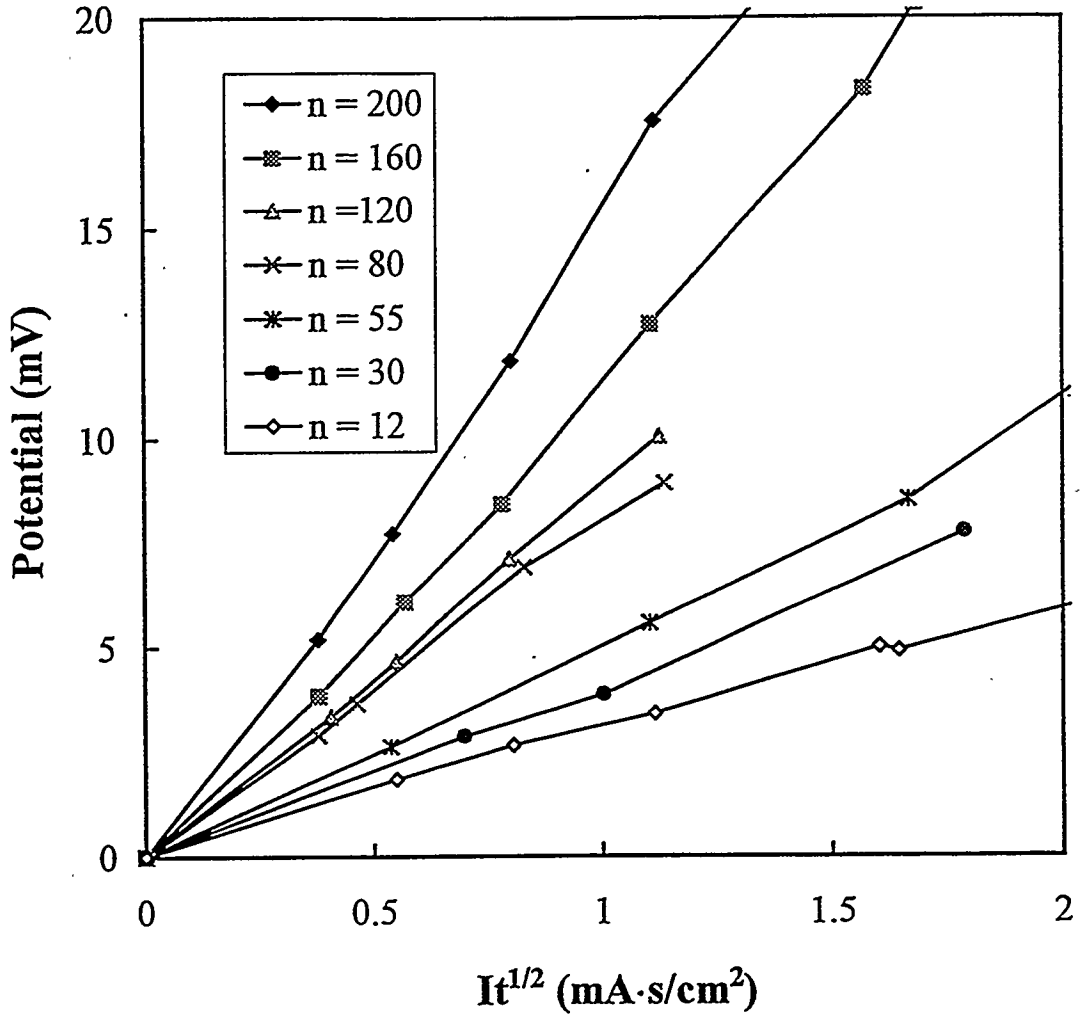

Figure 4-7. Data measured from galvanostatic polarization experiments on $Na/PEO_nNaCF_3SO_3/Na$ cells at 85°C. Cells were polarized by passing a constant current of about 0.1 mA/cm^2 to 0.3 mA/cm^2 for a time period on the order of 1 min.

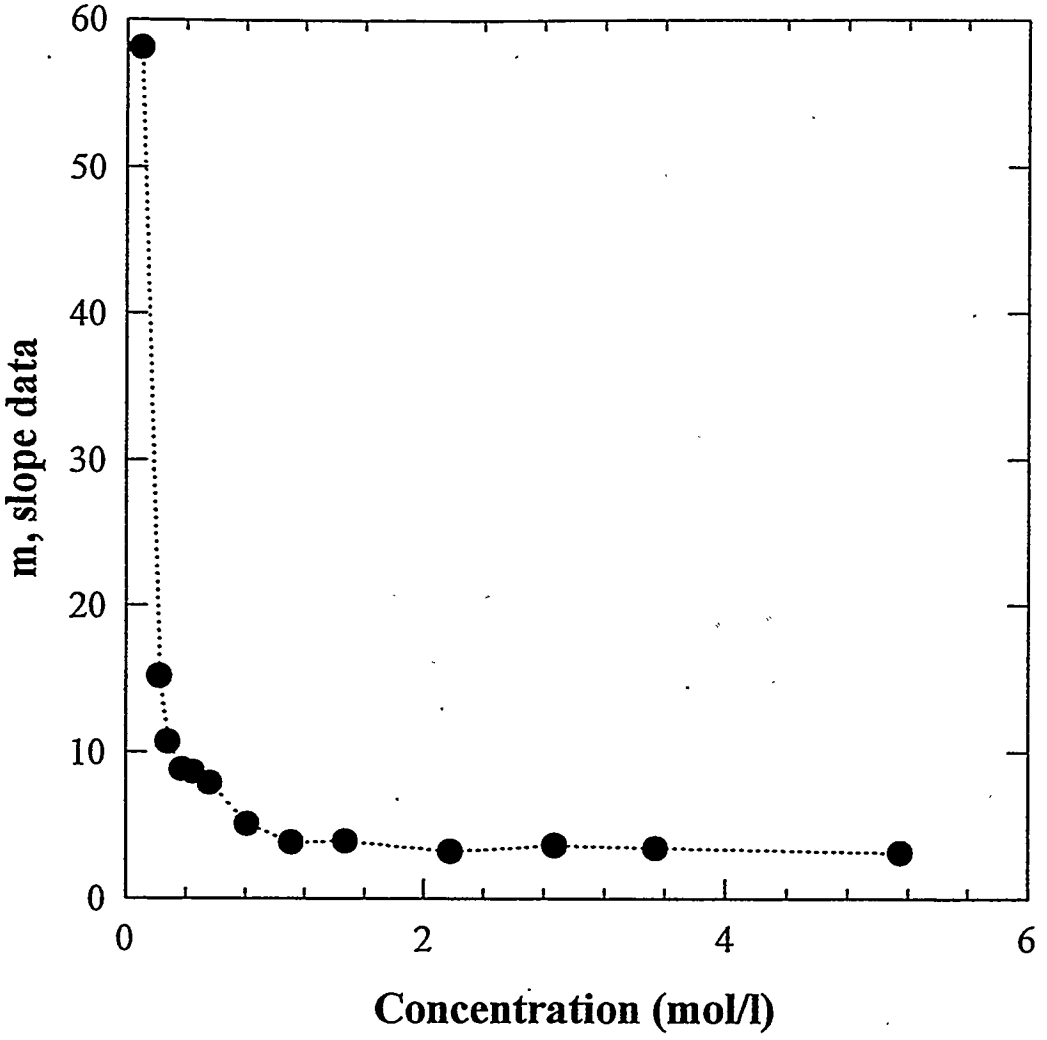

Figure 4-8. Slopes of galvanostatic polarization plots of $Na/PEO_nNaCF_3SO_3/Na$ cells as a function of electrolyte concentration at 85°C. The slopes were taken at the origin of the polarization plots.

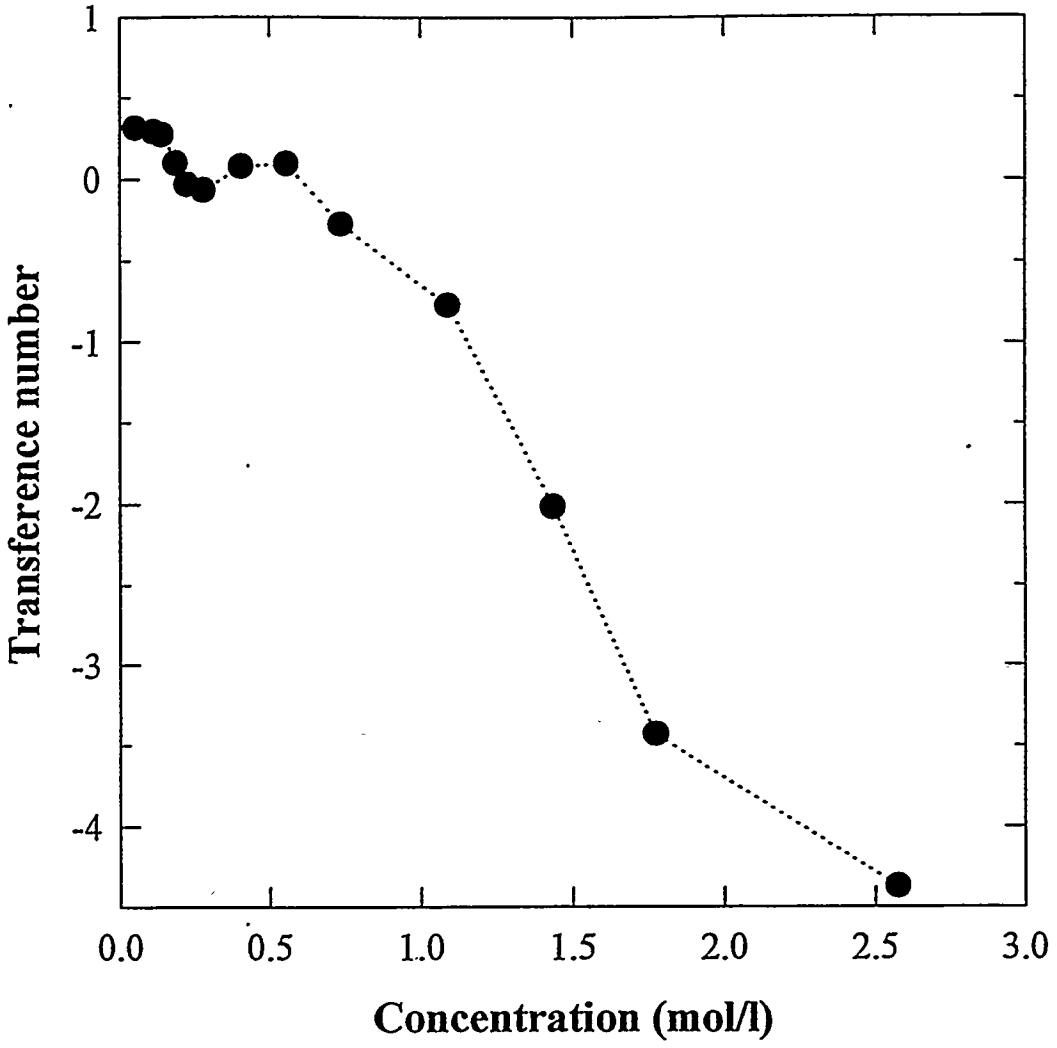

Figure 4-9. Transference numbers for the sodium ion in $PEO_nNaCF_3SO_3$ at 85°C using the galvanostatic polarization method developed in the present work.

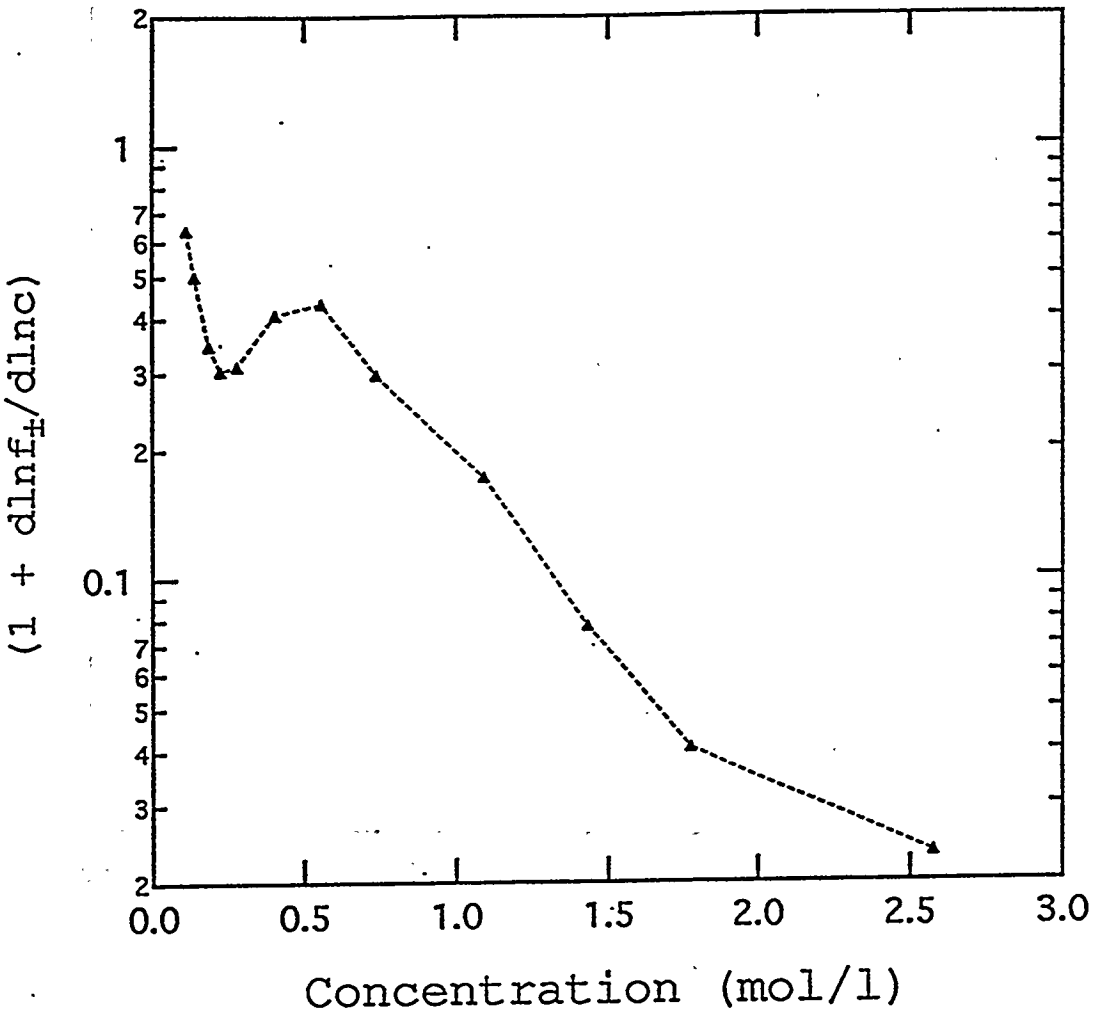

Figure 4-10. Semilogarithmic plot of the thermodynamic factor for $NaCF_3SO_3$ in PEO at 85°C as a function of the electrolyte concentration.

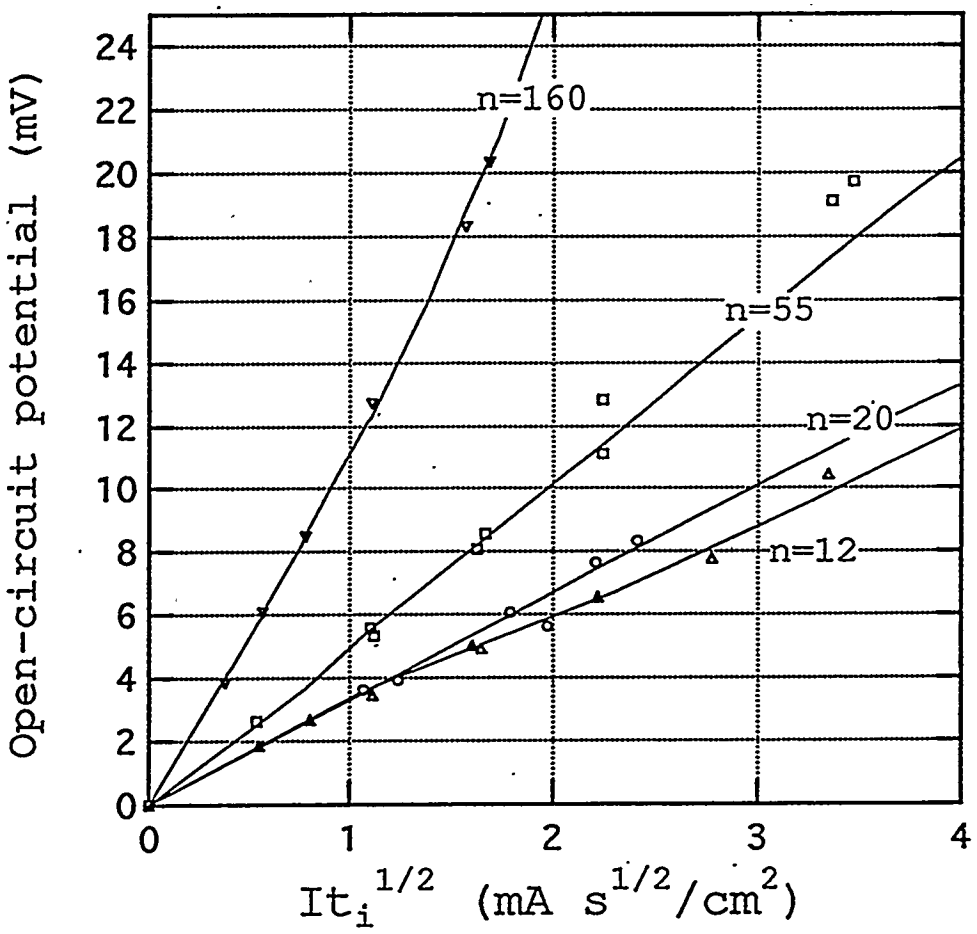

Figure 4-11. Comparisons between the galvanostatic polarization data and the results of numerical simulations for various bulk concentrations. The solid lines are the simulation results.

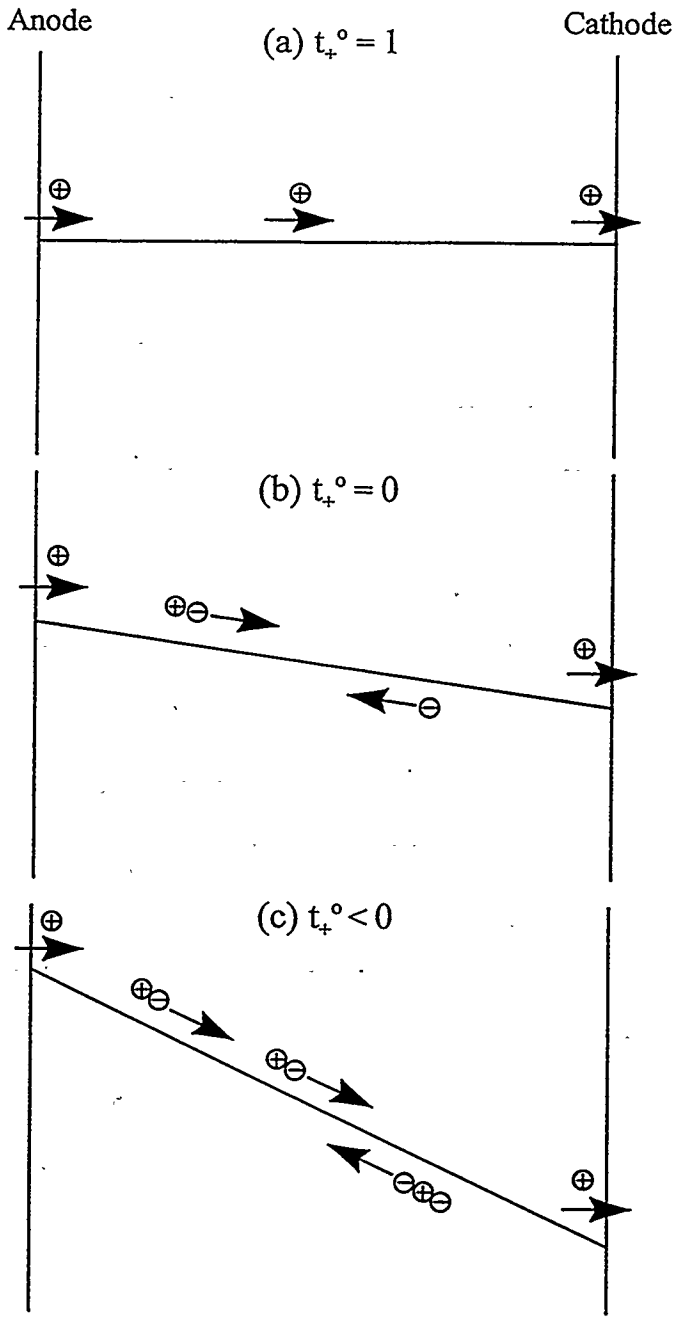

Figure 4-12. Schematics of mass transportation processes in a polymer electrolyte in the case of (a) unity sodium ion transference number, (b) zero sodium ion transference number, and (c) negative sodium ion transference number. These sketches only serve to illustrate that a cell can be discharged regardless of the value of sodium ion transference number.

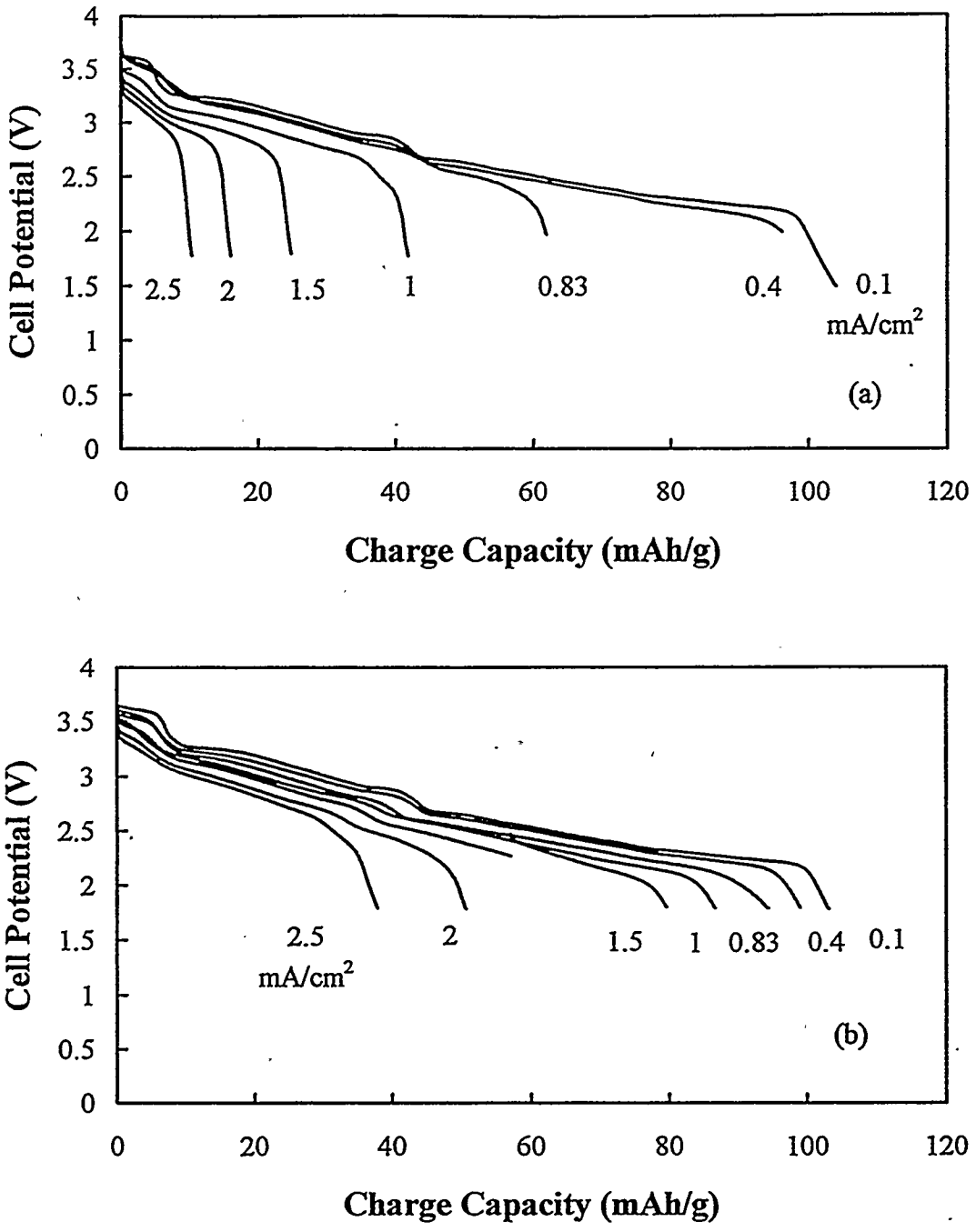

Figure 5-1. Discharge curves for $Na/PEO_nNaCF_3SO_3/Na_xCoO_2$ Cells at 85°C, where (a) n = 8, and (b) n = 20. The two cells were cycled in the same sequence to minimize the electrode capacity fading effect. The current density was in the range of 0.1 mA/cm^2 to 2.5 mA/cm^2.

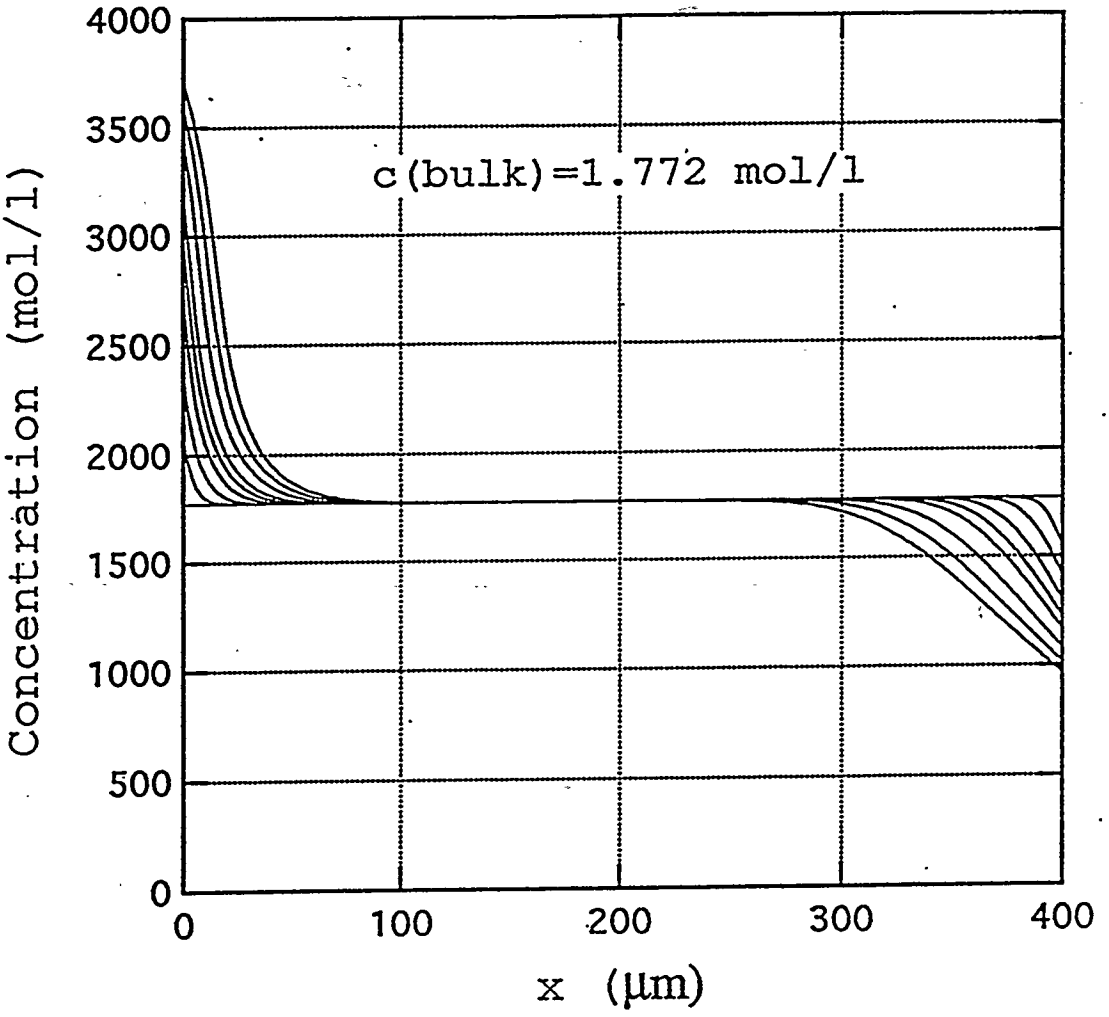

Figure 5-2. Concentration profiles across a $Na/PEO_{12}NaCF_3SO_3/Na$ cell during a galvanostatic polarization for four minutes at 85°C at 0.4 mA/cm^2. The profiles are equally spaced in time at thirty-seconds intervals. These simulations use the variable physical properties measured in this work.

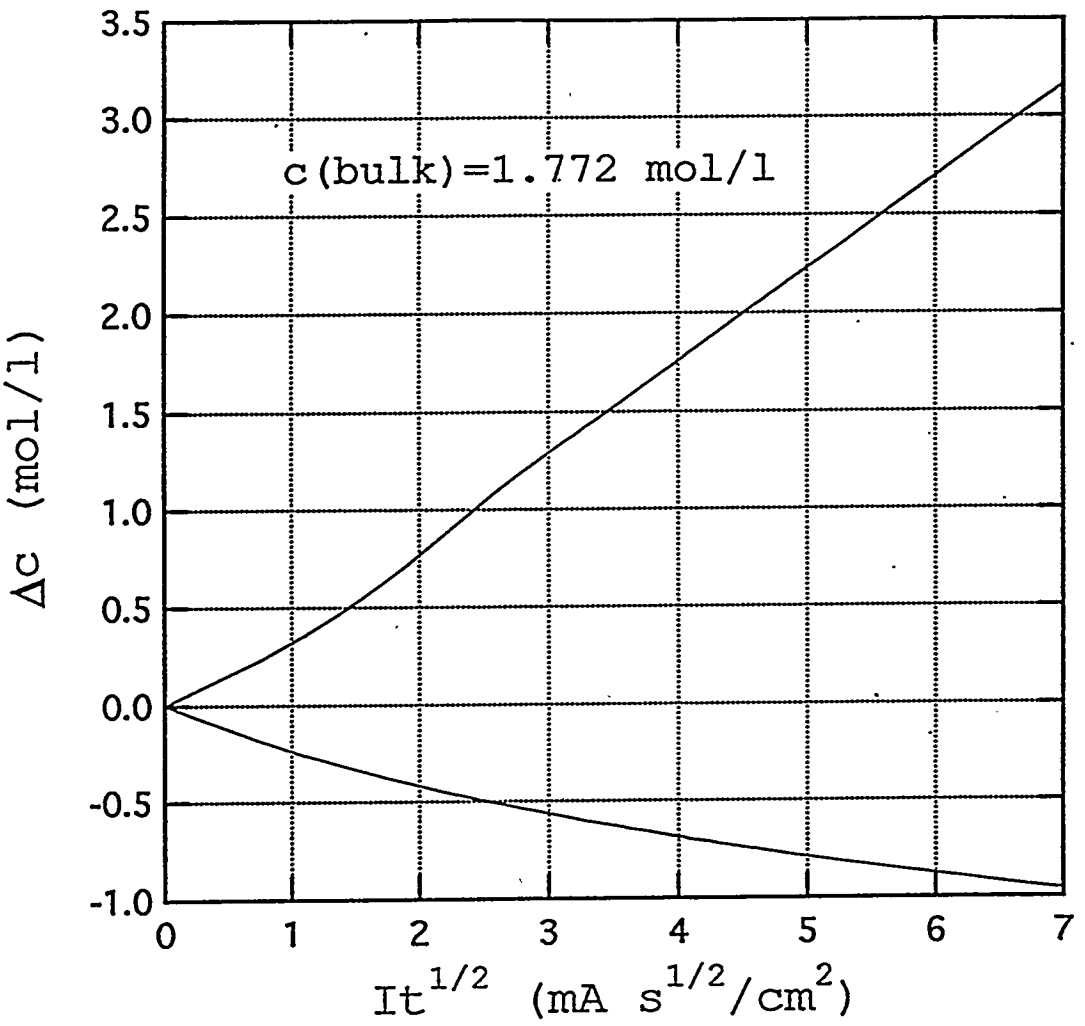

Figure 5-3. The difference between concentrations of the electrolyte at the electrode and the bulk. This is the theoretical prediction for galvanostatic polarization experiments for a $Na/PEO_{12}NaCF_3SO_3/Na$ cell at 85°C using the physical properties measured in this work.

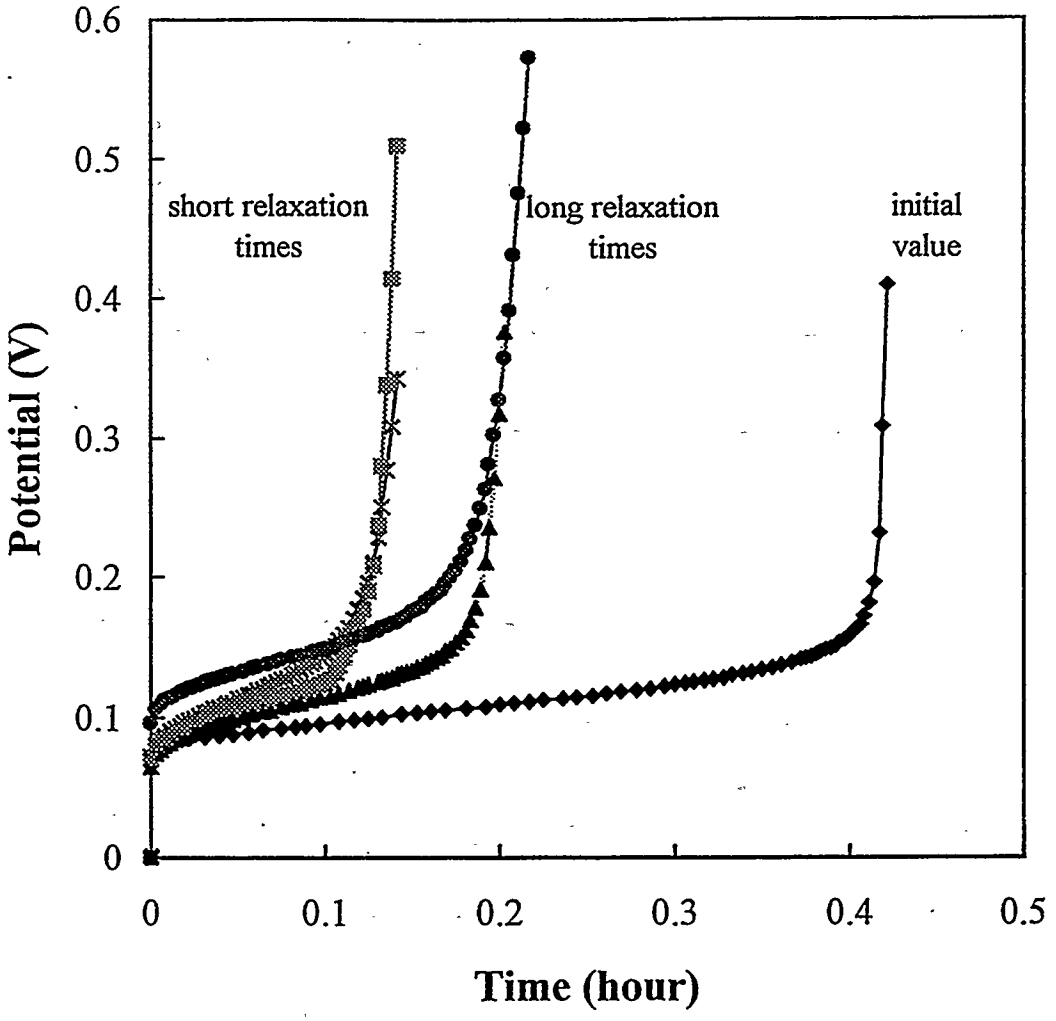

Figure 5-4. Transition-time experiments for the system $Na/PEO_8NaCF_3SO_3/Na$ at 85°C. A current density of 0.55 mA/cm^2 was used in each of the tests. Different rest times were used between successive experiments.

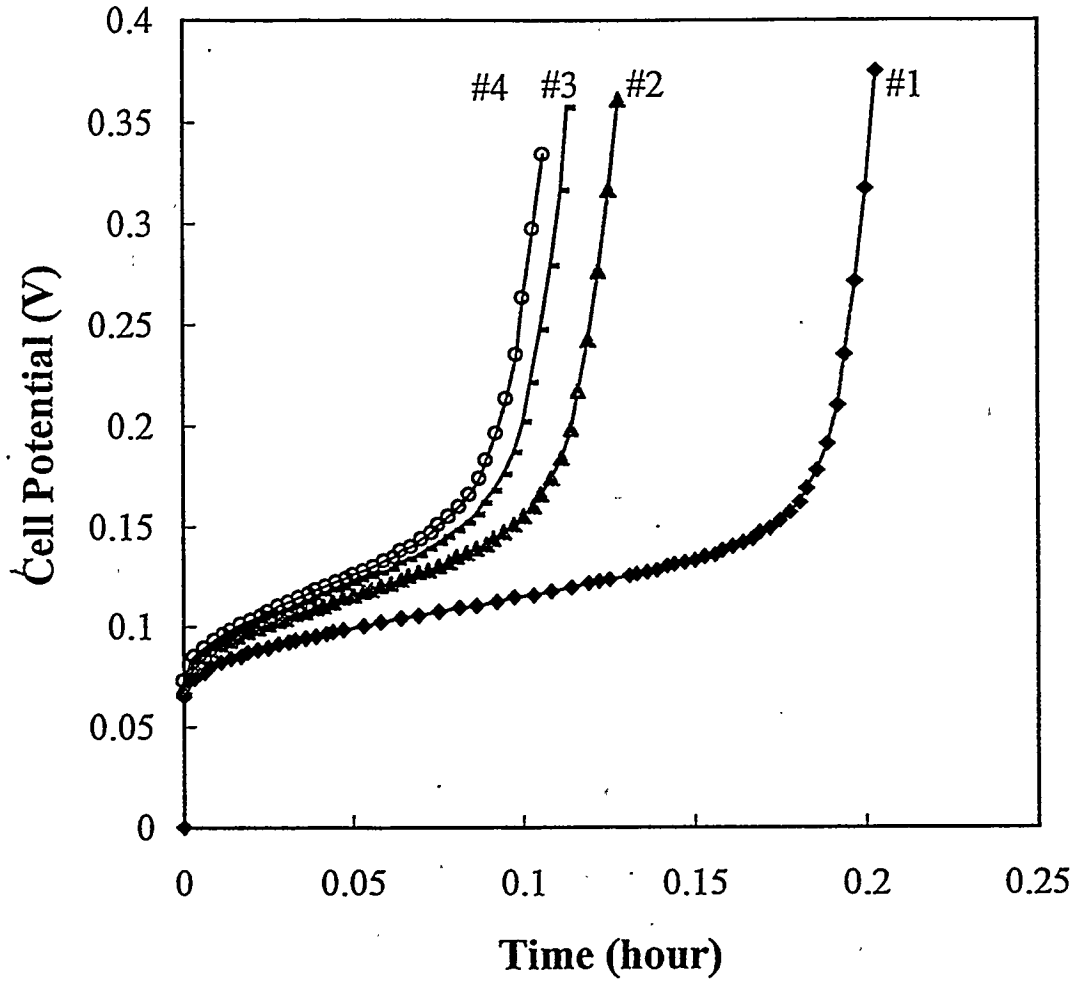

Figure 5-5. Transition time experiments for the $Na/PEO_8NaCF_3SO_3/Na$ system at 85°C. A current density of 0.55 mA/cm^2 was passed across the cell for all the tests. Each experiment is followed by one-hour rest period.

Chapter 6 Conclusions

Solid-state sodium cells using polymer electrolytes and sodium cobalt oxide positive electrodes are characterized in terms of discharge and charge characteristics, rate capability, cycle life, and energy and power densities. The P2 phase Na_xCoO_2 can reversibly intercalate sodium in the range of $x = 0.3$ to 0.9, giving a theoretical specific energy of 440 Wh/kg and energy density of 1600 Wh/l. Over one hundred cycles to 60% depth of discharge or better have been obtained at 0.5 mA/cm^2 and two hundred shallower cycles at the same rate. Experiments in which positive/positive cells were cycled suggest the Na/PEO interface is not the limiting factor to cell cycle life. Four-probe DC experiments also show that the sodium/electrolyte interface is stable and only has minor contributions to the cell resistance. Electrolyte modification due to mass polarization, disconnection of particles in the cathode are suggested as the factors contributing to eventual cell failure. Subtle chemical and structural changes are other possible factors, but x-ray diffraction experiments failed to reveal these changes in this study. In terms of cycle life, energy density, and rate capability, these are the best results obtained on a sodium/polymer electrolyte cell to date. These results are also comparable to the known lithium/polymer systems, indicating that the sodium polymer battery is an attractive alternative of the lithium/polymer system.

The effect of carbon black additive on the composite $Na_{0.7}CoO_2$ electrode is evaluated in terms of electronic conductivity and cell performance. Although $Na_{0.7}CoO_2$ is highly conductive (10^2 to 10^3 S/cm), the conductivity of the electrodes is dominated by the

volume fraction of carbon. Adding 10 v/o of carbon black can effectively increase the electrode conductivity from about 10^{-7} to 10^{-1} S/cm. Carbon additive is also essential to cell performance. The electrode containing 10 v/o of carbon exhibits significantly better performance than the one containing the same or larger volume fraction of solid phase ($Na_{0.7}CoO_2$) but no carbon additive. These effects may be attributed to the better connections between $Na_{0.7}CoO_2$ established by the very fine carbon particles.

The transport properties of polymer electrolytes are crutial factors for the performance. These properties, the ionic conductivity, the salt diffusion coefficient, and the ion transference number, are measured for the $PEO_nNaCF_3SO_3$ system over a wide range of concentration (0.1 to 2.6 mol/l) at 85°C. The ionic conductivity was measured using the standard ac-impedance technique, and the diffusion coefficient using the restricted method. The concentration difference was extracted from the potential signal for diffusion coefficient measurements. The measurement of transference number is complicated by the nonideality of polymer electrolytes. A novel method is therefore developed from concentrated solution theory in this work. It is rigorous for any binary electrolyte and also simple experimentally. The method is based on dc polarization experiments in combination with concentration cell measurements. The thermodynamic factor, in addition, can be determined from this method.

All the three transport properties of the $PEO_nNaCF_3SO_3$ system are very electrolyte-concentration dependent. The conductivity increases with concentration at low concentrations, going through a maximum, and then decreases when more salt is added. The transference number, diffusion coefficient, and thermodynamic factor all vary with

concentration in a similar fashion. The salt diffusion coefficient is on the order of 10^{-7} to 10^{-8} cm^2/s, depending on the electrolyte concentration. The transference number decreases as concentration increases, going from around 0.31 in the most dilute solution (0.05 mol/l) to -4.37 in the most concentrated solution (2.58 mol/l). Some discussion of the impact of microscopic speciation on the macroscopic transport properties is given to rationalize the negative transference number obtained. The thermodynamic factor ($1+d\ln f_{\pm}/d\ln c$) is far less than unity especially for highly concentrated solutions, indicating that these polymer electrolytes are highly nonideal.

The transport properties are used to analyze and optimize the performance of $Na/PEO_nNaCF_3SO_3/Na_xCoO_2$ cells. The cell utilizing a moderately-concentrated electrolyte, $PEO_{20}NaCF_3SO_3$, has much better rate capability than the one using a more concentrated electrolyte, $PEO_8NaCF_3SO_3$. Contrary to what is generally believed, that more concentrated solutions are better electrolytes because there is less tendency for a limiting current to be reached, cells with $PEO_nNaCF_3SO_3$ have an optimum electrolyte concentration. The optimum is a compromise between avoiding salt depletion and salt precipitation. The rate-limiting process in the $PEO_8NaCF_3SO_3$ cell is believed to be salt precipitation at high discharge currents.